Schwann cell-sensory neuron complex and sensory mechanotransduction

Inaugural-Dissertation
to obtain the academic degree
Doctor rerum naturalium (Dr. rer. nat.)

submitted to the Department of Biology, Chemistry, Pharmacy
of Freie Universität Berlin

by
Julia Anai Ojeda Alonso
from La Paz, B.C.S., Mexico

2021

The present work was carried out under the supervision of Prof. Dr. Gary R. Lewin from March 2016 to March 2021 at the Max Delbrück Center for Molecular Medicine in the Helmholtz Association.

I declare that this thesis has been composed solely by myself and that it has not been submitted, in whole or in part, in any previous application for a degree. Except where states otherwise by reference or acknowledgment, the work presented is entirely my own.

1st reviewer: Prof. Dr. Gary R. Lewin

2nd reviewer: Prof. Dr. Ursula Koch

Date of defense: 28th of October of 2021.

1. Table of Contents

2. Abstract

The recent discovery of nociceptive Schwann cells has changed our vision of how mechanotransduction occurs in sensory neurons. We have described a diversity of sensory Schwann cells that participate on mechanotransduction in mechanoreceptors and nociceptors. Here, we have demonstrated that $Sox10^{+}$ Schwann cells display mechanosensitive currents by indentation. Optogenetic manipulation of $Sox10^{+}$ Schwann cells in Meissner corpuscles as in A-fiber and C-fiber mechanonociceptors demonstrated that these cells influence the mechanical threshold, sensitivity and adaptation of cutaneous sensory neurons. Particularly, sensory Schwann cells in Meissner corpuscles are compartamelized and influence different aspects of Aβ-fibers excitability. $Sox10^{+}$ Schwann cells are tightly coupled with sensory afferent terminal endings and participate in mechanosensitivity and AP initiation, while $Sox2^{+}$ are associated with excitability and adaption properties. Similar functional structure has been found in hair follicles innervated by Aβ-fibers and associated with $Sox2^{+}$ Schwann cells. In nociceptors, $Sox10^{+}$ Schwann cells seem to be directly coupled to the terminal endings and influence their mechanical threshold and adaption properties. Thus, the sensory Schwann cell and terminal endings of cutaneous sensory neurons are a diverse and conserved feature in specialized receptors for mechanotransduction.

The TMEM150C/Ttn3 transmembrane protein was recently proposed as a mechanosensitive ion channel. Here we have overexpressed TMEM150C/Ttn3 in naïve cells and stimulated with mechanical indentation, no mechanosensitive currents were observed or modulation of mechanically gated ion channels such as Piezo2. Additionally, we have used the *ex vivo* skin-nerve preparation to characterize the role of TMEM150C/Ttn3 in cutaneous sensory neurons function in two mutant mice where the gene was ablated. The $TMEM150C^{LacZ/LacZ}$ mouse line was generated by introducing a LacZ and neomycin cassette and disrupt the allele is expected. Skin nerve preparation recordings and mousewalk behavior test showed no difference between wild-type and knockout mice. However, it is possible that DRG neurons go through alternative splicing and part of the gene generates a truncated protein. The $TMEM150C^{-/-}$ mouse was generated using CRISPR/Cas technology where the N-terminal sequence of the allele is deleted, and no transcripts are produced. Preliminary results suggest that TMEM150C seem to participate in slowly adapting properties of mechanoreceptors and nociceptors.

Zusammenfassung

Die kürzlich erfolgte Entdeckung von nozizeptiven Schwannzellen hat unser Verständnis der mechanischen Reizweiterleitung in sensorischen Neuronen grundlegend geändert. Wir konnten eine Reihe von sensorischen Schwannzellen definieren, die an der Erfassung von mechanischen Reizen in Mechano- und Schmerzrezeptoren beteiligt sind. In der vorliegenden Arbeit zeigen wir, dass Sox10-positive Schwannzellen auf Druckreize mit mechanosensitiven Impulsen reagieren. Optogenetische Untersuchungen an $Sox10^+$ Zellen in Meissnerschen Korpuskeln als auch in Mechanonozizeptoren der Klassen A und C ergaben, dass diese Zellen sowohl Reizschwelle, Empfindlichkeit als auch neuronale Adaptation von Sinneszellen der Haut beeinflussen. Dabei liegen sensorische Schwannzellen in Meissnerschen Korpuskeln in Kompartimenten vor und wirken auf unterschiedliche Aspekte der Erregbarkeit von Aβ-Fasern. $Sox10^+$ Zellen liegen eng an den terminalen Enden sensorischer Afferenzen und modulieren Sensitivität sowie die Auslösung von Aktionspotentialen, während $Sox2^+$ Zellen Erregbarkeit und Adaptation beeinflussen. Eine ähnliche funktionale Einheit wurde in Haarfollikeln gefunden, die von Aβ-Fasern innerviert und mit $Sox2^+$ Schwannzellen assoziiert sind. In Nozizeptoren scheinen Sox10+ Schwannzellen direkt mit den terminalen Enden verbunden zu sein, um mechanische Reizschwelle und Adaptatation zu modulieren. Sensorische Schwannzellen und terminale Enden von sensorischen Neuronen der Haut scheinen daher eine konservierte und differenzierte Eigenschaft von Rezeptoren zu sein, die auf die Empfindung von mechanischen Reizen spezialisiert sind. Das TMEM150C/Ttn3 Transmembranprotein wurde kürzlich als mechanosensitiver Ionenkanal postuliert. Wir haben daher TMEM150C/Ttn3 in Wildtypzellen überexprimiert und diese mechanisch gereizt; dabei konnten wir keine mechanosensitiven Impulse noch eine Modulation von mechanisch aktivierten Ionenkanälen wie Piezo2 beobachten. Wir haben zudem zwei nullmutante Mausmodellen für TMEM150C/Ttn3 benutzt, um mit Hilfe von *ex vivo* Haut-Nerv-Präparaten die Funktion des Proteins zu bestimmen. Die $TMEM150C^{LacZ/LacZ}$ Linie wurde durch Insertion einer LacZ/neomycin Kassette in den Lokus des Gens hergestellt, um das Leseraster zu zerstören. Die Analyse von Haut-Nerv-Präparaten und Beobachtung der Schrittfolge von mutanten Mäusen zeigte allerdings keinen Unterschied zwischen Nullmutante und Wildtyp. Eine mögliche Erklärung dafür ist, dass in Spinalganglien durch alternatives Splicing der mRNA eine trunkierte Version des Proteins hergestellt wird. Die zweite Mutante, $TMEM150C^{-/-}$, wurde mittels CRISPR/Cas hergestellt, wobei der N-terminale Anteil des Gens deletiert wurde und kein Transkript gebildet wird. Erste Ergebnisse mit dieser Mutanten deuten darauf hin, dass TMEM150C eine Rolle bei der langsamen Adaptierung von Mechanorezeptoren und Nozizeptoren spielt.

3. List of abbreviations

AM	A-fiber mechanonociceptor
AP	Action potential
BFABP	fatty acid-binding protein
Cad19	cadherin 19
C-C	C-cold (thermoreceptor)
C-H	C-heat (thermoreceptor)
C-HC	C-heatcold (thermoreceptor)
C-M	C-mechanonociceptors
C-MC	C-mechanocold
C-MH	C-mechanoheat
C-MHC	C-mechanoheatcold
CNS	Central Nervous System
ChR2	Channelrhodopsin-2
DRG	dorsal root ganglia
DRAM	Damage-Regulated Autophagy Modulators
ECDs	extracellular domains
EMC	Extracellular matrix
HF	Hair follicle
HGF	hepatocyte growth factor
HSPC	High Speed Pressure Clamp
HTMRs	high threshold mechanoreceptors
LTMRs	low threshold mechanoreceptors
Jas	Jasplakinolide
JNK	c-Jun-amino (N)-terminal kinase
NCCs	Neural crest cells
K2P	two-pore domain K^+ channel
KCNK	K^+ channels subfamily K encodes for K2P
NGF	Nerve growth factor
Ngn1-2	neurogenin 1; neurogenin 2
NRG1	neuregulin 1

NT-3	Neurotrophin-3
PAX3	paired box gene 3
$p75^{NTR}$	p75 neurotrophin receptor
PI3-K	phosphatidylinositol 3’-kinase
PI4P	Phosphatidylinositol 4-phosphate
PI4KIIIIα	PI 4-kinase type IIIα
PLC- γ	phospholipase C-γ
PNS	Peripheral Nervous System
Potassium channel KCNQ4	Kv7.4
RA	rapid adapting receptor
RA-LTMRs	rapid adapting low threshold mechanoreceptors
SA	slow adapting receptor
SA-LTMRs	slow adapting low threshold mechanoreceptors
SCPs	Schwann cells precursors
SIF	Synthetic interstitial fluid
Sox2	Sex determining region Y (SRY)-box2
Sox10	sex determining region Y (SRY) box 10
STOML3	Stomatin-like protein 3
TLR4	Toll-like receptor 4
TSCs	Terminal Schwann cells
Trk	trombomyosin-receptor-kinase

4. List of Figures

5. List of Tables

6 Introduction

Awareness of internal and external stimuli is fundamental for organisms to survive. In the animal kingdom the sensory system is a conserved trait, animals rely on the sensory input to develop and refine their nervous system to perform complex motor movement and social interactions with other organisms. Since animals cannot detach from their physical world, sensing mechanical forces has ended up in the evolution of the somatosensory system.

The somatosensory system is able to discriminate from different qualities of light and noxious stimuli to create an interpretation of the physical world and generate a response to it by proprioception, touch and pain.

This work will focus on the cutaneous sensory system that underlie the sensation of touch and nociception, involving sensory receptors in the skin.

6.1 The somatosensory system

The somatosensory system is the largest sensory modality of the body. It comprises all sensory neurons located in the dorsal root ganglia (DRGs) that extend their axons to the periphery reaching specialized receptors at the skin, muscle and internal organs. All sensory neurons are pseudounipolar, one peripheral axon innervates sensory organs and conducts the action potential (AP) via the soma to a central axon, which forms the synapsis with the second order neurons in the spinal cord (Wolf & Ma, 2007).

The sensory information processed by the somatosensory system is classified into autonomic, proprioceptive and cutaneous (McGlone & Reilly, 2010). The autonomic system regulates function of internal organs and activation of the receptors of the viscera that often do not lead to conscious sensations such as cardiovascular, respiratory, digestive and renal systems (Kandel et al., 2013).

Proprioception is the sense of awareness of posture and movements of the body itself. To process information about limb position and muscle forces, animals use proprioceptors in skeletal muscle, joint capsule and skin (McGlone & Reilly, 2010; Woo et al., 2015; Assaraf et al., 2020).

This work is focused on the transduction of touch, temperature and nociception by sensory afferents innervating the skin. Traditionally, it is recognized that the terminal endings of sensory afferents are the key elements of transduction. However, the presence of nonneuronal cells in the skin, surrounding the sensory afferent and forming part of the specialized receptor morphology have led to the speculation that these cells may have a functional role in mechanical and thermal transduction.

Different kind of sensory neurons respond to external stimuli, although detecting distinct modalities such location, intensity and timing of stimulation. In order to understand their contribution, it is important to identify the underlying molecular mechanisms and connectivity to convey information to central circuits. External stimuli are transduced into a change of the membrane potential (receptor potential) which is able to initiate action potentials (APs) where the neurons activated reflects the sensitivity and the firing frequency reflects the intensity of the stimulation (Hao et al., 2015).

Information encoding depends on the cooperation of several factors as: i) the physicochemical communication of nonneuronal cells and neurons, both being potentially mechanosensitive; ii) mechanosensitive ion channels and their biophysical properties expressed in sensory neurons and nonneuronal cells; and finally, iii) the properties of voltage-gated ion channels that contritube to trigger APs.

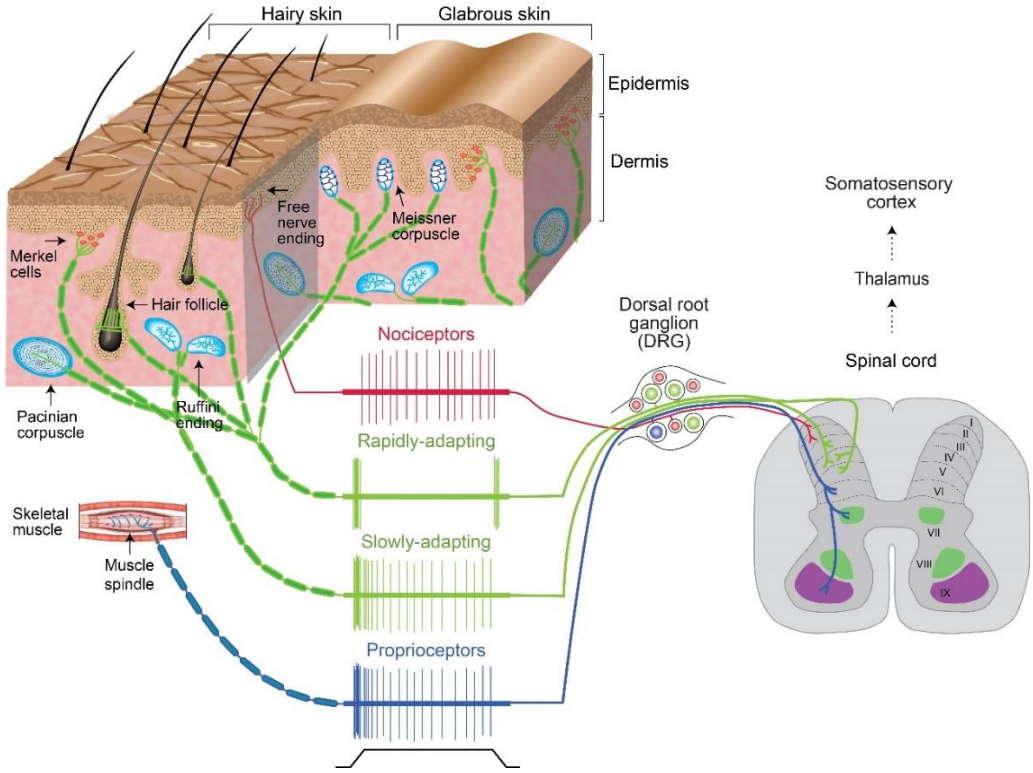

Figure 1. Cutaneous nervous system. Each DRG neuron afferent project one axon to the specialized sensory organ with in the glabrous or hairy skin and the other axon goes to the spinal cord. Usually nociceptors arrive between I-III layer of the dorsal horn, mechanoreceptors to the intermedium layers between III-IV and proprioceptors to the deeper layers as VI or connect to motoneurons in the ventral horn. In red nociceptors represented by Aδ- and C fibers are display as non- or slightly myelinated fibers that reach the upper layers of the epidermis and can respond with slowly adapting activity to mechanical stimulation. In green, mechanoreceptors represented by Aβ fibers innervate specialized receptors in the glabrous skin as well as different type of hairs in the hairy skin. Highly myelinated fibers can response to mechanical stimulation with a rapid adapting firing activity at the beginning and end of stimulation or slowly adapting

response along with the mechanical stimulation. Proprioceptors in blue innervate the muscle, not present in the skin, and display a slowly adapting response to muscle stretch. Adapted from Omerbašić et al., 2015).

6.1.2 The skin is a complex sensory organ

The skin is the largest organ innervated by specialized sensory receptors, it comprises two main layers: epidermis and dermis (Figure 1). The epidermis is where first contact with mechanical and thermal stimulation occurs. It acts as a protective barrier consisting of keratinocytes organized in the upper layer and forming a stratified squamous epithelium: basal, spinous, granular and cornified; of ectodermal origin. The dermis is a supporting layer of connective tissue of mesodermal origin, composed of loosely packed fibroblast and a collagen-rich extracellular matrix that form an upper papillary dermis and a lower reticular dermis (Jenkins & Lumpkin, 2017). Underneath the dermis, a layer of fat cells forms the hypodermis.

Most cutaneous sensory afferents are mechanosensitive and can be roughly classified in mechanoreceptors when their firing responses are generated by innocuous mechanical stimulation or nociceptors where the responses are activated by harmful stimuli. Mechanoreceptors are found in the epidermis to dermis transition forming lanceolate endings that innervate different types of hair and in the glabrous skin as Meissner corpuscles, Pacinian corpuscles, Merkel cells domes or Merkel cell-neurite complex and Ruffini endings (Figure 1); other myelinated fibers such as sympathetic efferents and motoneurons can innervate a variety of cutaneous structures as sweat glands (Fleming and Luo et al., 2013).

Nociceptors have thinly myelinated or unmyelinated axon which project through the dermis to forming a horizontal sub-epidermal neural plexus at the dermo-epidermal border. Single branches project into the keratinocytes layer in the epidermis (Johnson, 2001; McGlone & Reilly, 2010). Keratinocytes in the skin have been proposed as mechanotransducers several times due to their disposition at the first layers of the skin, able to release ATP and influence in C-fibers and Merkel cells activity (Baumbauer et al., 2015). ATP secretion and communication might be too slow to be involve in light touch and fast pain process, however glial cells are normally in direct contact with the sensory terminal ending or in between the neuron and other nonneuronal cells in the skin as in the hair shaft (Lee & Ginty, 2014; Abdo et al., 2019).

6.1.3 Sensory Neurons

Sensory neurons are a heterogeneous population of neurons with their somas in the dorsal root ganglion and trigeminal ganglia (Roudaut et al., 2012; Li et al., 2011). Sensory neurons can be

classified according to the different modalities of somatic sensation that they subserve such as touch, temperature and nociception (Figure 1).

Sensory neurons can also be classified in several ways according to their morphology like soma size and level of myelinization, where normally large-soma and thickly myelinated neurons correspond to mechanoreceptors and small-soma and thinly or nonmyelinated axons are nociceptors. They can also be classified as their electrophysiological properties, such as conduction velocity, threshold and AP shape. Thus, mechanoreceptors have fast conduction velocities (>10m/s), low threshold and narrow AP; and nociceptors usually display slow conduction velocities (1m/s to 5m/s), high thresholds and humped AP shape during repolarization. Finally, in response to mechanical stimulation mechanoreceptors respond with different rates of adaptation to sustained mechanical stimulations as rapidly adapting (RA) and slowly adapting (SA), while nociceptors only display slowly adapting responses (Figure 1) (Smith & Lewin, 2009; Li et al., 2011).

The molecular diversity of sensory neurons is also reflected by their phenotypic heterogeneity. For instance, mechanoreceptors for light touch and nociceptors for potentially noxious stimuli express a myriad of cell adhesion proteins, receptors and ion channels allowing them to respond to mechanical stimuli showing mechanically activated currents (McCarter et al., 1999; Cho et al., 2002; Hu & Lewin, 2006). The protein complex where mechanosensitive (MS) ion channels are immersed along with scaffold proteins that connect the extracellular matrix and cytoskeleton, and their interaction with nonneuronal cells allows sensory neurons expressing similar MS ion channels generate unique receptor responses ((Delmas & Coste, 2013; Bragriantsev et al., 2014).

6.1.4 Peripheral glia cells

Peripheral glial cells derive from the neural crest and can be divided into three categories: satellite cells of the sensory and autonomic ganglia; myelinating and nonmyelinating Schwann cells; and enteric glia (Figure 2) (Douarin et al., 1991). These three glial types have varying functions according to their location such as myelination, neuronal support, regulation of synaptic connectivity and even sensory functions (Bunge, 1993; Kastriti & Adameyko, 2017).

Schwann cells wrap axonal processes to protect and ensure AP conduction in two ways: ensheathing groups of small-diameter axons in a structure called the Remak bundle; or forming myelinating cells that surround large-diameter axons with a multilamellar sheath (Figure 2) (Jessen & Mirsky, 2005). Myelinating Schwann cells form a glial sheath that covers most of the surface of the neuronal cells and axon membrane is not in direct contact with the connective tissue. Although, forming interdigitation with the membrane of the glial cells which interacts with

the microenvironment of the neurons and reflecting the complex interaction between both cell types (Woodhoo & Sommer, 2008; Lee & Ginty 2014). In the Remak bundle, nonmyelinating Schwann cells are arranged along the small-diameter axons surface acompanied by a process denominated differentiation brake. Immature and nonmyelinating Schwann cells are similar in morphology and antigenic markers (Jessen & Mirsky, 2015).

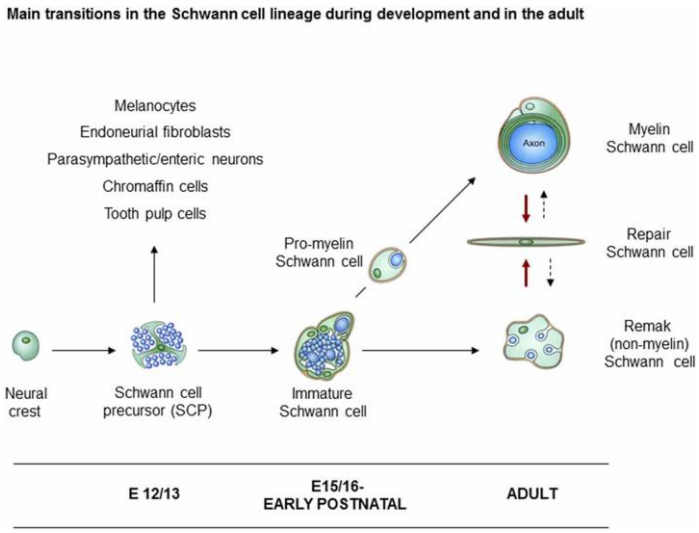

Figure 2. Different types of Schwann cells. Schwann cells precursors (SCP) can form several types of Schwann cells involve in development and nerve repair. Immature Schwann cells can be reversibly induced to form myelin and non-myelin Schwann cells of adult nerves as well as can be part of sensory receptors as in Meissner corpuscles, sensory glia-neuron complex and terminal Schwann cells in hair follicles. Figure taken from Jessen & Mirsky, 2015.

Schwann cell generation includes two main processes: gliogenesis, whereas neural crest cells form Schwan cells precursors (SCPs), a process highly depending on axon-associated survival signaling mostly by neuregulin 1 (NRG1); and maturation, where immature Schwann cells acquire their final fate by secreting autocrine survival signals (Figure 2). SCPs migrate along growing axons and actively divide during peripheral nerve formation (Jessen et al., 2015).

SCPs found in the outer margin of the axonal nerves and in between them start to envelop large numbers of axons forming axon-Schwann cells bundles and become immature Schwann cells (Woodhoo & Sommer, 2008; Jessen et al., 2015). Some of them start a process called radial sorting, consisting of individual Schwann cell surrounding single large-diameter axon where several neurotrophic factors participate such as neuregulin 1 (NRG1), Insulin-like growth factors (IGFs), neurotrophin-3 (NT3) and brain-derived neurotrophin factor (BDNF). Then, the number of Schwann cells start to decrease because some of the glial cells lose contact with the axons and undergoes apoptosis. One of the most prominent death signals is promoted by the p75

neurotrophin receptor ($p75^{NTR}$) which is required to enhance Schwann cell death in development and after nerve injury (Jessen & Mirsky, 2019).

SCPs not only will give rise to immature Schwann cells, but also provide trophic factors to sensory and motor neurons and form nerve fasciculation in late embryonic states as E18.5 (Riethmacher et al., 1997). It is only at postnatal stages where immature Schwann cells will become myelinating or non-myelinating mature Schwann cells (Figure 2) (Bunge Jessen & Mirsky, 2005). To avoid nonmyelinating Schwann cells to become myelinating Schwann cells, the c-Jun-amino (N)-terminal kinase (JNK) pathway activates and elevates transcription factors as paired box gene 3 (PAX3), necessary for proliferation, survival, differentiation and motility; and the Sex determining region Y (SRY)-box2 or Sox2, involve in stem cell pluripotency maintenance and cell fate determination and myelination inhibition (Woodhoo & Sommer, 2008; Kioke et al., 2014 Feng & Wen, 2015).

Several Schwann cell markers have been identified according to the developmental stage of peripheral glial cells and they can be divided in 1) developmental stages, the SRY-box 10 (or Sox10) and cadherin 19 (Cad19); 2) as soon as SCPs are generated some proteins are expressed, some of these proteins are also present in immature Schwann cells like brain fatty acid-binding protein (BFABP); and finally, 3) markers expressed after immature Schwann cells develop as GFAP and S100 (Jessen & Mirsky, 2005).

The transcription factor Sox10 is essential for glial fate, it regulates the ability to respond to NRG1, which is necessary for neural crest cells migration and serves as an axon-derived factor for mitotic SCPs (Jessen & Mirsky, 2005). However, Sox10 is also present in all migrating neural crest cells as satellite glial cells in DRG neurons and SCPs in spinal nerves, although later in development it is downregulated in neurons and most of Schwann cells except for specialized Schwann cells present in Meissner corpuscle, called lamellar cells, and nociceptive glia-neuron complexes (Abdo et al., 2019). Schwann cells that retain Sox10 or Sox2 expression form part of the specialized sensory receptors in the skin and are known as sensory Schwann cells or nociceptive Schwann cells (Abdo et al., 2019). Although it is still not clear what the function of specialized sensory Schwann cells in the adult is, recent evidence indicates that nonneuronal cells such as, Merkel cells, keratinocytes, and Schwann cells can influence transduction of touch, temperature and pain (Abdo et al., 2019; Nikolaev et al., 2020; Baumbauer et al., 2015).

Interestingly, Schwann cells are very plastic and already mature cells can revert to SCPs after nerve injury and again start to proliferate like neural crest-derived cells, fibroblast and endothelial cells of mesodermal origin, which related to their ability to express transcription factors as Sox10 and Sox2 even in adult stages. (Douarin et al., 1991).

After peripheral nerve injury, Schwann cells can regenerate and surround proximal and distal axonal stumps after section. Specifically, after distal or Wallerian degeneration, myelin and Remak cells go through dedifferentiation to participate in processes such as regeneration and repair (Figure 2) (Jessen & Mirsky, 2019).

6.1.5 Projections to the spinal cord and cortex

Sensory afferents project one axon to the spinal cord in the dorsoventral axis providing the first level of anatomical and functional framework of sensory and motoneurons (Caspary & Anderson, 2003). Rostro-caudal and mediolateral topography forms a somatotopic map on the spinal cord (Wolf & Ma, 2007), where DRG neurons come to their final location according to their initial position in the neural tube and their time of birth (Caspary & Anderson, 2003).

In general, five parallel layers (or laminae) form the spinal cord dorsal horn and receive most of the projection inputs from the DRG neurons and their positions are sorted out according to their sensory modality. Touch, mediated by mechanoreceptors, normally carried by Aβ-fibers goes to internal dorsal laminae III-V of the spinal cord (Figure 1); while nociceptive information carried by Aδ-fibers project to layers III, and nociceptive C-fibers project to superficial laminae I-II (Figure 1) (Li et al., 2011; Lechner & Lewin, 2013).

Sensory afferents, with different physiological properties reach overlapping areas of the spinal cord and according to their interaction with specific interneurons indicate that spatiotemporal patterns of APs.

In the next section each kind of cutaneous receptor will be described with their own properties and how they contribute to the full cutaneous sensitivity.

6.2 Specialized receptors in the skin

6.2.1 Mechanoreceptors

Mechanoreceptors that sense skin deformation, brush, motion, stretch and vibration are responsible for the sense of touch (Roudaut et al., 2012). Innervated by Aβ-fibers with medium and large diameter somas and thickly or thinly myelinated axons, fast conduction velocity and a low-threshold to mechanical stimulation are known as low-threshold mechanoreceptors (LTMRs) (Lewin & Moshourab, 2004). According to their response to mechanical stimulation sensory afferents innervating mechanoreceptors can also be more specifically classified as rapid adapting (RA-LTMRs) firing action potentials at the beginning and end of ramp and hold mechanical

stimulation, examples are Meissner corpuscle, Pacinian corpuscle and hair follicle afferents (Figure 3). Slow-adapting (SA-LTMRs) corresponds to mechanoreceptors that continue firing to sustained mechanical stimulation such as Merkel-neurite complex and Ruffini endings (Figure 3) (Lewin & Moshourab, 2004; Roudaut et al., 2012).

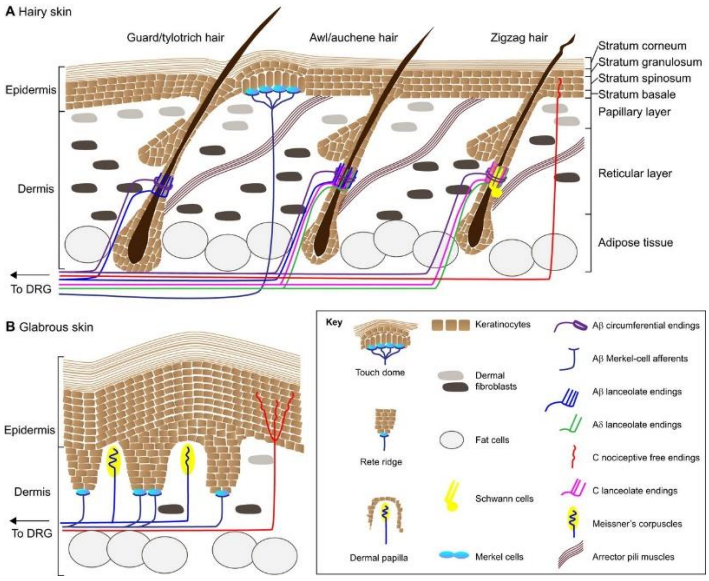

Figure 3. Cutaneous receptors in hairy and glabrous skin in mouse. (A) Hairy skin in the mouse is composed by three types of hair. Guard/tylotrich hairs are the longer but less abundant. Awl/auchene hairs and zigzag hairs form most of the mouse fur coat. Lanceolate and circumferential endings wrap around after the bulge of the hair. All lanceolate endings intercalate with terminal Schwann cells protrusions. Besides hair innervation, Aβ fibers reach touch domes formed by Merkel cells in the epidermis in adjacent to guard hairs. (B) Glabrous skin includes invaginations of the epidermis called rete ridges where Merkel neurite complex are found, and dermal zones in between are called dermal papillae where Meissner's corpuscle are founded. Figure taken from Jenkins & Lumpkin, 2017.

6.2.2 The Meissner corpuscle

The Meissner corpuscles are fine touch receptors sensitive to low-medium vibration frequencies. Also known as Wagner-Meissner corpuscle or tactile corpuscle, found mostly at digits, palmar and sole skin as well as lips, palate, tongue and genitalia (Johnson, 2001). Localized underneath the epidermis in the dermal papillae of the glabrous skin, formed by one to three encapsulated Aβ-fiber nerve endings forming ellipsoid structures (Figure 3) (Johnson, 2001; Walcher et al., 2018; Piccini et al., 2021). They have rapidly adapting (RAI) responses to light indentation, dynamic deformation and vibration to low frequency motion transduction in the range of 1-300Hz, and in cats are best tuned to 50 Hz (Piccini et al 2021). The receptive field of Meissner corpuscle afferents are relatively small compared to other mechanoreceptors such as Merkel cell-neurite

complex or D-hairs. After activation, their response is normally uniform along the receptor field which indicates good spatial discrimination (Árnadóttir & Chalfie, 2010; Piccini et al., 2021).
Recently, it was proposed that there are two types of Aβ-fiber innervating the Meissner corpuscles in the mouse skin according to the neurotrophic receptor that they express. Some express TrkB and depend on BDNF signaling; the rest of Meissner corpuscles express c-Ret, another neurotrophic receptor (Neubarth et al., 2020). An additional innervation by peptidergic and non-peptidergic unmyelinated C fibers has been described in Monkeys and rats (Figure 4) (Idé, 1976; Paré et al., 2001). Supported by the plethora of sensory ion channels like ASIC2, ASIC3 and Piezo2 expressed in the terminal endings of the Meissner corpuscle which could correspond to different kind of sensory afferents like Aβ- and C-fibers (Chen & Wong, 2013; Omerbašić et al., 2015; Ranade et al., 2015).
The capsule of the Meissner corpuscle is derived from endoneurial-perineural fibroblastic connective tissue, an interlamellar matrix composed by collagen and microfilaments. The apex of the corpuscle is abundant in fibroblast and extracellular matrix, while at the base the capsule attaches the receptor to the basal epidermis (Paré et al., 2001). The Schwann cells within the capsule are flattened and elongated with a disk-like lamellar shape (Figure 4), stacked one after each other with the unmyelinated sensory afferent in between ascending through the corpuscle with a spiral shape (Fleming & Luo, 2013). Lamellar cells in Meissner corpuscle and Pacinian corpuscle are specialized Schwann cells that develop after birth and acquire similar morphology and organization in relation with the Aβ-fiber that innervates the corpuscle (Idé, 1977; Zelená, 1978; Nikolaev et al., 2020). The highly myelinated Aβ-fiber loses its myelin sheath at the corpuscle, supporting the idea of a direct communication between Lamellar cells and the sensory afferent in mechanotransduction (Nikolaev et al., 2020).

6.2.3 The Pacinian corpuscle

Pacinian corpuscles are innervated by Aβ-fibers encapsulated in an “onion shaped” end organ composed of modified Schwann cells called Lamellar cells (Figure 1), which may work as high-pass filters (Johnson, 2001). Pacinian afferents are classified as rapidly adapting (RAII) mechanoreceptors. Pacinian corpuscles have large receptive fields and are sensitive to very high frequency vibration tuned to 150-300Hz and are able to detect distant events transmitted due vibration (Hao et al., 2015). However, there is almost no Pacinian corpuscle in the mouse skin (Lewin & Moshourab, 2004), most of them are found very close to the bones (Schwaller et al., 2020).

The development of Pacinian corpuscles is not well understood but, it is known at least in rats, that the corpuscle formation starts with accumulation of inner core cells which are most probably Schwann cells that can aggregate in the outer capsule layer during embryonic development. By the time of birth, Schwann cells are already specialized in Lamellar cells (Zelená, 1978).

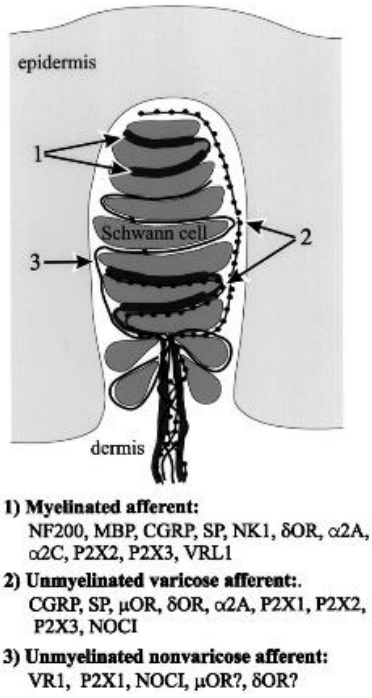

Figure 4. Meissner corpuscle structure and innervation from glabrous Monkey skin. Meissner corpuscle are mainly innervated by (1) myelinated Aβ-fibers, (2) Unmyelinated CGRP-positive C-fibers and (3) unmyelinated TRPV1 positive nonpeptidergic C-fibers. The Schwann cells are distributed between the innervation at the base and apex of each Meissner corpuscle. Figure taken from Paré et al., 2001.

For a long time, modulating and filtering properties of Lamellar cells has been their suggested function within the Pacinian and Meissner corpuscles. It has also been suggested that neurotransmitters like GABA regulate axonal excitation during the static phase of mechanical stimulation released of Lamellar cells from Meissner and Pacinian corpuscles (Hao et al., 2015). Eastwood and collaborators (2015) proposed a model for ON/OFF responses in mechanoreceptors in *C. elegans*, which is compatible with rapidly adapting mechanoreceptors response from vertebrates as Meissner and Pacinian corpuscles. Showing that the dynamic response depends on common physical mechanism, where single or multiple elastic filaments tethered directly mechanosensitive ion channels or occludes the ion permeation pathway, such filaments could be anchored to the ECM or cytoskeleton. Extracellular filaments coming from

membrane of large-size DRG neurons have been shown to be essential for evoking mechanosensitive RA currents, a characteristic current type for mechanoreceptors (Hu et al., 2010). Moreover, recently the Usher2A protein has been found expressed in Meissner corpuscle Lamellar cells and is necessary to tune mouse vibrotactile responses (Schwaller et al.,2020). Additionally, Lamellar cells have been proposed as nonneuronal mechanosensitive cells expressing R-type Ca^{2+} channels with role in mechanotransduction in Pacinian and Meissner corpuscle (Nikolaev et al., 2020), corroborating their active role in mechanotransduction.

6.2.4 Merkel-neurite complex and touch dome

Merkel cells are sensory receptors cells that form synapse-like contacts with a single sensory afferent known as Merkel cell- neurite complex and touch domes specialized for discriminative touch (Figure3) (Maricich et al., 2009; Maksmovic et al., 2014). Merkel cell are epidermal-derived cells clustered in close apposition to an enlarged nerve terminal from a Aβ fiber in the finger pads, whisker follicles and Guard hairs. Merkel cell afferents express TrkC, which is the receptor for NT-3 (Morrison et al., 2009).

In the hairy skin, Merkel cells form a touch dome which involves around 150 Merkel cells innervated by a single Aβ-fiber. On the glabrous skin, Merkel cells from a Merkel cell-neurite complex with an Aβ-fiber that can contain from 4-40 Merkel cells (Maricich et al., 2009; Maksmovic et al., 2014).

The slowly adapting Aβ-LTMRs (SAI) of the Merkel cell complex and touch domes transmit a precise spatial image of the tactile stimuli, shape and texture and to some extent vibrotactile information in a frequency range of 1-100Hz and are tuned to low frequencies around 5Hz (Roudaut et al., 2012; Jenkins & Lumpkin, 2017).

Merkel cells are mechanosensitive neuron-like cells and display mechanosensitive currents which make them indispensable for proper encoding of SA Aβ-LTMRs responses (Maricich et al., 2009; Maksmovic et al., 2014) due to expression of the MS ion channel Piezo2 (Woo et al., 2014; Ikeda et al., 2014).

Merkel cells can be identified in the skin by the expression of the neuronal transcription factor *Atoh1*, serving as molecular marker for these epidermal cells in the skin. Downstream activation of *Atoh1*, the transcription factor Sox2 is required to maintain *Atoh1* expression, working together to initiate and maintain Merkel cell fate (Maksmovic et al., 2014; Jenkins & Lumpkin, 2017). Thus, Sox2 is also a Merkel cell marker (Abdo et al., 2019).

6.2.5 Ruffini endings

Ruffini endings are encapsulated sensory endings innervated by one to three Aβ-fiber, with an elongated cylindrical shape lying in the collagen strands on the deep epidermis (Figure 1). Ruffini receptors contribute to direction of an object motion sensation and stretch, firing with regular slow adapting (SAII) to mechanical stimulation (Johnson, 2001). Their sensitivity to stretch and localization suggest that they have are sensitive to horizontal tensile strain.

Ruffini endings are present in human glabrous skin, where the expression of TrkB receptor indicates that their development requires BDNF (Fleming and Luo., 2013). However, Ruffini endings have never been found in mice or monkey skin (Lewin & Moshourab, 2004).

6.2.6 Hair follicles: Guard, Awl/auchene and zigzag hairs cover the mouse coat

Hair has an important sensory function in mammals, provides information about their own space and position in the surrounding environment. In addition to regulate body temperature, facilitate perspiration and social behavior (Lechner & Lewin, 2013).

The hair follicles have specialized receptors able to detect light touch. There are three kinds of hairs in most of the mammals: guard hairs or monotrich, awl/auchene and zigzag hairs (Figure 3) (Li et al., 2011). Sensory fibers associated with hair follicles respond to indentation, stretch, vibration, hair motion and harmful stimuli with different rates of adaptation to sustained mechanical stimulation. The afferent endings are arranged as lanceolate endings in parallel to the hair shaft or as circumferential endings, and their innervation distribution give them particular sensorial properties. (Lechner & Lewin, 2013; Jenkins & Lumpkin, 2017).

In the mouse, the most abundant kind of hair is zigzag covering around 76% of the skin, then awl/auchene with 23% and finally guard hairs making up only 1% of the total hairs (Figure 3) (Li et al, 2011; Lechner & Lewin, 2013; Jenkins & Lumpkin, 2017).

Guard hairs are innervated by RA and SA Aβ-LTMRs, around 20% and 80% respectively, detecting movement and tuned to a specific range of frequencies between 5 and 50Hz, slightly overlapping with Meissner corpuscle and Merkel cell-neurite complex responses (Li et al., 2011; Owens & Lumpkin 2014). Awl/auchene and Zigzag hairs are found mostly in the trunk of the hairy skin, innervated by Aβ-, Aδ- and C-fibers, and Aδ- and C-fibers, respectively. With a lower proportion of Aβ-fibers (around 20%) compared to Aδ- and C-fibers (around 80%) in both type of hair (Li e et al., 2011; Abraira & Ginty, 2013). C-LTMRs are special kind of sensory afferents that innervate the hair follicles, also form longitudinal lanceolate endings and show an intermediate adaptation between RA- and SA-LTMRs of mechanoreceptors with a putative a role in pain

inhibition (Li et al., 2011; Roudaut et al., 2012). C-LTMRs have been proposed to be involve in gentle touch and social touch behavior.

All sensory fibers forming a lanceolate sensory ending arranged in parallel to the hair long axis along with finger-shaped terminal Schwann cells (TSCs) processes that extend to the skin surface in increasing number respectively to the type of hair zigzag, awl/auchene and guard hairs. Forming intercellular junctions between the axon terminal and the hair follicle outer root sheath of cells (Figure 5) (Li & Ginty, 2014). Their location and morphology suggest these cells could have a function in mechanotransduction to the sensory afferent to detect hair movements. Moreover, each kind of hair seems to have a different organization of Schwann cells and density (Figure 5). C-LTMRs and Aδ- LTMRs intercalate glial cells and sensory afferent lanceolate digits with process coming from the same glial cells; while Aβ-LTMRs has an individual Schwann cells in between the terminal ending and the hair (Li & Ginty, 2014).

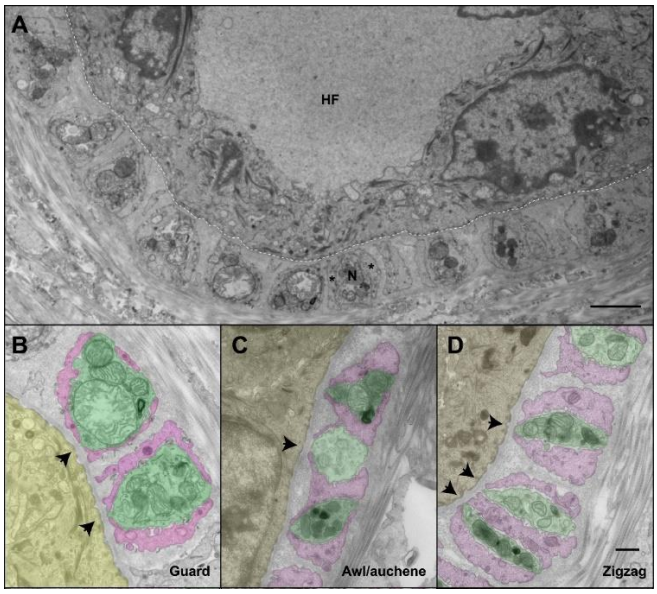

Figure 5. The ultrastructural relationship between LTMRs, TSCs and hair follicle epithelial cells at the three hair follicle subtypes. (A) A transmission microscopic image of a cross section through a lanceolate complex at a guard hair follicle. Repeating units of axon terminal and TSC processes are regularly arranged in a single layer surrounding the hair follicle (HF). (B) A cross section of the same guard hair shown in A. Axon terminals are pseudo-colored in green; TSC processes are pink, the hair follicle epithelial cell is in yellow. Each unit is composed of one axonal terminal encased by two or three TSC processes. (C) A cross section of a lanceolate complex of an awl/auchene hair follicle. Each axon terminal is encased by two TCS processes on two sides which can be in contact with an adjacent axon terminal forming a complex unit. (D) A cross section of a lanceolate complex associated with a zigzag hair follicle; each axon is also encased by two TSC processes on two sides. Figure taken and modified from Li & Ginty, 2014.

6.3 Nociceptors

Nociception is the ability to detect potential or actual harmful stimuli; while pain is the perception of nociceptive stimuli companied by an emotional response. Nociceptors appear very early in animal evolution, flatworms with a rudimentary nervous system already show escape responses to pinprick noxious stimulation (Smith & Lewin, 2009; Sneddon, 2018; Dudin & Patapoutian, 2010) their morphology is highly conserved in mammals like mice and humans. Nociceptors and thermal receptors are formed by medium and small diameter DRG neurons with thinly but mostly nonmyelinated axons.

For a long time, nociceptors have been considered as “free endings” in the epidermis (Figure 3) that, if myelinated, lose it at the terminal ending and accompanied by Schwann cells in the epidermis for structural stability and support functions (Smith & Lewin, 2009). It has also been suggested that there is direct communication between nonneuronal cells in the skin and the “free nerve endings” of sensory afferents (Smith & Lewin, 2009; Li & Ginty, 2014; Sneddon, 2018). The recent work from Abdo and collaborators (2019) has shown that Schwann cells closely associated with free nerve endings are mechanosensitive and may communicate directly with sensory nerves to transmit mechanical noxious stimuli.

6.3.1 Sensory glia-neuron complex

Schwann cells are recognized as myelinating and nonmyelinating cells that surround nerves in the peripheral ends working as supporting cells and produce recovering sheath that can support saltatory conductivity of action potentials. However, there are other kinds of Schwann cells in the skin that can form part of specialized mechanoreceptors, called Lamellar cells that form part of Meissner corpuscles, Pacinian corpuscles, Ruffini endings, Krause end bulbs and the most recently described nociceptive glia-neurite complex (Kastriti & Adameyko, 2017; Abdo et al., 2019).

The recently described nociceptive glia-neurite complex consists of epidermal Schwann cell forming a mesh-like network in a close functional connection with the traditionally considered free endings of nociceptive sensory neurons (Figure 6). Nociceptive Schwann cells not only work as a relay station between the noxious stimuli and the terminal ending, but they are also intrinsically mechanosensitive, and able to transmit nociceptive information (Abdo et al., 2019).

Sox10 is a neural crest specific transcription factor for migration, specification and later maturation of all types of cells coming from the neural tube to form the Peripheral Nervous System (PNS). However, Sox10 is downregulated during neurogenesis (Kastriti & Adameyko, 2017).

Nociceptive Schwann cells were found using is Sox10 as a glial-specific marker, as Sox10 expression persists after birth. To determinate if activation of nociceptive Schwann cells could evoke nocifensive responses in mice, Sox10 reporter mouse was crossed to Channelrhodopsin-2 (ChR2), allowing the activation of Schwann cell optogenetically. Nocifensive behaviors responses such as paw lifting, and licking were observed during blue light activation of nociceptive Schwann cells. Using the same strategy but crossing the Sox10 reporter line with Archaerhodopsin in nociceptive Schwann cells, a proton pump that activates with yellow light and induce hyperpolarization in the expressing cell, nocifensive behavior was reduced to noxious mechanical stimulation (Abdo et al., 2019).

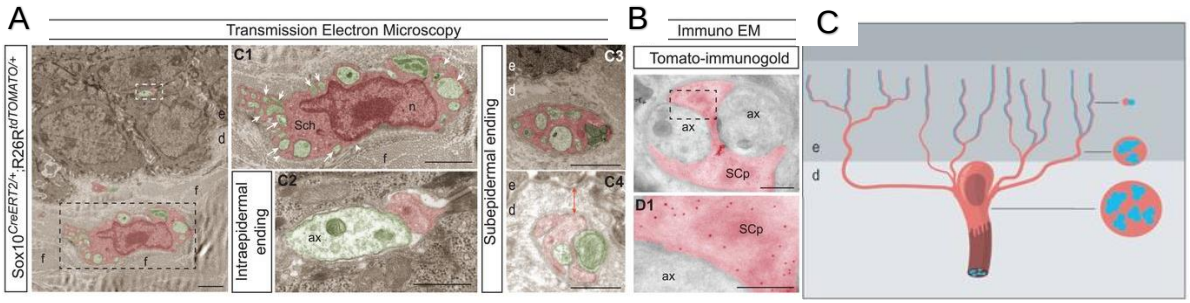

Figure 6. Cutaneous Schwann cells form a glio-neural end organ. Using the glial-specific Cre line Sox10-CreERT2 coupled to the Rosa26-enhanced YFP reporter line, recombination in Schwann cells dilucidated their close association to nociceptive sensory neurons. (A and B) Transmission electron microscopy of the glio-neural complex. Images are pseudocolored with axons in green and Schwann cells and processes in red. (B) Immuno-electron microscopy wit anti-dsRed antibody showing specific expression of TOMATO in Schwann cell process and not at the axons. (C) Schematic illustration of a Schwann cell with full processes arriving to the epidermis and surrounding nociceptive fibers that were considered free endings. Figure taken and modified from Abdo, et al., 2019.

Nociceptive sensory afferents are a complex group of Aδ- and C-fibers, with distinct morphology and tuned to specific stimuli, but have overlapping range of modality and similar responses to noxious stimuli.

6.3.2 Aδ-fiber mechanonociceptors respond to pinprick

Aδ-fiber mechanonociceptors (AMs), also known as A-fiber nociceptors, have thinly myelinated axons and convey fast pain responses such as pin prick, and control withdrawal reflexes. Their somas are medium-size and conduction velocity varies between more than 1m/s and less than 10 m/s (Lewin & Moshourab, 2004; Dubin & Patapoutian, 2010). AMs are activated by high intensity static indentation and display a slowly adapting response, what placed them as slowly-adapting high threshold mechanoreceptors (SA-HTMRs). A subpopulation, around 20%,

responded to heat or cold stimulation in hairy skin (Smith & Lewin, 2009). In the skin, AMs sensory afferent lose their myelin before arriving to the epidermis when they are associated with Schwann cells or keratinocytes (Light & Perl, 1979; Lewin & Moshourab, 2004; Abdo et al., 2019).

6.3.3 C-fibers: C- Mechanonociceptors, C-Polymodal and C-Thermoreceptors

C-fibers correspond to 60-70% of the afferents that innervate the skin. They have unmyelinated fibers, packed into individual Remak bundles ensheathed by nonmyelinating Schwann cells, very slow conduction velocities (<1m/s), and display slow adapting response to static mechanical stimulation (Smith & Lewin, 2009).

C-fiber nociceptors are subclassified according to their modality response to noxious stimuli. C-mechanonociceptors (C-M) respond to noxious mechanical stimulation only, part of these C-fibers respond to mechanical and thermal stimulation called C-fiber polymodal receptors. C-fibers polymodal can be classified as C-mechanoheat (C-MH), C-mechanocold (C-MC), a few of these C-fibers are able to respond to heat and cold (C-MHC) (Lewin & Moshourab, 2004).

C-thermoreceptors detect change in temperature such as warm and cooling, as well as noxious heat and cold. Thermosensitive C-fibers activated by temperatures lower than10°C and higher than 40°C, are considered thermal nociceptors. Because C-thermoreceptors and C-thermonociceptors can have overlapping responses to mild and noxious thermal stimuli, they are grouped together in the same classification as C-heat (C-H), C-cold (C-C) and C-heatcold (C-CH) (Lewin & Moshourab, 2004; Smith & Lewin, 2009).

Other C-fibers found in the skin correspond to tactile C-fibers respond to gentle touch and cold (described in the hair follicle section). Additionally, silent nociceptors comprise around 10-25% of C-fibers in the skin, do not respond under physiological conditions, but after applying irritant to the skin such as mustard oil or capsaicin, silent C-fibers are sensitizing and respond displaying tonical response to further mechanical or thermal stimulation (Kress et al., 1992; Lewin & Moshourab, 2004; Smith & Lewin. 2009). Sensitization can be achieved by inflammatory agents or even by repeated stimulation (Kress et al., 1992). It does not only activate silent C-fibers, also decreases threshold and enhance responsive C-fibers, modulating the expression or membrane accumulation of receptors and ion channels.

Nociceptor function is very plastic which is a key property for peripheral sensitization, setting lower thresholds and increased receptor potential response (Lechner & Lewin, 2013) could will lead to major signal integration that enhance firing activity of secondary dorsal horn neurons and pain-generated responses (Kress et al., 1991; Wolf & Ma, 2007).

Although it is yet not clear which are all the processes involve in peripheral sensitization. The same growth factors such as neurotrophins and their receptors (Trk receptors and $p75^{NTR}$) involved in sensory neurons development, have a crucial role during peripheral sensitization changing membrane protein expression and even sensitivity of thermo- and mechanosensitive ion channels. In the next section, grow factors are described according to the sensory neuron target that they act on during development and potentially under nerve injury in adult organisms.

6.4 Growth factors receptors and their function in sensory neurons

Somatosensory neuros arise from dorsal lamina of neural crest cells (NCCs) that migrate ventrally to the periphery into the ventromedial line to form clusters on each side of the neural tube that will become DRGs in the intervertebral space (Jenkins & Lumpkin, 2017). During migration and agglomeration to form the ganglion, neurons are exposed to spatiotemporal cues from adjacent somites and spinal cord to induce cell fate. For example, the expression the transcription factor Sox10 to maintain multipotency and high rate of proliferation (Marmigère & Ernfors, 2007). As shown in figure 7, somatosensory neurons start to diversify by expressing one of the members of the RUNX family that work as organizer of transcription factors and later on axonal growth and appropriate targeting of the central axon in the spinal cord lamina. RUNX1 is normally found in small neurons that will become nociceptors while and RUNX3 in large diameter neurons of mechanoreceptors and proprioceptors (Marmigère & Ernfors, 2007).

DRG neurons express at least one member of the family of the trombomyosin-receptor-kinase (Trk). Nociceptors express TrkA, the nerve growth factor (NGF) receptor; mechanoreceptors express TrkC, the neurotrophin-3 (NT-3) receptor; or brain-derived neurotrophic factor (BDNF) receptor TrkB (Marmigère & Ernfors, 2007; Lechner et al., 2009; Usoskin et al., 2015). TrkA and TrkB bind and be activated by NT-3 and NT-4/5 respectively. The Trk receptors are transmembrane proteins, their extracellular domain is distinguished by their IgG-C2 repeats in their extracellular domain, cysteine rich regions flanking a leucine-rich repeat; and their main function is increase phosphorylation in phospholipase C-γ (PLC- γ) and phosphatidylinositol 3'-kinase (PI3-K) (Roux & Barker, 2002). Sensory afferents require neurotrophin signaling not only to develop their identity in the ganglion, but also to reach the skin where they form specialized receptor endings along with the nonneuronal cells surrounding them. Mechanoreceptors and proprioceptors expressing $TrkC^{+}$ and $TrkB^{+}$ are the first born (around E13) and display mechanically activated currents. In a second wave nociceptors expressing TrkA (at first) are

develop and mechanosensitivity acquisition in nociceptors is observed in two waves: one starts at E15.5, the second dramatically after birth between P0-P1 (Lechner et al., 2009).

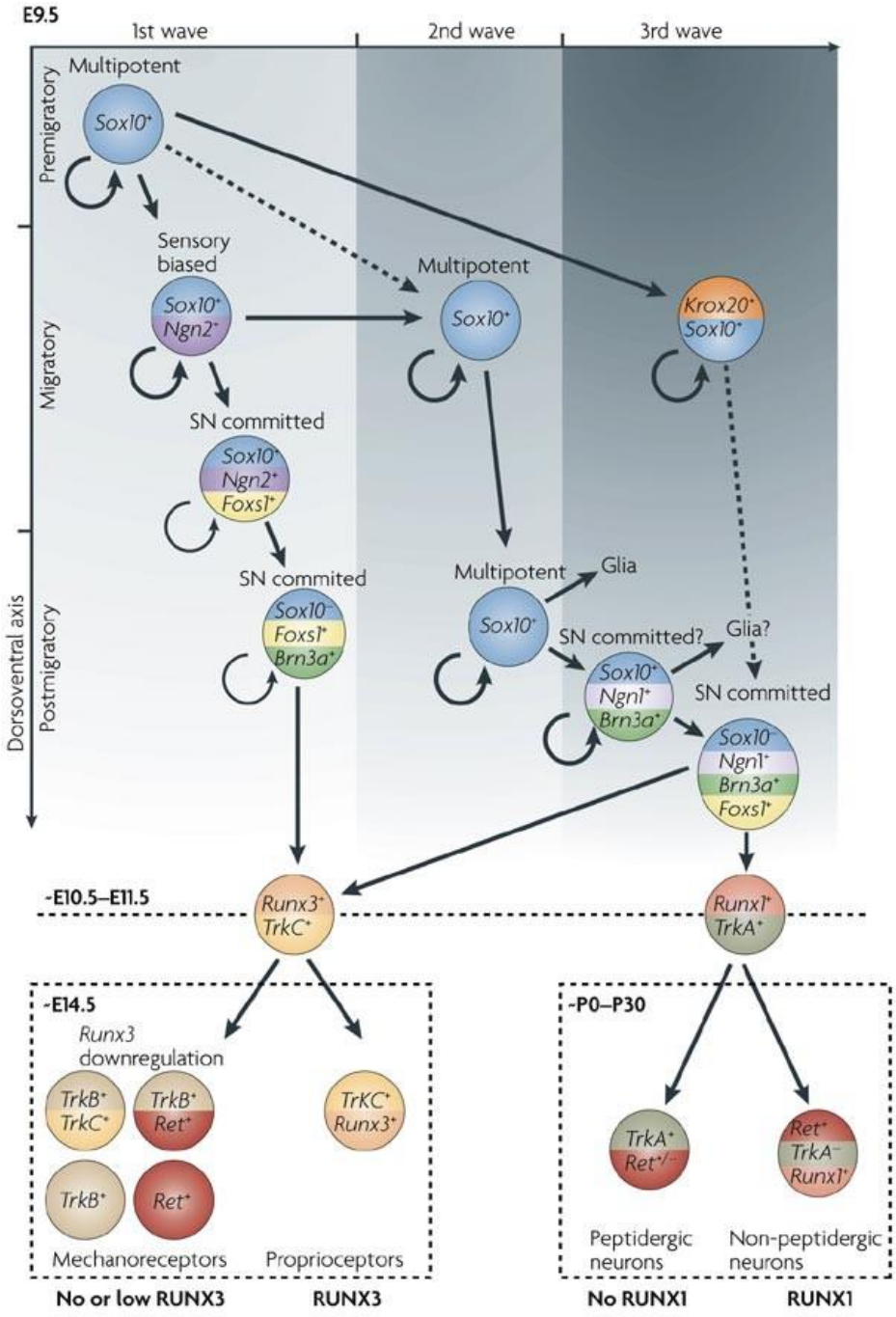

Figure 7. Distinct genetic cascades control the first two waves of neurogenesis in the dorsal root ganglion (DRG). The vertical axis represents the dorsoventral position and migratory status of the cells during development. In the first wave, SRY (sex determining region Y) box 10-containing ($SOX10^+$) cells migrate and express neurogenin 2(Ngn2), which biases them towards a sensory fate. Cells with high levels of NGN2 subsequently commit to a sensory neuronal fate (SN). Postmigratory pioneering neurons of the first wave express Brn3a and form large proprioceptive

and mechanoreceptive neurons expressing runt-related transcription factor 3 (Runx3) and neurotrophic tyrosine receptor kinase C (TrkC) at early developmental stages. In the second wave of neurogenesis, cells are characterized by the continuous expression of Sox10 throughout migration and in the DRG, where they continue to divide at a high rate. These cells start to express Foxs1, Brn3a and Ngn1 in the DRG, before they express RUNX factors. They might produce both the $TrkA^+$ and $TrkC^+$ populations of neurons by expressing Runx1 or Runx3, respectively. The third wave of neurogenesis arises from boundary cap cells expressing Sox10 and Krox20; they contribute mainly to the RUNX1/TrkA population of neurons and to glia. Cells from the first wave that maintain Runx3 expression keep TrkC and become proprioceptors, whereas cells that lose or reduce Runx3 expression make TrkB and TrkC, TrkB alone, RET alone or RET and TrkB mechanoreceptive neurons. Among small neurons, maintained Runx1 expression drives a $TrkA^-$ non-peptidergic phenotype ($TrkA^-/Ret^+/Runx1^+$ cells), whereas downregulation of Runx1 allows the cells to acquire a peptidergic phenotype ($TrkA^+/Ret^{+/-}/Runx1^-$). Figure reprint from Marmigère & Ernfors, 2007.

6.5 Mechanosensitive ion channels in DRG neurons

Mechanotransduction is the conversion of mechanical stimuli into a biological response and mechanosensitivity is the ability to detect mechanical stimuli. Mechanotransduction is a ubiquitous process among all living organisms from the earliest eubacteria to the latest eukarya domains in evolution (Delmas et al., 2011). At the cellular level, it is important for migration, proliferation and differentiation which activates ion channels, transmembrane proteins and receptors that transduce mechanical signals into intracellular signaling cascades (Murthy et al., 2017). On the other hand, mechanosensory neurons rely on mechanosensitive ion channels and auxiliary subunits to set their biophysical properties and response to external mechanical stimuli. MS ion channels are characterized for fast response, high sensitivity and dynamic range of mechanosensory signaling, and yet, the diversity of all the MS ion channels expressed by sensory neurons and how intrinsic neuronal mechanisms differ between them to produce unique response to the same stimuli or differentiate mechanical stimulation is poorly understood (Delmas & Coste, 2013; Walsh et al., 2014).

There are 3 types of mechanically activated currents identified in sensory neurons (Figure 8) with similar biophysical characteristics such as fast activation and amplitude (Hu & Lewin, 2006); but differentiated in others like threshold, inactivation, ion selectivity and pharmacological sensitivity. Rapidly adapting (RA-type) current have low thresholds and inactivate between 3-6ms, are found in all types of DRG neurons but mostly mechanoreceptors; whereas intermediately adapting (IA-type) currents have a low thresholds and are found mostly in middle to small-size neurons, and they can inactivate around 15-30ms; finally, slowly adapting (SA-type) currents are normally present in higher proportion in cells with small-size diameter, they can have low- or high-

thresholds and very slow inactivation 200-300ms, sometimes these currents are subdivided into SA-currents and ultra-slow adapting currents, up to 2seconds after initial stimulation (Cho et al., 2002; Hu & Lewin, 2006; Hao & Delmas, 2010). Since three types of mechanically activated currents have been found in DRG neurons, it has raised the questions if the different kinetics between them reflects the activation of different kind of mechanosensitive ion channels.

In the skin, all types of sensory neurons that innervate a specialized receptor can display different shapes of mechanically activated currents coming from the same or different mechanosensitive ion channels. The mechanosensitive currents do not necessarily reflect sensory neuron identity. The receptor potential kinetics of rapidly and slowly adapting mechanoreceptors depends on the interaction between the cells involve that form the specialized receptor as well as mechanosensitive ion channels biophysical properties and the complex in which are immerse in the membrane (Hao & Delmas, 2010; Delmas et al., 2011).

Characterization of mechanically activated ion channels has been a complicated endeavor in the somatosensory system. First, mechanosensitive ion channels are usually expressed at low levels in the endogenous cells, they are associated with auxiliary proteins and can form complex microdomains and finally, there is an intrinsic level of basal mechanical forces that all cells are able to respond and adapt, masking truly mechanoreceptors and mechanosensitive ion channels (Delmas et al., 2011). Certain requirements have been established to propose a candidate gene as MS ion channel: 1) the gene must be expressed by mechanosensitive cells and should affect its mechanosensitivity when the cell is lacking the candidate gene, but not development or other functions; 2) heterologous expression of the candidate gene should confer mechanosensitivity to a naïve cell; 3) point mutations in the potential pore-forming subunits should alter conductance or ion selectivity of the endogenous mechanically activated currents; 4) finally, if the candidate gene does not need any subunit to gate or transfer mechanical activation, the candidate gene should be able to be activated in artificial lipid bilayers (Árnadóttir & Chalfie, 2010; Ranade et al., 2015).

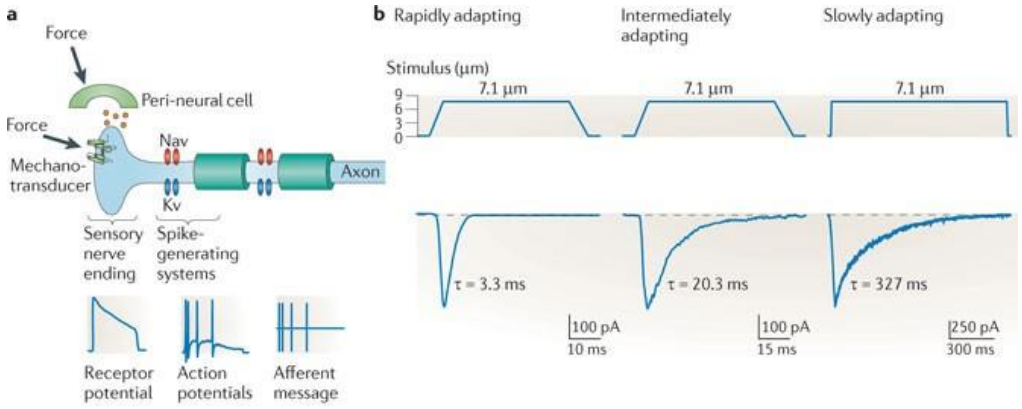

Figure 8. Mechanosensitive ion channels activation elicits currents in sensory neurons. (A) Sensory nerve ending. Mechanical stimulation of the receptive field activates mechanosensitive ion channels expressed in the nerve axon. The ion flow through these channels generates a local depolarization (receptor potential) that brings the membrane potential to the threshold for triggering action potentials. Mechanoreceptors encode the parameters of the mechanical stimulus into a discharge of APs, whose firing frequency reflects the main features of the stimulus. Perineuronal cells have been proposed to modulate receptor potential properties. (B) Representative traces of mechanosensitive currents recorded in sensory neurons while current amplitude and activation kinetics is similar between them, threshold and inactivation kinetics allow to classify them in: Rapidly adapting, intermediately, slowly adapting and ultra-slowly adapting. Figure taken from Delmas et al., 2011.

6.5.1 Piezo channels

Piezo channels were characterized as mechanically activated ion channels by Coste and collaborators (2010), using mechanical indentation and pressure clamp in mouse neuroblastoma cells (N2A), they characterized Piezo channels mechanosensitive currents as cationic nonselective with a low permeability to chloride, fast-activated and RA kinetics, and are blocked by ruthenium red and gadolinium. Thereafter, it was also shown that Piezo currents are desensitized slowly to positive voltage, indicating that Piezo channels are also voltage- modulated (Bagriantsev et al., 2014; Moroni et al., 2018). Voltage modulation and voltage gating of Piezo channels indicates adaptation to the variety of roles that these channels have in different cell types.

Piezo1 and Piezo2 proteins are encoded by the *Piezo1/FAM38A* and *Piezo2/FAM38B* genes (Coste et al., 2010) and form trimeric large transmembrane proteins with 38 transmembrane domains, which make them the proteins with the largest number of TM domains highly conserved among plants and animals (Cox et al., 2017). Piezo1 and Piezo2 share around 50% identity, and different isoforms have been found for Piezo channels, especially for Piezo2 (Murthy et al., 2017; Szczot et al., 2017). Piezo1 is high expressed in bladder, colon, kidney, lung and skin; while Piezo2 expression is observed in bladder, colon, lung and DRG neurons (Szczot et al., 2017).

Piezo1 has been proven to be inherently mechanosensitive gated by membrane stretch, force is transmitted by lipids to the channel using isolated Piezo1 channels in a reconstitute droplet lipid bilayer (Syeda et al., 2016). Piezo1 channel is important in endothelial cell types under static and shear stress conditions, acting as a sensor of blood flow and erythrocyte volume regulation. Piezo1 is expressed in red blood cells, vascular endothelial cells and the uroepithelial cells sensing share stress (Murthy et al., 2017; Wu et al., 2017). Piezo1 channels have been also implicated in cell-cell interactions and motility by integrins activation and participate in cell migration, proliferation, and elongation (Nourse & Pathak, 2017).

Piezo2 is expressed in most of DRG neurons and the sensory endings where the protein has been detected in structures like lanceolate endings and circumferential afferents around hairs; and glabrous skin such as Meissner corpuscles and Merkel cells-neurite complex (Ranade et al., 2014; Woo et al., 2014). Also, Piezo2 channels are expressed in proprioceptors participating in stretch sensing (Woo et la., 2015). Piezo2 is also expressed in the sensory neurons that innervate the lungs and has a function in stretch-induced firing of afferents of the vagal nerve (Murthy et al., 2017). Lately, it has been identified Piezo2 channel is expressed in the urinary tract and sensory neurons that innervate it (Marshall et al., 2020). Early reports have shown that DRG neurons where Piezo2 has been ablated lost most of their mechanically activated RA currents, but not IA- or SA-currents, (Murthy et al., 2017). The Piezo2 gene undergoes extensive alternative splicing which generates unique variants with differences in rate of inactivation; ion permeability; and modulation by intracellular calcium; and are expressed in a cell-type specific manner that could generate sensory properties diversification (Szczot et al., 2017).

It has been proposed that Piezo1 and Piezo2 channels have four states: closed, open and at least two inactivated states (Murthy et al., 2017; Moroni et al., 2018). Lewis and collaborators (2017) have proposed that channel inactivation mechanism and channels localization in the membrane synchronize their activity as bandpass filters depending on the stimulus waveform and duration.

In conclusion, Piezo channel properties can be modulating according to the cell and microenvironment where the channels are being expressed producing different kinds of current kinetics necessary for distinct biological processes.

6.5.2 Looking for a slow-inactivating MS ion channels

Given the great diversity of processes and responses by cells using mechanotransduction, indicates that there are still mechanosensitive ion channels waiting to be identified. Recently, two types of transmembrane proteins have been proposed to be mechanosensitive or even

mechanically gated and may participate in sensory neurons mechanotransduction: OSCA/Tmem63 family and Tmem87/Elkin.

The Tmem63 family is homologous to OSCAs channels present in the plant *Arabidopsis thaliana* that can mediate MS currents following indentation or membrane stretch stimulation. (Murthy et al., 2018). The mammalian Tmem63 family has three members Tmem63A, Tmem63B and Tmem63C, proposed as putative hyperosmolarity activated ion channels or mechanosensitive ion channels. When the three subunits are simultaneously overexpressed in HEK293 cells, high threshold and slow activation/inactivation currents can be activated by mechanical stimulation (Zhao et al., 2016). It is important to note TMEM63B gene is highly expressed in the nervous system including DRG neurons.

Elkin1/Tmem87a has been reported as a transmembrane protein required for MS ion channel activity involve in inside-out mechanical signaling in the development and metastatic process of melanoma cells (Patkunarajah et al., 2020). Using pillar array substrate deflection and indentation techniques, metastatic melanoma cells have shown to have deflection-dependent currents required for cell migration. However, the mouse variant mElkin1/Tmem87 evokes a very small MA currents when is overexpressed, but its presence in DRG neurons indicate a possible role in mechanotransduction. The mouse Elkin1/Tmem87a protein is also highly expressed in lung and bladder (Patkunarajah et al., 2020).

6.5.3 Proteins associated with mechanosensitive sensory neurons

Only a few channels have been proven to be intrinsically mechanosensitive implying that they possess a mechanically gated subunit that is directly activated by membrane stretch like Piezo 1 channels (Delmas & Coste, 2013). However, other channels seem to acquire mechanosensitivity in the presence of other proteins that have couple the mechanical energy to gate the ion channel in the membrane, these proteins are modulatory subunits that can interact with the ion channel, membrane, cytoskeleton and the ECM (Poole et la., 2015). Adaptation and inactivation regulate mechanosensitive currents, adaptation allows the channels to be available to new mechanical stimuli that arrive to the sensory neurons and inactivation of MEC channels supports filtering and protects the sensory neurons in cases of exacerbating stimulation by limiting the cell input (Roudaut et al., 2012).

How MS ion channels are gated is one of the major questions in the mechanotransduction field. The molecular complexes in the membrane interacting with the cytoskeleton and the extracellular matrix could facilitate the gating of mechanosensitive ion channels and account for the diversity of mechanosensitive currents that can be found in the same sensory neuron (Hu & Lewin, 2006;

Poole et al., 2015). Mechanosensitive ion channel inactivation seems to be common denominator regulatory mechanism that leads to slowly adapting responses and hypersensitivity. Enhancing adaptation can be achieve by intrinsic channel modifications but also by auxiliary subunits in the channel microenvironment such as TMEM120A/TACAN or TMEM150C/Tentonin3.

TMEM120A/TACAN

The TMEM120 family has to members, TMEM120A and TMEM120B, has been identified as nuclear envelope proteins with roles in adipocyte differentiation and metabolism (Batrakou et al., 2015). The TMEM120A gene encodes a transmembrane protein known as TACAN and proposed as a mechanically activated ion channel expressed in nociceptors and participating in the transduction of mechanical pain (Beaulieu-Laroche et al., 2020). The TACAN protein was selected from a proteomic screen as a putative ion channel because it possessed 6 transmembrane domains and high expression in medium- and small-size DRG non-peptidergic neurons. Expression of TACAN in cells lead to mechanosensitive currents membrane to induced-stretch with high-speed pressure clamp and pillar arrays substrate deflection in cell models and lipid bilayers that could be block by gadolinium and GsMTx4. (Beaulieu-Laroche et al., 2020). In addition, non-peptidergic nociceptors shown impairments of mechanosensitivity when the TACAN protein is knockout in mouse, and von Frey behavior test showed a reduction in nocifensive response using the same TACAN knockout mouse ((Beaulieu-Laroche et al., 2020).

Recently, it has been questioned TACAN as a mechanosensitive ion channel by two research groups unable to reproduce indentation or stretch-induced mechanosensitive currents associated with TACAN heterologous expression in cells and reconstituted membranes (Niu et al., 2021; Rong et al., 2021 in bioRxiv). TACAN structure was determined by cryo-EM showing that it does not have a typical ion channel constitution in the membrane, and it is associated to a coenzyme-A molecule (CoASH) that stabilize the channel in its closed state (Rong et al., 2021 in bioRxiv). It is still possible that TMEM120A/TACAN forms a mechanosensitive ion channel that responds to specific mechanical stimuli like cell-substrate perturbation, or indirectly modulate mechanosensitive ion channels by lipid metabolism-related signaling pathways that change the membrane constitution (Batrakou et al., 2015; Niu et al., 2021; Rong et al., 2021 in bioRxiv).

TMEM150C/Tentonin3

TMEM150C/Tentonin3 is a small protein with 6 transmembrane domains encoded by the gene *TMEM150C* expressed by DRG neurons. The protein Tentonin3 is highly expressed in DRG neurons, epididymis, pancreas, eye, brain, and spinal cord (Yue et al., 2014).

This protein was identified as a putative mechanosensitive protein from at least two different and independent screens (Hong et al., 2017; Hergert, Regina unpublished data). In 2017, Hong and colleagues showed mechanically activated currents when Tmem150c/Tentonin3 was overexpressed in a heterologously system. The MS currents displayed high thresholds, rapid kinetics of activation and a two-phase inactivation kinetics, rapid and slowly even after the end of indentation. In line with other MS ion channels, Tenontin3 candidate is nonselective cationic channel with high permeability to calcium ions and was blocked by mechanosensitive ion channel blockers as gadolinium, ruthenium red, FM1-43 and GsMTx4.

Tmem150c/Tentonin3 is found in myelinated large-sized neurons and colocalize with parvalbumin and TRPV1 positive neurons which are markers for proprioceptors and nociceptors, respectively. The high expression in parvalbumin positive neurons indicated a potential role in proprioceptors function. Using a Tentonin3/TMEM150C KO mice which had no expression of the protein, Hong and collaborators (2017) showed a reduction in SA-currents mechanically activated DRG neurons. In addition, extracellular recordings from the peroneal nerve that innervates the EDL muscle showed a reduced stretch-evoked activity in muscle spindle afferents. Finally, behavior tests such as inverted grid and mouse walk analysis display a reduction of clinging and a loss of motor coordination respectively in the Tentonin3/TMEM150C KO mice leading to the conclusion that this protein is necessary for proprioception (Hong et al., 2017).

Although Hong and colleagues (2017) did not explicitly claim Tentonin3/TMEM150C as a mechanosensitive ion channel, their work was certainly suggestive. However, their results were questioned by several expert groups in mechanotransduction arguing that endogenous Piezo1 currents activated by mechanical stimuli in wild type HEK293T possibly were mistaken for Tentonin3/TMEM150C intrinsic mechanosensitivity. Moreover, Dubin et al. (2017) overexpressed Tentonin3/TMEM150C in HEK293T cells in which Piezo1 had been deleted (HEK-P1KP, CRISPR/Cas9 system generated) and observed no mechanically gated currents after cell indentation.

The slow inactivating MS current generated after co-transfection of Piezo1 and Tentonin3 does not clarify if the observed currents belong to two different MS ion channels or, if there was a modulating role of Tentonin3/TMEM150C on Piezo1. Modification on the putative pore of Tentonin3/TMEM150C displayed in conductance variation, indicating the possibility of it forms an ion channel ion channel. (Hong et al., 2017). Further experiments done by Anderson and colleagues (2018) corroborated that Tentonin3/TMEM150C does not evoke mechanically activated currents in HEK293T P1KO cell. Although they observed that it prolonged inactivation kinetics of Piezo1 in addition to decreasing the threshold for Piezo2 channels when co-expressed

with Tentonin3/TMEM150C (Anderson et al., 2018). Since all these channels have different mechanical gating, it is possible Tentonin3/TMEM150C modifies the surrounding environment of the channel like cytoskeleton or acts as tether.

In the past 10 years, the knowledge of proteins, ion channels, cells and composition of cutaneous specialized receptors has been dramatically expanded. It is necessary to place their role in mechanotransduction and re-evaluate the role old known components to propose new functional models of mechanotransduction in the somatosensory system. Part of that effort are the aim of this project.

7. Aims of the study

The main goal of this project is to investigate the role of sensory Schwann cells and the candidate to mechanosensitive protein TMEM150C/Tentonin3 in sensory neurons mechanotransduction.

First, the recently proposed new structural organization of nociceptors as Schwann cells-nociceptor complex will be tested to investigate their contribute to sensory neurons terminal-endings function and sensitivity. Here, specialized Schwann cells will be stimulated with optogenetic tools to know what kind of mechanoreceptors and nociceptors are associated directly with them and their role in mechanotransduction or sensory afferent excitability.

Secondly, the role of the recently characterized TMEM150C/Tentonin3 protein to be associated with sensory neurons mechanosensitivity, will be characterize in cutaneous sensory neurons function. Here, two mutant mice with a deletion of TMEM150C gene will be tested for mechanotransduction in sensory neurons.

8. Material and methods

8.1 Materials

8.1.1 Chemicals

Name	Supplier	Catalog number
2'2-thiodiethanol (TDE)	Sigma Aldrich	88559
Agarose	Sigma Aldrich	A9414
Bovine serum albumin (BSA)	Sigma Aldrich	A2153-100G
Calcium chloride ($CaCl_2$)	Sigma Aldrich	C4901
Carbencillin	Carl Roth	6344.2
Cut smart buffer	NEB	B7200S
Dimethyl sulfoxide (DMSO)	PanReac AppliChem	A3672,0100
dNTPs	Invitrogen	P/N55082-85
(D)-Saccharose	Carl Roth	4621.1
EGTA	Sigma Aldrich	E4378
EHS Laminin	Gibco	23017-015
Ethidium bromide	Sigma Aldrich	67-66-3
Fugene	Promega	E2311
Glucose	PanReac AppliChem	A1422,0500
LB broth	Sigma Aldrich	L3022-1KG
Magnesium chloride ($MgCl_2$)	Merck	1.05833
Mineral oil	Sigma Aldrich	M8410-500ML
OCT Tissue Tek	Sakura, Alphen aan den Rijn	4583
Paraformaldehyde	Sigma Aldrich	158127
Penicillin/Streptomycin	Sigma Aldrich	P4333
Polydimethylsiloxane (PDMS) Sylgard 184 silicone elastomer	Dow Corning Corporation	(240)4019862
Poly-L-lysine (PLL)	Sigma Aldrich	P1524
Potassium chloride (KCL)	Carl Roth	7986.1
Sodium chloride (NaCl)	Carl Roth	3957.1
Sodium hydroxide (NaOH)	Carl Roth	P031.1
Taq Polymerase	NEB	M0267L

Taq Polymerase buffer	NEB	B9014S
Triton X-100	Sigma Aldrich	X-100-500ML

8.1.2 Reagents for cell culture

Name	Supplier	Catalog number
Dulbecco's modified eagle medium (DMEM)	Thermo Fisher Scientific	31966
Fetal calf serum (FCS)	Sigma Aldrich	P-0781
Opti-MEM	Thermo Fisher Scientific	31985070
Phosphate-buffered saline (PBS)	Gibco	D8537

8.1.3 Buffer and solutions

Name	Composition
Extracellular solution for HSPC (High Speed Pressure Clamp)	150 mM NaCl, 5 mM KCl, 2 mm $CaCl_2$, 1 Mm $MgCl_2$, 10 mM glucose, 10 mm HEPES; adjusted to 7.4 with KOH
Extracellular solution for whole-cell patch clamp	140 mM NaCl, 4 mM KCl, 2 mM $CaCl_2$, 1 mM $MgCl_2$, 4 mM glucose, 10 mM HEPES; adjusted to pH 7.4 with NaOH
Intracellular solution for HSPC	140 mM KCl, 1 mM $MgCl_2$, 1 mM EGTA, 10 mM HEPES; adjusted to pH 7.3 with KOH
Intracellular solution whole-cell patch clamp	110 mM KCl, 10 mM NaCl, 1 mM MgCl, 10 mM HEPES, 1 mM EGTA; adjusted to pH 7.3; 290 mOsm
Paraformaldehyde solution (PFA, 4%)	4% paraformaldehyde in 0.1M PBS, adjusted to pH 7.2-7.4 with NaOH and HCl
Synthetic interstitial fluid (SIF)	2 mM $CaCl_2$, 5.5 mM glucose, 10 mM HEPES, 3.5 mM KCl, 0.7 mM $MgSO_4$, 123 mM NaCl, 1.5 mM NaH_2PO_4, 7.5 mM saccharose, 9.5 mM Na-gluconate; adjusted to pH 8.4 with 10

	N NaOH; carbogene was used for oxygenation during the experiment and bring pH to 7.4
Section-Blocking	5% of Invitrogen normal goat serum, 95% PBS
Washing buffer	5% of Invitrogen normal goat serum, 95% (0.1% Triton X-100) PBS
Dent's bleach	10% H_2O_2, 13.3% DMSO and 53.3% methanol
Dent's fix	20% DMSO, 80% methanol

8.1.4 Commercial kits

Name	Supplier	Catalog number
TaqMan Universal PCR Master Mix	Roche	4304437
Quiagen Plasmid Midi kit	Quiagen	12843

8.1.5 Plasmids

Name	Marker	Obtained from
Empty vector		Raluca Fleisher, PhD Student
Vector_green	GFP	Dr. Mirko Moroni
Vector_red	tdTomato	Dr. Mirko Moroni
mousePiezo1	GFP	Dr. Mirko Moroni
mousePiezo2	GFP	Dr. Mirko Moroni
mouseStoml3	GFP	Raluca Fleisher, PhD Student
mouseTmem150c		Dr. Regina Herget

8.1.6 Antibodies

Primary antibodies

Name	Species	Dilution	Supplier	Catalog number
Anti-NF200	Chicken	1:1000	Abcam	AB72998
Anti-S100	Rabbit	1:1000	Dako	Z0311
Anti-PGP9.5	Rabbit	1:400	Thermo Fisher Scientific	PA5-29012
Anti-Sox2	Rabbit	1:10	Gift from T. Edlund	
Anti-Tmem150c	Rabbit	1:2000	Sigma Aldrich	ABN2266

Secondary antibodies

Name	Host	Dilution	Supplier	Catalog number
Anti-Chicken488	Goat	1:1000	Abcam	Ab150169
Alexa Fluor Anti-Rabbit488	Goat	1:1000	Sigma Aldrich	A11034
Alexa Fluor Anti-Rabbit555	Goat	1:1000	Invitrogen	A31630
Alexa Fluor Anti-Rabbit568	Donkey	1:1000	Invitrogen	A10042
Alexa Fluor Anti-Rabbit647	Donkey	1:1000	Thermo Fisher Scientific	A21245
DAPI		1mg/ml	Thermo Fisher Scientific	62248

8.1.7 Cell culture

Name
Neuro 2a cells (N2A) from mouse

8.1.8 Equipment

Name	Supplier
Axiovert 200 inverted microscope	Carl Zeiss
Borosilicate standard wall capillaries, 1.5 OC x 0.86 ID x 100 L mm	Harvard Apparatus
Camera HD IC80	Leica
CoolSnapEZ camera	Visitron Systems
DM5000B light microscope	Leica
DMZ universal puller	Werner Zeitz
EPC-10	HEKA Elektronik
Force sensor (Ultra-precise Force Measurement System FMS-LS)	Kleindiek Nanotechnik

Glass coverslips, Thickness No. 2, 22x22mm	VWR
Glass coverslips, 12mm diameter	Thermo Fisher Scientific
High Speed Pressure Clamp	ALA Scientific
Laser scanning microscope LSM710	Carl Zeiss
Lamp LCD KL1500	Leica
Magnetic Base	Kametec
Microelectrode platinium Kaptom (1mΩ)	World Precision Instruments
Micro Forge MF-830	Narishige
Micromanipulator MM3A	Kleindiek Nanotechnik
Micromanipulator MM33	Märzhäuser Wetzlar
Microscope for dissection MS5/M26	Leica
Nanodrop spectrometer 2000	Kleindiek Nanotechnik
Nanomotor	Kleindiek Nanotechnik
NeuroLog System including Stimulator and Amplifier Modules	Digitimer Ltd
Objective 40X, LD Achroplan 40x/60 Korr Ph2 ∞/0-2	Carl Zeiss
Oscilloscope (Digital Storage Oscilloscope TDS 220)	Tektronix
Peltier device	Esys
Peristaltic pump Miniplus 3	Gilson
Piezo actuator	Physik Instrumente (PI)
Piezo amplifier	Physik Instrumente (PI)
PowerLab 8/35	ADInstruments Ltd
Skin-nerve chamber	Custom-made at the Max Delbrück Center for Molecular Medicine in the Helmholtz Association
Table (IG Breadboard)	Newport
Thermal stimulator	Esys
Tubing (E-3603)	Tygon
Vibratom VT 100S	Leica
Waterbath	Julabo

8.1.9 Consumables

Name	Supplier
Forceps Dumont Mirror Finish #5	Fine Science Tools
Falcon tube	Eppendorf
Vannas Spring Scissors	Fine Science Tools
Pasteur pipette	Brand
Razor blade	Braun
Syregine	

8.1.10 Software

Name	Supplier
Fiji (ImageJ)	Open source
Fitmaster	HEKA Elekectronik
GraphPad Prism 8	Graphpad Software
Igor Pro	Wavemetrics Inc.
LabChart 8 (including Spike Histogram extension)	ADInstruments Ltd
Office 365	Microsoft
Nanocontrol 4.0	Kleindiek Nanotechnik
Patchmaster	HEKA Elektronik
ZEN 2010	Carl Zeiss

8.2 Animals

All animal experiments were carried out according to the German and EU animal protection laws. Mice were kept and handle through animal house of the Max Delbrück Center. All mice strains genetically modified were bred under a C57BL/6N background.

8.2.1 TMEM150C$^{LacZ/LacZ}$ mice

The first TMEM150C KO mutant mouse used in this project was generated by the trans-National Institute of Health Mouse initiative Knockout Mouse Project (KOMP). A LacZ and neomycin cassette were inserted between exons 5 and 6 of the Ttn3 locus with a stop codon, which resulted in the expression of a truncated Ttn3 fused to LacZ (Figure 9).

Figure 9. TMEM150C knock out vector construct. Scheme taken and modified from Hong et al., 2017).

8.2.2 TMEM150C$^{-/-}$ mice

A second mouse was generated with a deletion of TMEM150C allele using CRISPR/Cas9 technology by the Ingenious Targeting Laboratory (iTL). Valérie Begay (from Gary Lewin's lab) designed the guide RNA (gRNA) indicated with red arrow in Figure 10. The sequence between the end of intron 1-2 and the beginning of intron 5-6, leading to the deletion of exon 2-5 with a frame shift. The mouse was generated by the company ingenious targeting laboratory and the founders, two pairs of heterozygous mice, were provided to stablish the line.

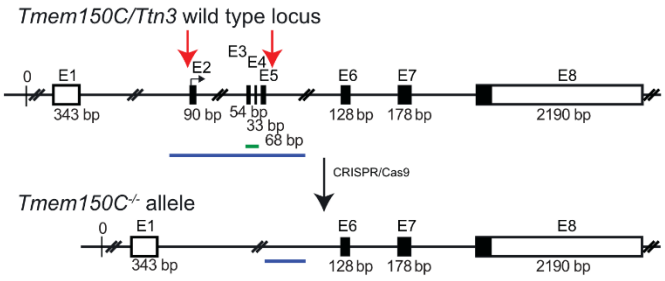

Figure 10. TMEM150C gene deletion using CRISPR technology. On the top, schematic representation of the wild-typeTMEM150C allele. Red arrows indicate the gRNA designed to delete the regions between the end of intron 1-2 and the beginning of intron 5-6. The blue line represents a fragment sequence of the wild-type allele, the green line represents fragment sequence that was used for WT genotyping. On the bottom, the resulting allele after CRISPR/Cas9 deletion, named TMEM150C$^{-/-}$. The blue line represents the fragment amplicon for the knockout ($^{-/-}$) genotyping.

Line	Provider	Genotyping
Tmem150c$^{tm1a(KOMP)Wtsi}$	KOMP project	3' Universal (CSD-Neo-F): GGGATCTCATGCTGGAGTTCTTCG (fwd from genetrap cassette) 5' Universal (LR-5En2frt-R): GGTGGTGTGGGAAAGGGTTCGAAG (rev from genetrap cassette)
Tmem150C$^{-/-}$ (CRISPR/Cas)	Ingenious targeting Laboratory	MEMT 1.0F: 5'-CTCAATAACAGCCACAAGGAAAG -3' MEMT 1.0R: 5'- ACTGGCAGGGTTGTGTAAG -3'

8.2.3 Sox10-ChR2, Sox10-TOM, Sox2-ChR2, Sox10-ArchT and Sox2-ArchT

The Sox10^{CreERT2} mouse strain targeting strategy have been previously described by Laranjeira et al., (2011). Briefly, Sox10::iCreER^{T2} transgenic mice were generated by pronuclear injection of a modified PAC expressing a tamoxifen-inducible Cre recombinase (iCreER^{T2}) under the control of Sox10 regulatory sequences. The original PAC (RP21-529-I6 from RPCI mouse PAC library 21, UK HGMP Resource Center) was modified by homologous recombination in bacteria using a targeting vector containing 5' (AscI-SalI 460-bp) and 3' (SpeI-PacI 440-bp) homology regions; an iCreER^{T2} cassette (3.3 kb), and the chloramphenicol resistance gene (Cm^{R}) was flanked by FRT sites and therefore removed by Flp recombinase activation in bacteria. Sox2^{CreERT2} (stock number 017593), Rosa26R^{tdTomato} (stock number 007914), Rosa26R$^{ChR2\text{-}EYFP}$ (stock number 012569) and Rosa26R$^{ArchT\text{-}EGFP}$ (stock number 021188) were ordered from The Jackson Laboratory.

Sox10^{CreERT2} mice were crossed to R26R^{TOM} mice for histological and Schwann cell isolation experiments and to R26R^{ChR2} and R26R^{ArchT} for functional experiments. Tamoxifen (Sigma, T5648) was dissolved in corn oil (Sigma, 8267) at a concentration of 20 mg/ml and delivered by intra peritoneal (i.p.) injection to adult mice or pups (P10) (Abdo et al., 2019).

For this project, adult mice from Sox10-ChR2, Sox2-ChR2, Sox10-ArchT and Sox2-ArchT were imported after tamoxifen injection from Patrik Ernfors's Lab in the Karolinska Institute, Stockholm. All genotyping and mice treatment were carried out before shipment by Laura Enrique-Calvo.

8.3 Methods

8.3.1 Skin nerve preparation

Electrophysiological recordings from cutaneous sensory fibers of the tibial nerve and saphenous nerve were made using an *ex vivo* skin nerve preparation following the method described previously by Milenkovic et al., 2008; Walcher et al., 2018).

Hairy skin – saphenous nerve preparation

The animal was sacrificed by cervical dislocation and the hair of the limb was shaved off. The saphenous nerve was dissected with the skin of the hindpaw attached and mounted inside-out in a bath chamber which was constantly perfused with warm (32°C) oxygen-saturated interstitial fluid. The saphenous nerve was gently pulled through a narrow channel to an adjacent recording chamber embedded in mineral oil where teased fibers were used for single-unit recordings over a platinum wire electrode for monopolar recording with a reference electrode.

Glabrous skin – tibial nerve preparation

The glabrous skin from the hind paw was removed along with the tibial nerve dissected up to the hip and cut. The glabrous skin along with the tibial nerve still attached to the hindpaw was transferred to a bath chamber which was constantly perfused with warm (32°C) oxygen-saturated interstitial fluid. The remaining bones, muscle and ligament tissue were gently removed as much as possible, allowing the glabrous skin and tibial nerve preparation to last at least 6 hours of recording in healthy a stable condition in an outside-out configuration. The tibial nerve was passed through a narrow channel to an adjacent recording chamber embedded in mineral oil.

Isolation of single units

Fine forceps were used to remove the perineurium and fine nerve bundles were teased and placed on a platinum wire recording electrode. Mechanical sensitive units were first located using blunt stimuli applied with a glass rod. The spike pattern and the sensitivity to stimulus velocity were used to classify the unit as previously describe (Milenkovik et la., 2008; Walcher et al., 2018). Raw data were recorded using an analog output from a Neurolog amplifier, filtered and digitized using a Powerlab 4/30 system and Labchart 8 software with the spike-histogram extension (ADInstruments Ltd., Dunedin, New Zealand).

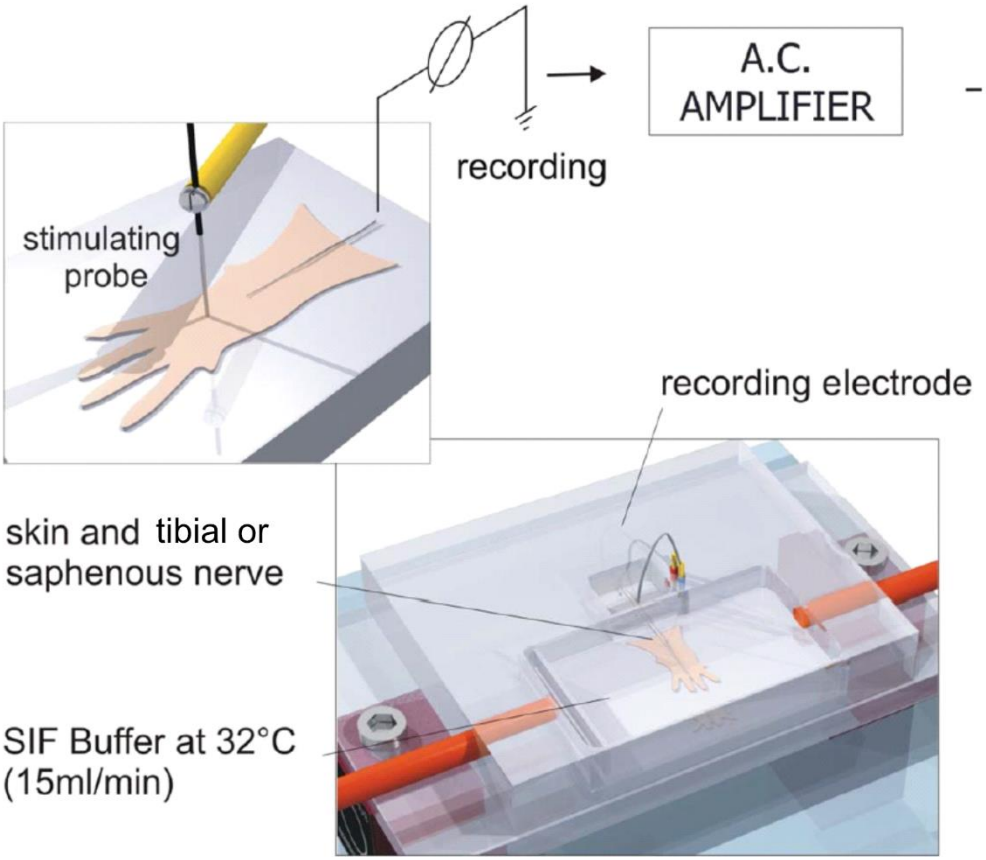

Figure 11. The skin nerve preparation. Scheme of the of the experimental chamber where the skin is placed constantly perfused with SIF buffer at 32°C. On the bottom, the skin is stretch out and pinned down, the nerve is lead through a narrow channel into the small recording chamber isolated with mineral oil. The nerve fibers are placed over the recording electrode. On the top, mechanical stimulation on the skin triggers action potential that can be recorded and amplified. Ilustration from Paul Heppenstall.

8.3.2 Electrophysiological recordings from skin-nerve preparation

Conduction velocity measurement

The conduction velocity (CV) was measuring the formula CV = distance/time delay, in which CVs > 10ms^{-1} were classified as RAMs or SAMs (Aβ, <10ms^{-1} as Aδ and <1ms^{-1} as C-fibers. All mechanical, thermal or optogenetically driven responses analyzed were corrected for the latency delay between the electrical stimulus and the arrival of the action potential at the electrode.

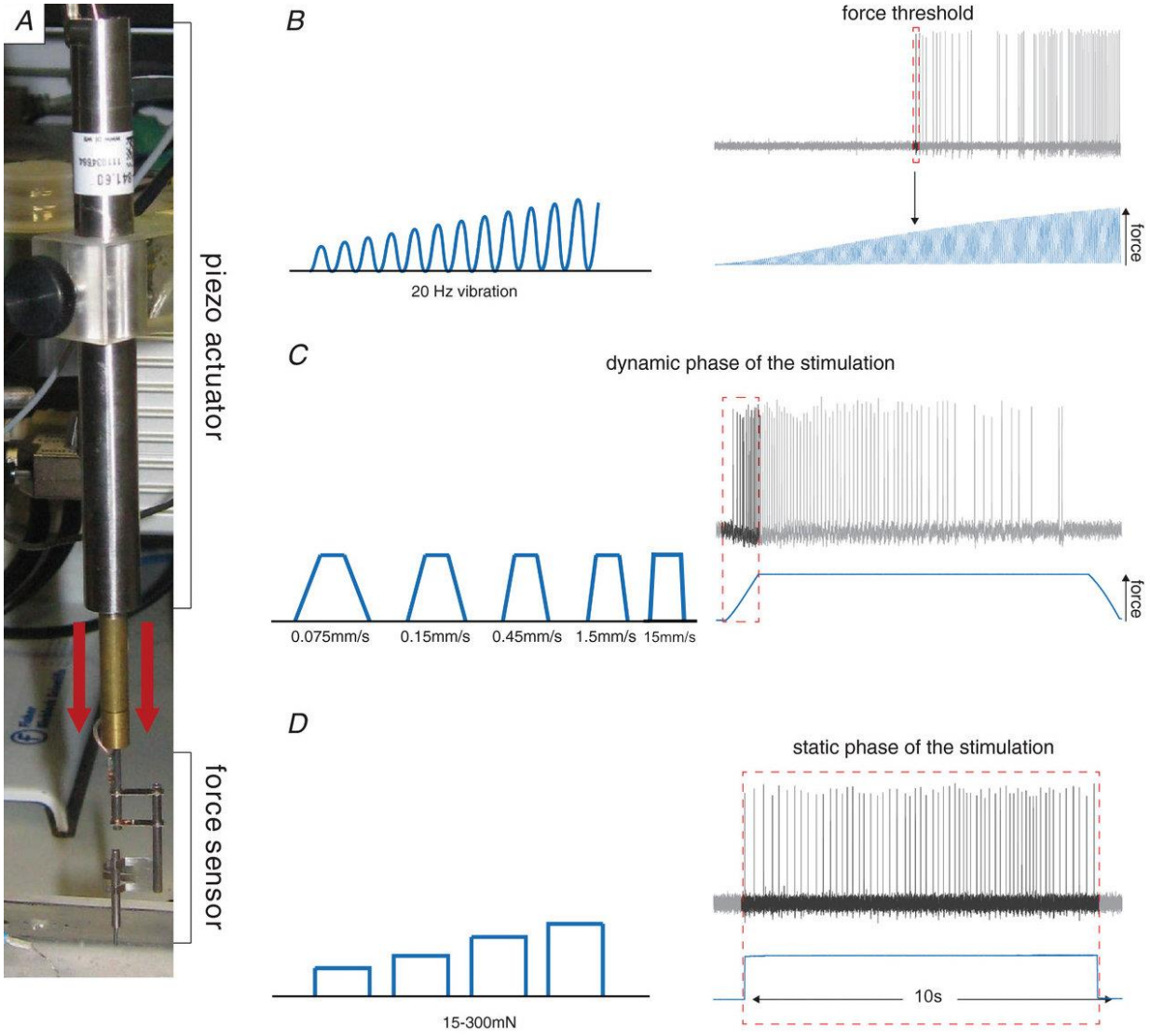

Figure 12. Mechanical stimulation protocols. (A) Piezo actuator used apply mechanical stimulation protocols and the force sensor feedback system for the actual stimuli applied on the skin. (B) Left, schematic representation of the sinusoidal wave of 20Hz, or vibration stimulus, with increasing force intensity. Right, Example trace of a sensory afferent responding to the vibration stimulus. Notice that the mechanical or force threshold is measured as the force necessary to evoke the first action potential. (C) Left, schematic illustration of the ramp and hold mechanical stimulation using 5 different ramp velocities. Right, example trace of a sensory afferent responding to the ramp, or dynamic phase of the stimulation. Only the spikes of the at the dynamic phase are measured for this protocol. (D) Left, schematic representation of the ramp and hold stimulation where the ramp velocity is fixed but four different indentation intensities are applied. Right, example trace of a sensory afferent responding to the static face of the stimulation and used for quantification.

Mechanical stimulation

Mechanical stimulation of the receptor field of the recorded fibers was performed using a piezo actuator (Physik Instrumente, Germany, P-602.508) connected to a force measurement device (Kleindiek Nanotechnik, Reutlingen, Germany, PL-FMS-LS) (Figure 12A). Different mechanical stimulation protocols were used to identify and characterize the sensory afferents. Mechanoreceptors were tested with a vibrating stimulus with increasing amplitude and 20 Hz frequency. The force needed to evoke the first action potential was measured (Figure12B). Additionally, a ramp and hold step was used with sustained force (around 100mN) and repeated with varying probe movement velocity (0.075, 0.15, 0.45, 1.5 and 15 mm/s) (Figure 12C). Only the firing activity evoked during the dynamic phase were analyzed. SAM mechanoreceptors and nociceptors were tested with a mechanical stimulus with a constant ramp (1.5-2 mm/s) and increasing force amplitude, spikes evoked during the static phase were analyzed between 15-300mN (Figure 12D).

Thermal stimulation

Thermal stimulation was carried out in two ways. First, a qualitative classification of C-fiber nociceptors was made applying cold and hot SIF buffer directly to the receptors field of the terminal ending with a 1ml pipette. Cold buffer was kept on ice at 4°C and reach approximately 10°C at stimulation. Hot buffer was kept in a shaker incubator at 80°C and cold down to approximately 50°C at stimulation (Figure 13A). Thereafter, a thermostimulator connected to a thermocouple and Peltier that could be placed in direct contact with the skin was used. Two sequential temperature ramps were applied to test the thermoreceptors sensitivity. First, a cold ramp starting at 32°C (the skin basal temperature) and decreasing in 2 degrees per second rate until reaching 12°C and coming back to 32°C as fast as possible, a global change of 20 degrees in 10 seconds allows recording of cool thermoreceptors as well as noxious cold thermonociceptors responses. Thereafter, a heat ramp was starting from 32°C was applied with an increasing temperature of 2 degrees per second rate until reaching 52°C and coming back to 32°C as fast as possible, a global change of 20 degrees in 10 seconds allows recording of warmth thermoreceptors as well as noxious heat thermonociceptors responses (Figure 13B). A gap of 30 seconds between the two thermal ramp stimulation was used for sensory afferents to recover.

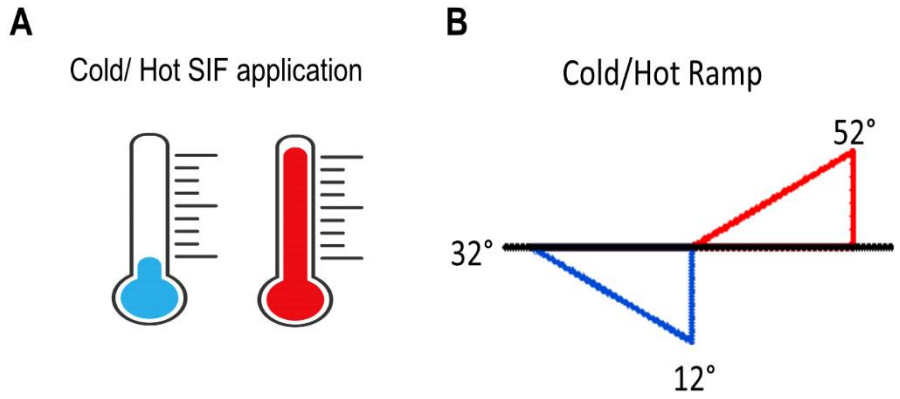

Figure 13. Thermal stimulation protocols. (A) SIF buffer at 4°C and 80°C was applied with a 1ml pipette to the receptor field of C-fiber terminal ending for qualitative classification of cold and heat sensitive. In the experimental chamber the temperature was kept at 32°C, then the expected temperature of SIF buffer at the time of stimulation changed to approximately 10°C and 50°C, respectively. (B) Cold and heat ramp stimulation were generated with a thermostimulator connected to a thermocouple and Peltier. To test C-fiber thermosensitivity, a cold ramp was applied from 32°C to 12°C cooling down 2°C/s during 10s and reaching back the basal temperature in less than 1 second. Secondly, a heat temperature was applied from 32°C to 52°C heating up 2°C/s during 10s and reaching back the basal temperature in less than 1 second.

Optogenetic stimulation

Cultured Schwann cells from Sox10-ChR2 mice were activated with blue light at 470nm at different intensities for 5 seconds and inward currents recorded in whole-cell patch clamp.

In glabrous skin-nerve preparation of Sox10-ChR2 and Sox2-ChR2 mice, receptive fields of mechanoreceptors or nociceptors were exposed to blue light stimulation for 10 seconds applied through a flexible optical fiber bundle with 90° angle with increasing light power from 0.5, 2.6, 3.9 and 4.3 mW/mm^2. During photostimulation, AP firing rate from sensory afferents associated with cutaneous Schwann cells activation was recorded, 10 seconds in between light stimulations was used to allow cutaneous Schwann cells and sensory terminal endings recover (Figure 14A).

Silencing of Schwann cells was achieved by expression of Archaerhodopsin in the same Sox10$^+$ Schwann cells. In glabrous skin-nerve preparation of Sox10-ArchT and Sox2-ArchT mice, yellow light of 565 nm was exposed for 10 minutes in the receptor field of sensory afferent previously characterized by mechanical or thermal stimulation. The light intensity was 0.5 mW/mm^2, in an intermittent cycle of 10:1 second ON/OFF. After light stimulation, mechanical stimulation such as

20Hz vibration, ramp and hold of 250mN or cold/hot thermal ramps were applied three times every 10 minutes (Figure 14B, C).

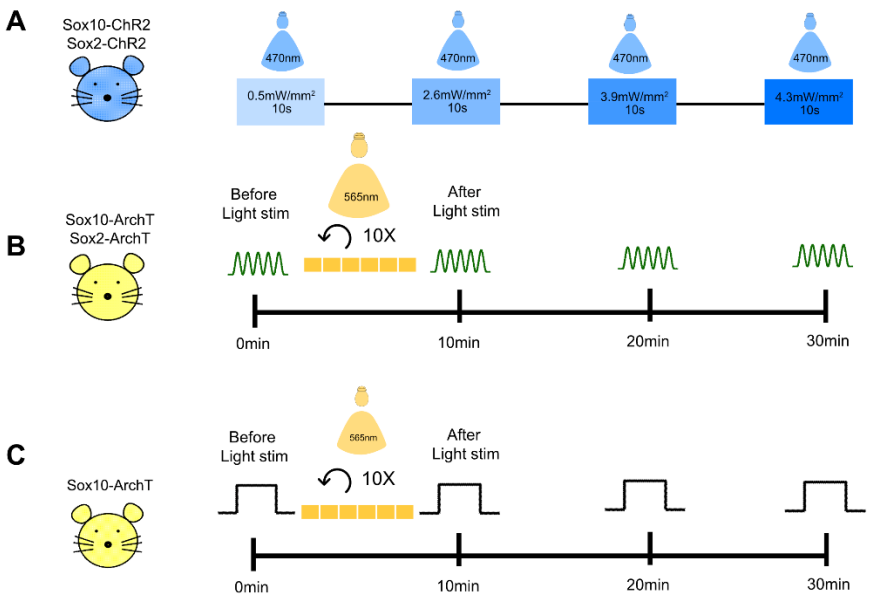

Figure 14. Optogenetic stimulation of Schwann cells. (A) Blue light stimulation protocol to Sox10-ChR2 and Sox2-ChR2 mice. A blue light LED (470nm) was used to photostimulated the receptor field of sensory afferents after they have been characterized by mechanical or thermal stimuli as mechanoreceptors and nociceptors. Four blue light intensities: 0.5mW/mm^2, 2.6mW/mm^2, 3.9mW/mm^2 and 4.3mW/mm^2 were applied for 10 seconds with pauses of 10 seconds in between. (B) Mechanoreceptors recorded from Sox10-AchT and Sox2-ArchT were characterized mechanically with a vibration protocol of 20Hz and velocity ramps stimulation (not shown). Sensory Schwann cells were silenced by constant yellow light (565nm) exposure for 10 minutes. Then, mechanical stimulation such as vibration and ramp and hold velocity stimuli were repeated three times every 10 minutes. (C) Nociceptors recorded from Sox10-AchT were characterized by mechanical or thermal stimuli with a ramp and hold mechanical ramp and cold/hot thermal ramp. Sensory Schwann cells were silenced by constant yellow light (565nm) exposure for 10 minutes. Then, ramp and hold stimuli at 250mN was repeated three times every 10 minutes.

8.3.4 Electrophysiological recordings from single cells

Cell culture

For whole-cell patch clamp recordings Neuro 2a cells (N2a) from mouse were used, except for the Schwann cells Sox10$^+$ experiments. N2a cells present endogenous mechanically gated currents due to the expression of Piezo1. For that reason, in most of the experiments N2a cells

where Piezo1 was deleted (N2a-P1KO) via CRISPR/Cas technology were used (Moroni et al., 2018).

Patch clamp

Whole-cell recordings in voltage clamp were performed from the N2A cell line and on $Sox10^{TOM}$ and $Sox10^{ChR2}$ cultured terminal Schwann cells at room temperature (20–24 °C). Patch pipettes were pulled from borosilicate glass with a tip resistance of 3–5 MΩ were filled with intracellular solution (in mM): 100 KCl, 10 NaCl,1 $MgCl_2$, 10 HEPES, and pH adjusted to 7.3 with KOH. The extracellular solution contained (in mM): 140 NaCl, 4 KCl, 1 $MgCl_2$, 2CaCl2, 4 glucose and 10 HEPES. Cells were clamped to a holding potential of −60 mV for N2A cells and -40mV for primary cell cultures of Schwann cells. Recordings were made using an EPC-10 amplifier (HEKA, Germany) with Patchmaster and Fitmaster software (HEKA). Pippette and membrane capacitance were compensated using the auto function of Patchmaster and series resistance was compensated by 70% to minimize voltage errors. Recordings from fluorescent cells were performed using Multiclamp 700B amplifier (Molecular Devices) and analyzed off-line in Clampfit software (Molecular Devices).

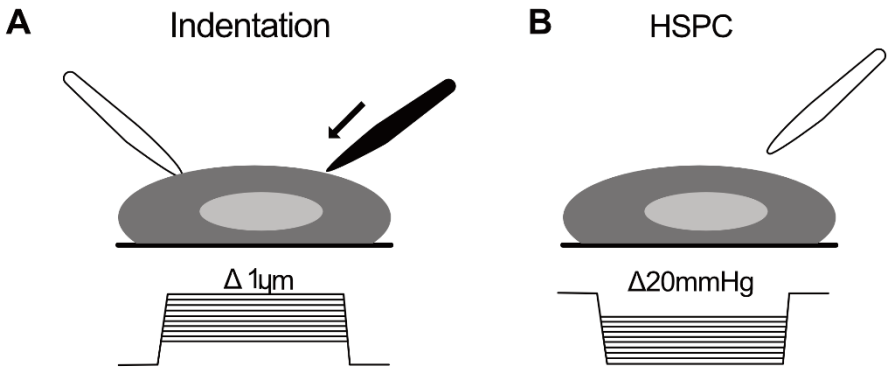

Figure 15. Mechanical stimulation in whole-cell patch clamp. (A) N2a-P1KO cells in whole-cell patch clamp configuration (transparent probe) were mechanically stimulated with a fire-polished glass pipette (in black). Once the cell was touch with the mechanical probe, it was taken one step back and considered as position zero. After, the soma of the cell was indented with 10 steps from 1-10µm approximately. The step duration was between 300-500ms, with 500ms pause in between the steps. (B)

Indentation

Mechanically activated currents were recorded as described earlier (Hu & Lewin, 2006; Wetzel et al., 2007). The mechanical probe consisted of fire-polished glass pipette (tip size 2-3µm) was manipulated by a piezo-driven micromanipulator (Nanomotor MM3A; Kleindiek Nanotechnik). The nanomotor can work in two operation modes: fine and course. For this project, course mode was the only used. Calibration of a single-step size was achieved moving a large number of steps and measuring the distance, repeated three times. Motor's velocity of movement was set at 3.5 µm/ms. The voltage signal sent to the nanomotor by the control unit was simultaneously monitored by a second channel at the EPC10 amplifier, allowing to measure the delay between the nanomotor movement and mechanically activated current, or latency. The probe was positioned at 60° near to the cell body and movements of the mechanical probe were executed in the in/out axis of the device (axis C) for 300-500ms with 500ms pause in between steps (Figure 15A). A voltage divider box (MM3-LS trigger, Kleindiek Nanotechnik) was connected that provided analog voltage output signal corresponding to the piezo signals. Depending on the movement of piezo micromanipulator, the voltage signal was registered as small pulse or just a change in a DC voltage. Only the somas were stimulated, the evoked currents were recorded with a sampling frequency of 200kHz. For the analysis of the kinetics properties of mechanically activated current traces were fitted with single-exponential functions using Fitmaster (HEKA). For optogenetic stimulation, see section "Excitatory optogenetic". All the experiments were carried out between 12 to 48h after plating.

High Speed Pressure Clamp

To test ion channels membrane stretch sensitivity, High Speed Pressure Clamp (HSPC) recordings were performed in excised outside-out patches pulled from N2a cells at room temperature. Recording pipettes were prepared using a DMZ puller and subsequently polished to a final resistance of 6–8MΩ for outside-out patches. Currents were elicited by negative pressure stimuli, with an Ala Instrument device, applied through the recording pipette holding at -60mV. A protocol of pressure steps from 10mmHg to 150mmHg in 20 mmHg steps during 600ms was used. Uncompensated series resistance values were less than 2MΩ. The recorded currents responsive to the pressure curve from each cell were fitted to a Boltzmann equation using the FitMaster program (HEKA, Elektronik GmbH, Germany). It is worth mentioning that construct such as Piezo2 and TMEM150C are not responsive to membrane-stretch and therefore these data are not shown.

8.3.5 Immunohistochemistry

Cryosections

Cryosections were used for immunohistochemical stainings on thin glabrous and hairy skin slices. The skin was dissected and fix as for gelatin sections, then washed with PBS 3 times for 10 minutes and left overnight to 24 hours in a 30% sucrose solution. Thereafter, the tissue was embedded in OCT Tissue Tek on dry ice and store for short term at -20°C or to preserve better at -80°C. The samples were sectioned at 14µm using a cryostat.

For immunohistochemical stainings, the cryosections were dried at room temperature for at least an hour and then washed with PBST (PBS-Triton X100 0.1%) 4 times for 7 minutes. Then, washed with blocking solution (in this case 10% serum of the secondary antibody species, 1% bovine serum albumin (BSA) in PBST) for one hour at room temperature. Primary antibodies were added using the same solution without BSA overnight at 4°C or 1hour at room temperature.

The next day, the slides were washed with PBST 5 times for 7 minutes and added the secondary antibodies 1:300 with Fluo-label. The previous washing steps were repeated, and the slices were mounted using Dako Fluoerescent medium, letting dried the slices out for1-2 hours and kept in the fridge afterwards.

8.3.6 Statistical analysis

To process raw data, in the patch clamp experiments the tau (τ) value of activation and inactivation of a current trace was calculated as exponential fit of different phases using Clampfit 10.7 software. To calculate p value and statistical significance unpaired t-test was performed.

In the skin nerve experiments, raw data were stored and processed using excel Microsoft Excel. All statistical tests and graphs were originally generated in Prism 8 (GraphPad Software, San Diego, CA, USA). Using different type of test as for: normality, two tailed and unpaired T test or Mann-Whitney U-test, one way analysis of variance (ANOVA) or Kruskal-Wallice test with Bonferroni multiple comparison test. Finally, in case necessary two-way repeated-measures analysis of variance (ANOVA) and post-hoc tests performed with Bonferroni's multiple comparisons test.

Significance values are reported as: * denotes P value $\leq$ 0.05; ** denotes P value $\leq$ 0.005; *** denotes P value $\leq$ 0.0005. All error bars are standard error of the mean (SEM).

9. RESULTS

9.1 Cutaneous Schwann cells- sensory neuron complex

Recently, cutaneous Schwann cells have been described as a specialized cell type associated with nociceptive sensory afferent endings forming a mesh-like glio-neural complex at the subepidermal border of the skin (Abdo et al., 2019). Activation of cutaneous Schwann cells, expressing channelrhodopsin, with blue light was shown to initiate nocifensive behaviors in mice. It was also shown that these cells were intrinsically mechanosensitive in patch clamp recordings from isolated Schwann cells showing membrane voltage changes to indentation stimuli (Abdo et al., 2019). These experiments suggested that the glio-neural complex has a physiological role in the mechanosensitivity of nociceptors. However, the physiological identity of the sensory afferents that are functionally coupled to the Schwann cell complex and how tightly they are coupled remained unclear.

9.1.1 Cutaneous Schwann cell selective connectivity to nociceptive sensory afferents

Mice expressing channelrhodopsin in Schwann cells under Sox10 transcription factor promoter, from now on called Sox10-ChR2 were used to perform *ex vivo* skin-tibial nerve preparation. This allowed to use blue light to stimulate specific Schwann cells and directly record from the associated afferent fiber. Mechano- and thermoreceptors were strongly activated by blue light stimuli and showed sustained firing during the light pulse (Figure 16A-B).

A-M nociceptors fibers are associated to pinprick nocifensive responses, showed responses to blue light stimulation of Schwann cells with only a few APs concentrated at the beginning of the stimulation. In the first four seconds of blue light photostimulation the firing rate varies between 2.19±0.77 to 1.13±0.51Hz, and then decayed to almost zero. Mechanical stimulation of A-M nociceptors typically displays a slow adapting firing to sustained static force with a firing rate between 21±3.08 to 7.45±1.36Hz, indicating a poor coupling between Schwann cells and A-M nociceptor, or it may be that nociceptive Schwann cells are only necessary for AP initiation rather than tonic firing in AMs (Figure 16A, B, E).

C-fibers can be classified according to their activation modality into C-fiber mechanonociceptors (or C-Ms); C- fiber polymodal responding to thermal and mechanical cues divided into C-mechanoheat (C-MH), C-mechanocold (C-MC) and C-mechanoheatcold (C-MHC).

All these C-fibers mechanosensitive recorded were considered nociceptors because their mechanical responses are in the noxious range. The mechanical response of C-Ms and C-polymodal fibers are comparable, with slightly higher firing rates seen in C-polymodal fibers in these recordings (Figure 16B, F, G). C-Ms firing rate to photostimulation was also slower compared to mechanical stimulation, 6±1.04 to 2.3±0.64Hz and 15.1±2.9 to 5.87±1.5Hz, respectively. Interestingly, similar responses were observed particularly in C-polymodal mechanonociceptors firing rate after Schwann cells photoactivation, 19±3.3 to 2.9±0.41 and 20±2.83 to 7.5±1.13, respectively. C-polymodal fibers display almost identical firing rates to mechanical activation as they do to blue light stimulation of nociceptive Schwann cells in the first 5 seconds of stimulation of each stimulus (Figure 16G).

It is important to note that response latency of C-M and C-polymodal fibers were significantly lower to light stimulation of Schwann cells (C-M= 23.4±11.76ms; C-polymodal= 64.89±10.64ms) than to mechanical activation (C-M= 17.57±5.3ms; C-polymodal= 81.02±13.82ms) respectively of the nociceptive sensory afferents (Figure 16D) indicating a direct coupling between the Schwann cells and the sensory afferent terminal ending.

C-thermoreceptors respond only to thermal stimuli. C-thermoheat (C-H) responses to heat, C-thermocold (C-C) to cold, and small proportion of C-thermoreceptors responded to heat and cold classified as C-thermoheatcold fibers (C-HC). During nociceptive Schwann cell photoactivation, all C-thermoreceptors recorded responded with tonic AP activity (Figure 16A, H). Unfortunately, it was only possible to do a qualitative classification of C-thermoreceptors applying hot or cold extracellular solution, without being able to distinguish between thermoreceptors and thermonociceptors.

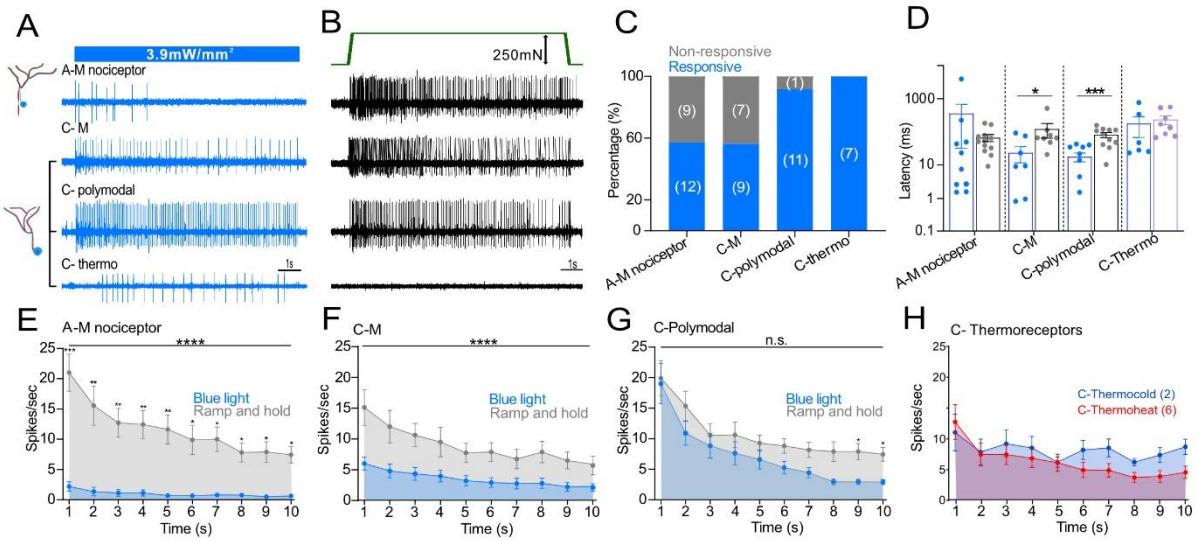

Figure 16. Nociceptive Schwann cells Sox10⁺ are strongly coupled to mechanonociceptors. (A-B) Representative traces of the different type of nociceptors recorded from ex vivo glabrous skin-tibial nerve preparation, firing activity recorded during blue light activation of Schwann cells (A) and mechanically evoked firing activity (B) of the same nociceptors previously recorded. (C) Number of nociceptors that responded to Schwann cells optogenetic activation. (D) Latency of Schwann cells activation by blue light compared to first AP generated to mechanical stimulation. (E-H) Time course of nociceptors AP firing activity during 10 seconds of blue light exposure. A-Ms (E) and C-Ms (F) firing rate is higher to mechanical than light stimulation, while C-fiber polymodal (G) (responding to mechanical and thermal stimulation) display similar activation of the sensory afferent to Schwann cell blue light activation as direct mechanical indentation (two-way ANOVA, $P<0.0001$ Bonferroni's multiple comparison test). Finally, C- fiber thermoreceptors (H) are display as responding to Schwann cells optogenetic, but not mechanical, stimulation. Data shown as mean ± SEM.

Nociceptive Schwann cell photostimulation was carried out using four increasing power intensities as described (Abdo et al., 2019). In Figure 16A, firing activity of the different type of nociceptors reached the maximum response already with the second intensity of blue light stimulation indicating the high sensitivity of nociceptors to Schwann cell photostimulation. However, as shown in Figure 16C, not all nociceptive sensory afferents recorded responded to the blue light protocols. Although, responsive and non-light responsive A-Ms, C-Ms, C-polymodal and C-thermoreceptors fibers have similar mechanical responsive properties to mechanical or thermal stimulation as well as threshold and conduction velocity (Figure 17E). Thus, a subpopulation with different mechanosensitivity does not appear to be specifically coupled to sensory Schwann cells.

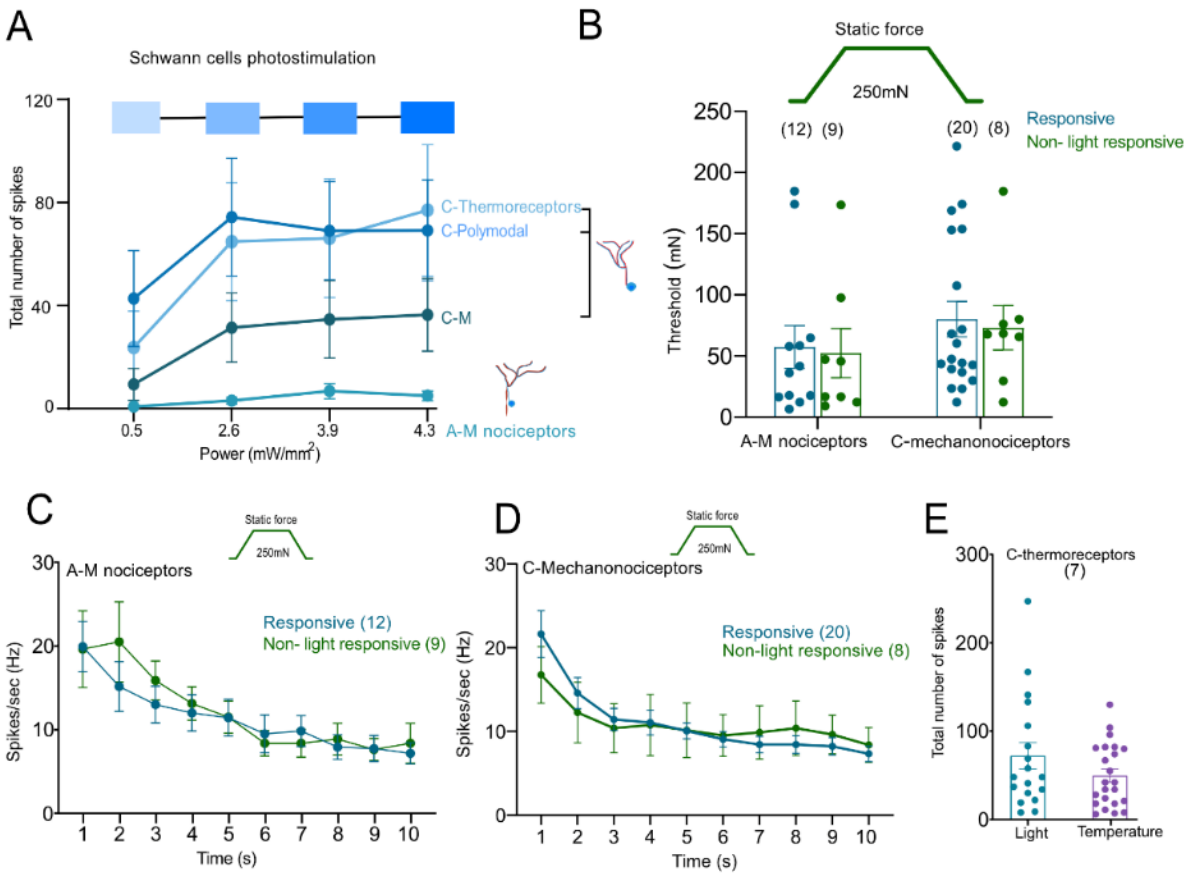

Figure 17. Responsive and non-light responsive nociceptors show similar responsive properties. (A) Action potential firing of nociceptors from Sox10-ChR2 mice to blue light stimulation (B) A-fiber nociceptors and C-mechanonociceptors show similar sensitivity and firing to increasing amplitude ramp-and-hold stimuli regardless of they were activated by blue light stimulation. (C) A-fiber nociceptors responsive and non-light responsive have similar firing frequency to 250mN ramp and hold stimulus. (D) C-mechanonociceptors, pulling out C-M and C-Polymodal have similar responses between responsive and non-light responsive to mechanical stimuli of 250mN. (E) C-thermoreceptors responded to light and thermal stimuli display similar firing rates. Data shown as mean ± SEM.

These results support a role for nociceptive Schwann cells in modulatory nociceptor sensitivity and excitability. Thus, C-fibers are more than free endings in the epidermis but exist in a functional complex with mechanosensitive Schwann cells. However, it does not imply a functional role of Schwann cells in mechanotransduction because the cations influx is artificially generated by ChR2 expression in Schwann cells. It is well known that sensory neurons possess a number of mechanosensitive ion channels that are necessary to transduce mechanical stimuli. Schwann cells being part of the nociceptive receptor could have a merely structural or sustaining role. Silencing the Schwann cells would shed light on whether they have a functional role in mechanotransduction.

Archeorhodopsin-3 (ArchT) is a yellow-green sensitive hyperpolarizing proton pump, that was expressed under the Sox10 transcription factor promoter to generate the Sox10-ArchT mice. An efflux of H^+ from the Schwann cells surrounding the nociceptive sensory afferents would hyperpolarize the membrane contrasting mechanosensitive depolarizing currents in the Schwann cells that could contribute to mechanotransduction in the nociceptive terminal ending.

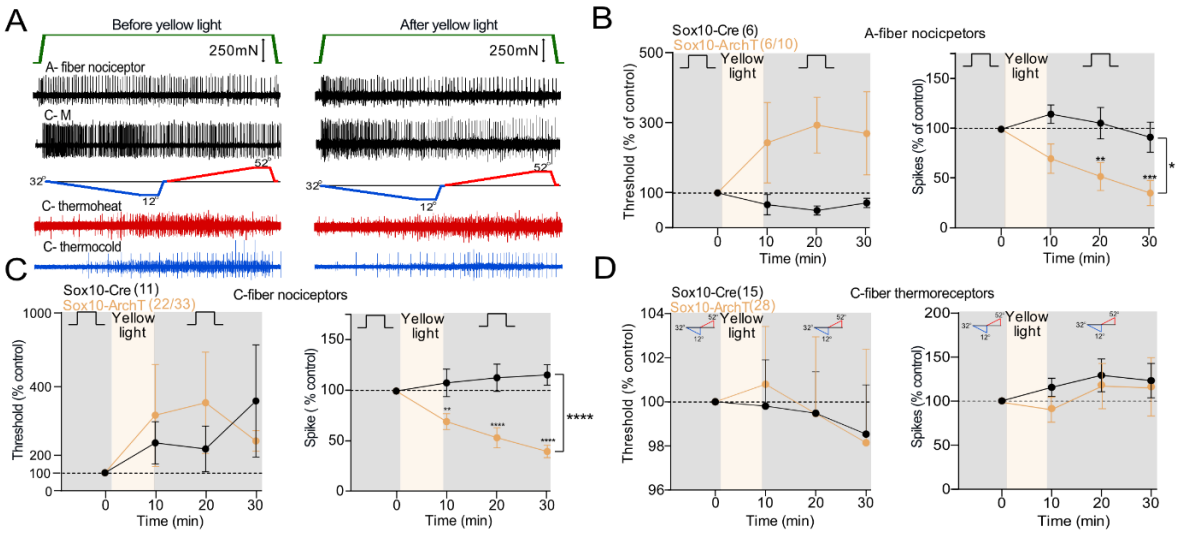

Figure 18. Silencing nociceptive Schwann cells reduce mechanical responses in nociceptive sensory afferents. (A) A-fiber nociceptors, C-Mechanonociceptors and C-thermoreceptors response before and after exposure of yellow light, only mechanical responses are diminished after silencing Schwann cells. (B) A-M fiber nociceptors recorded from Sox10-ArchT mice have a significant firing rate reduction during mechanical stimulation after yellow light exposure (two-way ANOVA, Bonferroni's multiple comparisons test, P< 0.05). (C) C-fiber nociceptors including C-M and C-polymodal firing rate to static force stimulation, whereas their threshold is unaffected to Schwann cells inactivation, their firing rate is significantly reduced after yellow light exposure (two-way ANOVA, Bonferroni's multiple comparisons test, P< 0.0001). (D) C-fiber thermoreceptors include C-polymodal fibers and C-thermoreceptors thermal respond to heat or cold ramps. Nor threshold or firing rate is affected after yellow light exposure of Schwann cells. Data shown as mean ± SEM.

All mechanosensitive nociceptors recorded from Sox10-ArchT were exposed to a 10 second mechanical ramp and hold stimulus of 250mN to evoke a maximal slowly adapting firing activity. Thereafter, $Sox10^+$ Schwann cells were silenced by exposure to yellow light for 10 minutes. The mechanical ramp and hold stimuli were repeated directly after yellow light photostimulation and monitored after photoinhibition and 10- and 20-minutes post-stimulation. Nociceptors recorded from Sox10-Cre mice, which did not express ArchT, were used as control using the same protocol.

A-fiber nociceptors mechanical threshold from Sox10-ArchT mice increased to more than 200% after yellow light exposure but it was very variable between sensory afferents recorded and not statistically significantly, but it was elevated compared to A-fiber nociceptors from Sox10-Cre mice that decreased to 702% after yellow light exposure (Figure 18B). The firing rate decreased to 65% of control after yellow light exposure and was reduced to 50% after 20 minutes after yellow light exposure (Figure 18B).

Similarly, C-fibers nociceptors mechanical threshold was variable in Sox10-ArchT and Sox10-Cre mice, increasing more than 200% and 400%, respectively, after yellow light exposure (Figure 18C). However, the firing rate after Schwann cells silencing decreased significantly and it was sustained 20 minutes after photoinhibition, to 70% and 40%, respectively in C-fiber nociceptors from Sox10-ArchT, while C-fiber nociceptors from Sox10-Cre kept firing at the same firing rate using the same stimulation (Figure 18C). These results indicate that nociceptive Schwann cells have a functional role in mechanotransduction of mechanical noxious stimuli to the nociceptive sensory afferent. Although further recordings are necessary, it is possible nociceptive Schwann cells set the threshold for AP firing in A-fiber nociceptors.

C-thermoreceptors electrophysiological properties were unaffected after yellow light inhibition of Schwann cells, regardless of their thermal sensitivity to heat or cold (Figure 18D). Thermal stimulation was achieved with a thermal device able heat or cool down a Peltier at the receptor field. Two types of ramps were generated: a heat ramp starting at 32°C and increasing 2°C per second until reaching 52°C after 10 seconds and coming back to the skin temperature of 32°C, as fast as possible; the second ramp was used to cool down the skin, starting at 32°C and decreasing 2°C per second until reaching 12°C after 10 seconds. This it might be because nociceptive Schwann cells do not express thermosensitive ion channels (Abdo et al., 2019). Besides the tight connection between Schwann cells and C-thermoreceptors, these nonneuronal cells do not appear to participate in the transduction of thermal stimuli.

All nociceptors recorded from Sox10-ArchT mice after Schwann cell inhibition by yellow light were compared with nociceptors recorded from Sox10-Cre mice, which do not express ArchT and therefore sensory afferent recorded are not affected by light stimulation, showing electrophysiological properties of nociceptive sensory afferents as increased threshold or reduced firing activity are directly related to Schwann cells silencing (Figure 18). In A-fiber and C-fiber nociceptors, spikes frequency response to a saturating ramp and hold stimulus of 250mN were comparable (Figure 19A, B). No significant differences were observed between the thermoreceptors recorded from Sox10-ArchT or Sox10-Cre (Figure 19C, D.

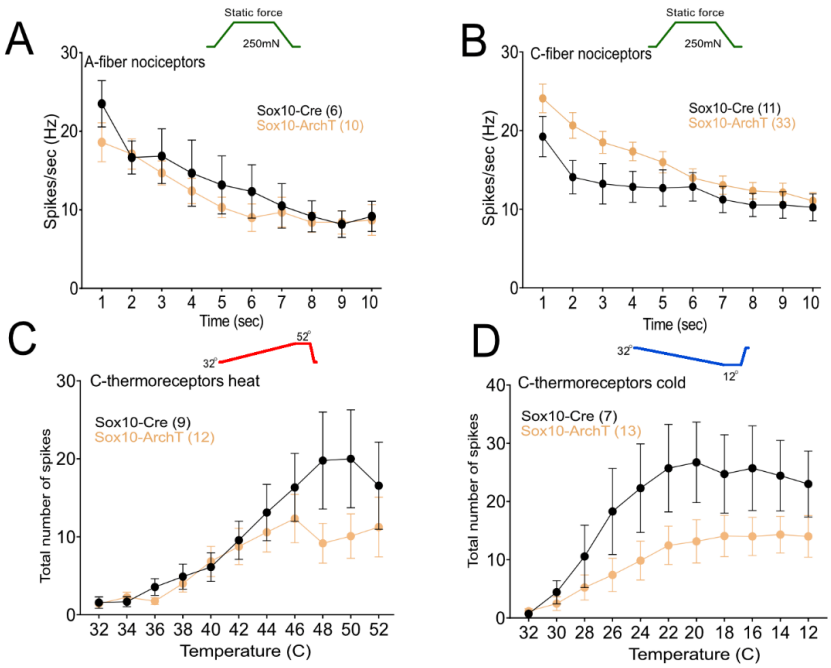

Figure 19. Nociceptors mechanical and thermal response in Sox10-ArchT and Sox10-Cre mice. (A) A-fiber nociceptors and C-fiber nociceptors (B) mechanical response to 250mN static force stimulation is comparable in Sox10-ArchT and Sox10-Cre. (C) C-thermoreceptors responding to heat ramp stimulation and (D) C-thermoreceptors sensitive to cold ramp stimulation are not different between Sox10-cre and Sox10-ArchT. Data shown as mean ± SEM.

9.1.2 Cutaneous Schwann cell participate in mechanotransduction in mechanoreceptors

Mechanoreceptors respond to touch, pressure, vibration and stretch. The ability to transduce different kinds of light mechanical forces requires specific electrophysiological properties in the sensory afferents as high sensitivity and adaptation. The functional properties observed in mechanoreceptors responses were attributed to the terminal ending of the sensory afferent. Besides that, unlike nociceptors, all cutaneous mechanoreceptors known form specialized receptors in the skin along with nonneuronal cells, these cells were thought to provide structural support. Meissner corpuscle and hair follicles are complex structures where cutaneous Schwann cells, or Lamellar cells, and sensory afferents are adjacent to each other and have a tight connection. In the Meissner corpuscle, Schwann cells form palisaded lamellar cells with Aβ-fibers in between that have been recently described as mechanosensitive in ducks (Nikolaev et al., 2020).

Using the same glia-specific Cre line (Sox10-CreERT2) coupled to the Rosa26-enhanced YFP ($R26R^{TOM}$) reporter line, from now called Sox10-TOM^{+}. Schwann cells $Sox10^{+}$ positive in the

Meissner corpuscle (Figure 20A), suggesting a similar functional connection in mechanoreceptors as was found in nociceptors. In most Meissner's corpuscles, we found 2-4 Sox10-TOM$^+$ cells to be intimately associated with the sensory endings of RAMs. Moreover, a subpopulation of these Schwann cells expressed another transcription factor known as Sox2. Using Sox10-TOM$^+$ reporter mice, a glabrous skin immunostaining against Sox2 showed that each Meissner corpuscle possess 1-2 Sox2-labeled cells located at the base of the end-organ (Figure 20B). Sox2$^+$ glial cells have been already described in satellite glial cells, non-myelinating Schwann cells, lamellar corpuscle Schwann cells in Meissner corpuscle, lanceolate endings in the hairy skin and in other epidermal components as Merkel cells forming part of the mechanoreceptor Merkel cell-neurite complex in the glabrous skin and touch domes in the hairy skin (Biernaskie et al., 2009; Kioke et al., 2014). However, the functional role of these two subtypes of Schwann cells in mechanotransduction is still elusive.

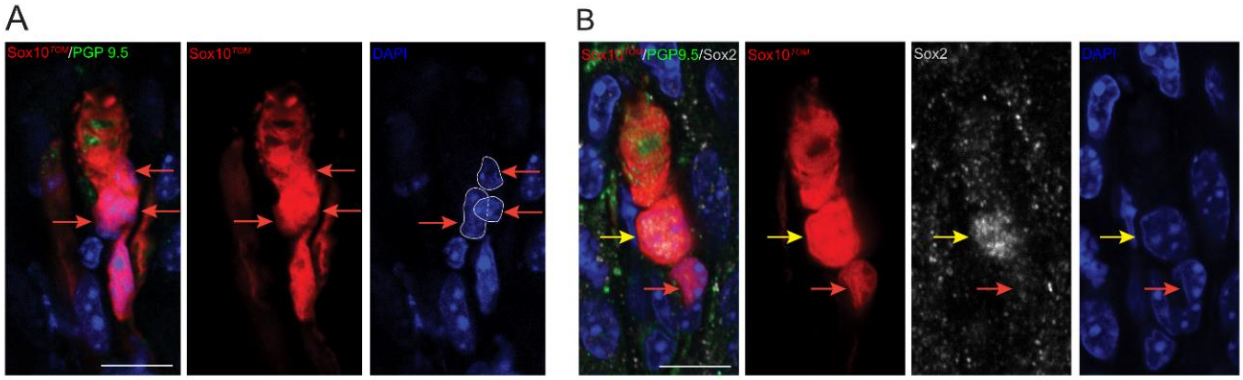

Figure 20. Targeted/specific recombination in Sox10-TOM mice selectively labels glial cells of Meissner corpuscles. (A) Recombination in glial cells of Meissner corpuscle in Sox10-TOM mice. Immunohistochemistry for TOMATO (recapitulating Sox10 expression) and PGP9.5 to label Meissner corpuscles. Right, individual channels. Arrows point to nuclei form recombined cells in the corpuscle. Scale bar: 20µm. (B) Sox2 represent a subpopulation of Sox10 Schwann cells in Meissner corpuscle. Immunohistochemistry for TOMATO (recapitulating Sox10 expression), for Sox2 and PGP9.5 to label Meissner corpuscles. Right, individual channels. Yellow arrow points to a nucleus from a recombined cell that also expresses Sox2, whereas red arrow shows a cell with just Sox10 expression in the corpuscle. Scale bar: 20µm. Immunostaining done by Laura Calvo-Enrique.

Meissner corpuscles in the glabrous skin are innervated by Aβ-fibers which display rapid adapting responses to mechanical stimulation, from now on called RAMs. Using Sox10-ChR2 mice, as previously described for nociceptors, RAMs sensory afferents were recorded and characterized according to their stereotypic mechanical response only during the dynamic phase of ramp and hold stimulation (Figure 21A).

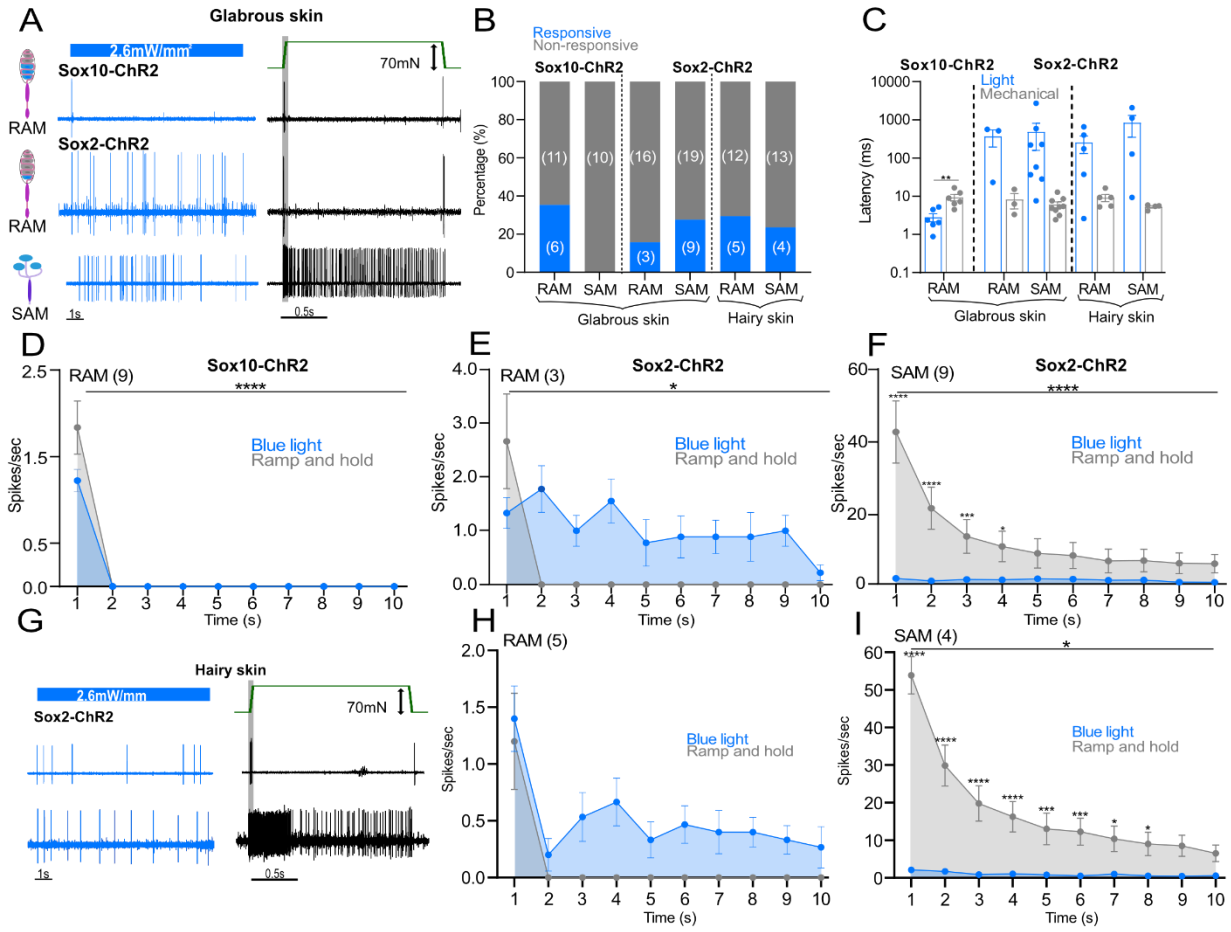

Figure 21. Sensory Schwann cells are necessary for rapid adapting mechanoreceptors sensitivity. (A) RAMs or SAMs activity recorded using the ex vivo hindpaw glabrous skin preparation. Left, blue traces correspond to blue light evoked activity. Right, black traces, activity evoked by ramp and hold mechanical stimuli to the same afferent. (B) Total number of mechanoreceptors (RAMs and SAMs) recorded from Sox10-ChR2 and Sox2-ChR2 mice, showing proportions of light responsive (blue) and non-responsive fibers (gray) mechanoreceptors. (C) First spike latencies for RAMs and SAMs comparing optogenetic activation of Schwann cells and mechanical activation of the same afferent during the ramp phase (in gray rectangle in A). RAMs recorded from Sox10-ChR2 mice respond faster to light stimulation than to ramp indentation applied at 15mm/s via piezo actuator (unpaired t test, $P < 0.05$). (D-F) RAMs (D) and SAMs (E, F) spiking activity plotted in 1 sec bins from Sox10-ChR2 10 and Sox2-ChR2 mice during 10sec of blue light or mechanical stimulation. In light-responsive RAMs from Sox10-ChR2, mechanical stimulation evoked much more spiking than light stimulation (two-way ANOVA, $P < 0.0001$). However, light-responsive RAMs from Sox2-ChR2 higher spiking rates to light stimulation than mechanical ramps (two-way ANOVA, $P < 0.05$, Bonferroni's multiple comparisons test). In addition, SAMs light-responsive spiking was lower to light stimulation than mechanical ramp and hold (two-way ANOVA, $P < 0.0001$, Bonferroni's multiple comparisons test). (G) RAMs or SAMs activity recorded from hindpaw hairy skin preparation. Left, blue traces correspond to blue light evoked activity. Right, black traces, activity evoked by ramp and hold mechanical stimuli to the same afferent. (H-I) RAMs and SAMs spiking activity plotted in 1 sec bins from Sox2-ChR2 mice during 10sec of blue light or mechanical stimulation recorded from hairy skin. Light-responsive RAMs from

Sox2-ChR2 exhibit higher spiking rates to light stimulation than mechanical ramps (two-way ANOVA, $P < 0.0001$, Bonferroni's multiple comparisons test). In addition, SAMs light-responsive spiking was lower to light stimulation than mechanical ramp and hold (two-way ANOVA, $P < 0.0001$, Bonferroni's multiple comparisons test). Data shown as mean ± SEM.

After photostimulation of $Sox10^+$ Schwann cells, similar responses in RAMs by mechanical stimulation were observed, with a few spikes at the beginning of the light exposure (Figure 21A, D). RAMs responsive to sensory Schwann cells photoactivation showed a statistically significantly shorter latency (2.8±0.69) for AP firing compared to RAMs latency (9.33±1.82) to a ramp mechanical stimulation (Figure 21C), indicating a direct coupling between Schwann cells and sensory afferents present in the Meissner corpuscle. It is important to note that only around a third part of all RAM sensory afferents recorded responded to blue light-activation of Schwann cells.

Slowly adapting sensory afferents found in the glabrous skin, now called SAMs, belong to Merkel cell-neurite complex. Merkel cells do not express $Sox10^+$ transcription factor and none of SAMs mechanoreceptors responded to blue light protocols (Figure 21B). This result shown that there is no non-specific effects of blue light photostimulation protocols in cutaneous mechanoreceptors.

As shown in Figure 20A, there is a subpopulation of glial cells $Sox10^+$ expressing $Sox2^+$ transcription factor, also found in Merkel cells. In order to test if Schwann cells $Sox2^+$ photostimulation can evoke firing activity of RAMs, a Sox2-ChR2 mice was generated as previously described in Abdo et al. (2019). Interestingly, activation of $Sox2^+$ Schwann cells evoked tonic firing activity in RAMs from Meissner corpuscle (Figure 21A, G). Similar results were found in RAMs recordings from in lanceolate terminals when $Sox2^+$ Schwan cells are photostimulated, indicating adaptation is not an exclusive property of the sensory afferent, at least depends on the interaction of sensory Schwann cells and the terminal ending (Figure 21E, H).

Previous work has shown that photostimulation depolarize Merkel cells in the touch domes and is sufficient to evoke action potential in SAI afferents when they express ChR2 under their epidermis-specific promoter K14, it was the first time using optogenetic tools to prove an excitatory connection between the epidermal Merkel cells and the cutaneous afferent that innervates them (Maksimovic et al., 2014; Shung et al., 2014). However, the light-evoked responses in Merkel cells can only explain the static phase of touch-evoked SAI responses and not action potential initiation or the high frequency response during the dynamic phase of mechanical stimulation. In our experiments, we have found comparable results stimulating $Sox2^+$ Merkel cells in recordings taken from skin nerve preparation from glabrous and hairy skin (Figure 21A, G).

$Sox2^+$ and $Sox10^+$ Schwann cells photostimulation generated a maximal response in mechanoreceptors at the low light intensity and progressively decreased with higher light intensity (Figure 22A). We compared the properties of non-responsive RAM mechanoreceptors to Schwann cell photostimulation in glabrous skin of Sox10-ChR2 and Sox2-ChR2 mice and found no differences in mechanosensitive properties such as threshold and response to velocity ramps (Figure 22B-D). In hairy skin from Sox2-ChR2 mice, RAM mechanoreceptors showed slightly lower sensitivity to ramp stimulation (Figure 22G).

SAMs responsive to Merkel cell photostimulation displayed a higher firing rate to ramp velocity and static force stimulation comparing to non-responsive SAMs recordings from glabrous skin of Sox2-ChR2 mice (Figure 22E, F). Responsive properties to mechanical stimulation of SAMs recorded from hairy skin of Sox2-ChR2 mice were not observed (Figure 22H, I).

In summary, there are two known types of sensory Schwann cells in Meissner corpuscles, $Sox10^+$ and $Sox10^+/Sox2^+$. These cells are compartmentalized, $Sox10^+$ positive Schwann cells are distributed along the Meissner corpuscle and are involved in threshold, sensitivity and transduction of mechanical forces to the terminal ending, while $Sox10^+/Sox2^+$ cells are closer to the bottom of the Meissner corpuscles presumably involve in AP firing rate.

As for nociceptors, Sox10-ArchT mice were used to silence sensory Schwann cells in mechanoreceptors recordings. A vibration protocol of 20Hz was used before and after 10 minutes yellow light exposure and repeated two times every 10 minutes to follow mechanoreceptors recovery, the same stimulation protocols were used in control mice Sox10-Cre and Sox2-ArchT. Figure 23A and B shown that there was a dramatic increase in the mechanical thresholds of RAMs in sensory Schwann cells $Sox10^+$ expressing, supporting a role for these cells in setting mechanotransduction sensitivity and threshold. A decreased following frequency from 60% to lower than 20% by the end of the recording indicates that RAMs coupling to Schwann cells is necessary to maintain Meissner corpuscle functional properties. In contrast, yellow light exposure to Schwann cells from Sox2-ArchT or Sox10-Cre mice, RAMs mechanical threshold decreased only 10% to vibration stimulus of 20Hz (Figure 21B).

Sox2 is also expressed in Merkel cells, yellow light exposure to SAMs showed no effect over threshold or firing rate (Figure 23C, D). However, it has been shown before that Merkel cells expressing ArchT and silenced with yellow light exposure only decreased their slowly adapting rate when the mechanical stimulation was simultaneously applied along with photostimulation (Maksimovic et al., 2014). In our experiments, light stimulation was followed by mechanical stimulation, then it is possible that Merkel cells and Aβ-fiber coupling is completely reestablished by the time SAMs activity was monitored.

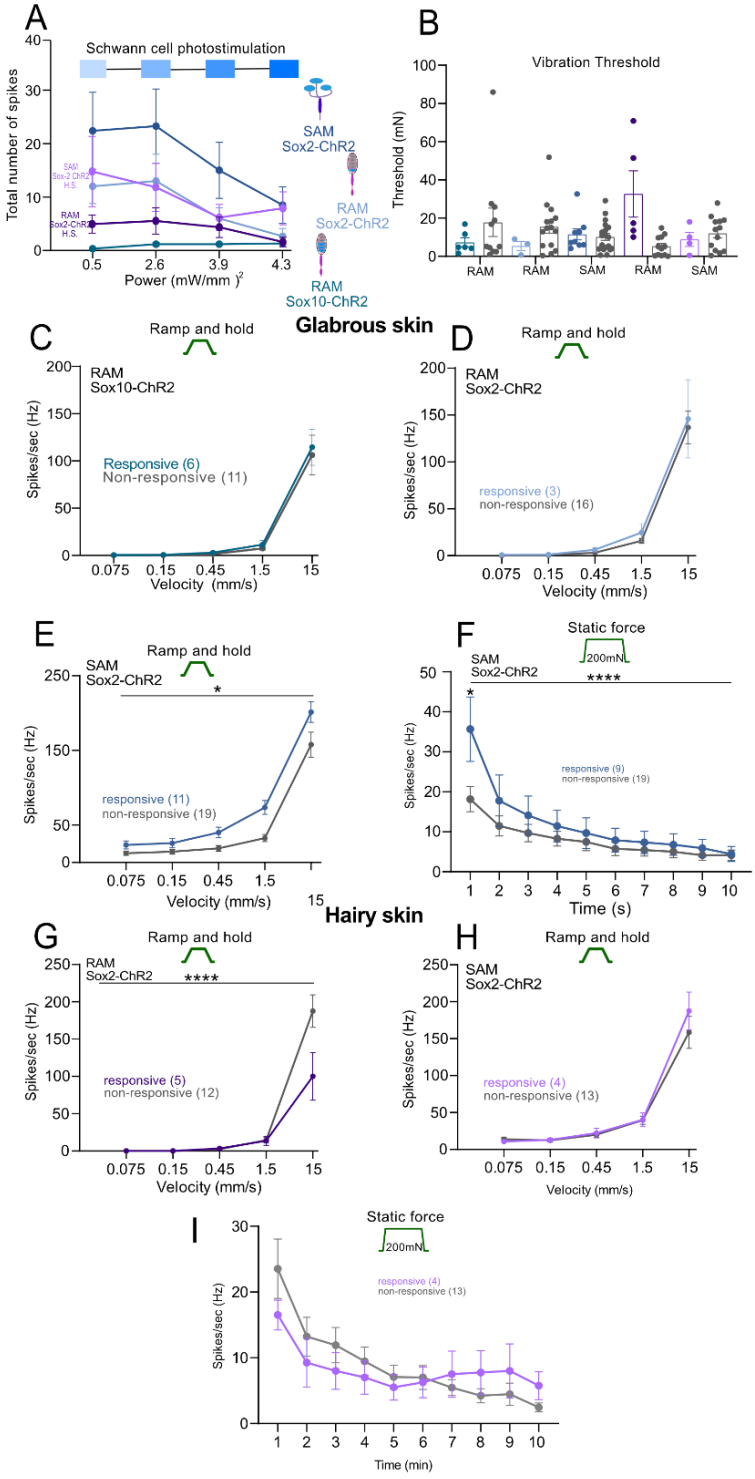

Figure 22. Mechanoreceptor properties of light responsive and light non-responsive afferents. (A) Action potential firing of RAMs and SAMs from Sox10 ChR2 and Sox2-ChR2 mice to blue light stimulation decreased slightly with increasing light intensity. (B) RAMs and SAMs show similar threshold irrespective of whether activated by blue

light. (C-D) RAMs responsive and light non-responsive to Schwann cells photostimulation have comparable ramp velocity responses in glabrous skin recordings from Sox10-ChR2 and Sox2-ChR2 mice. (E-F) SAMs responsive to photostimulation of Merkel cells Sox2^{+} have a higher firing rate to ramp velocity (E) and static force stimuli (F) (two-way ANOVA, P <0.001, Bonferroni multiple comparison's test). (G) RAMs responsive to Sox2^{+} Schwann cells blue light activation have a slight lower firing rate to ramp velocity compared to non-responsive sensory afferents (two-way ANOVA, P <0.001, Bonferroni multiple comparison's test). (H-I) SAMs recorded from responsive and light non-responsive to Merkel cell photostimulation have similar firing rate properties to ramp velocity (H) and static force stimulation (I). Data shown as mean ± SEM.

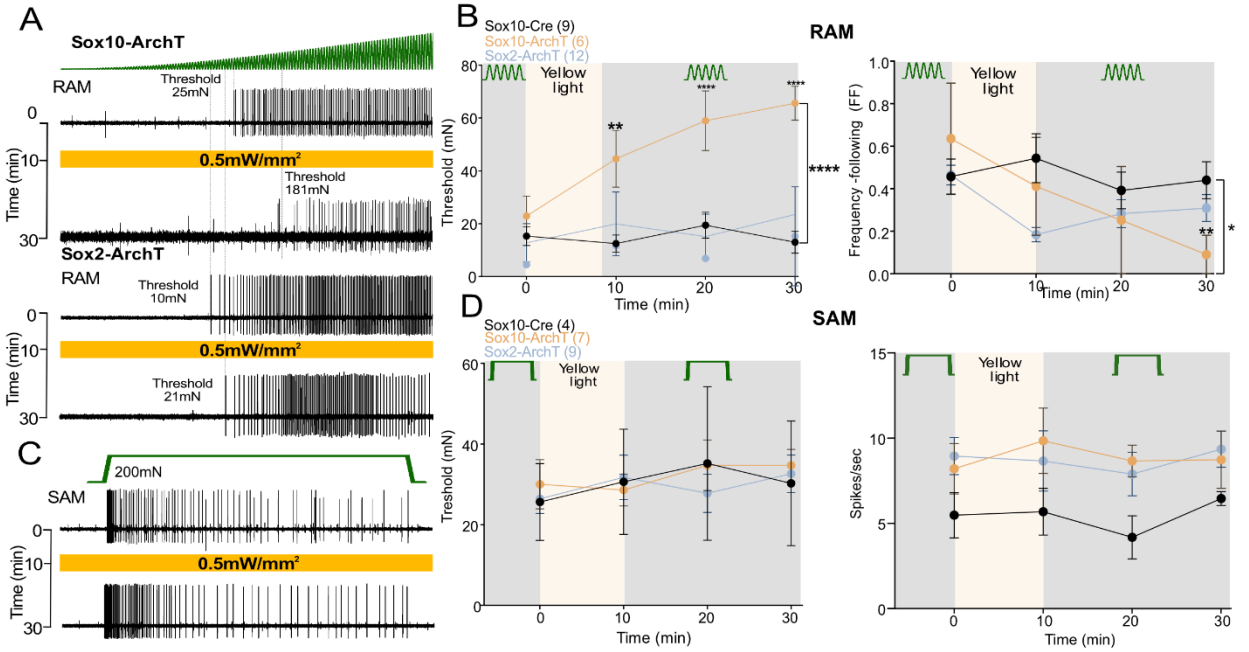

Figure 23. Sensory Schwann cells in the Meissner corpuscle are required for vibration sensing. (A) Mechanoreceptor spiking rates in response to 20Hz vibration stimulus before and after optogenetic inhibition of Schwann cells. Top, RAM representative trace of Sox10-ArchT mice; Bottom, the RAM representative traces from Sox2-ArchT mice. (B) Left, an increase in the absolute force necessary to evoke the first action potential was observed in RAMs recorded from Sox10-ArchT mice (Two-way ANOVA, P < 0.05, Bonferroni's multiple comparisons test); Right, the frequency-following rate decreased after yellow light stimulation in Sox10-ArchT+ mice 20 (two-way ANOVA, P = 0.05, Bonferroni's multiple comparisons test). (C) SAM representative traces of Sox2-ArchT mice to mechanical static force stimulation before and after yellow light photostimulation. (D) Left, absolute force necessary to evoke the first action potential to a ramp and hold stimuli, no changes are observed in SAM recorded from Sox10-ArchT, Sox10-Cre or Sox2-ArchT. Right, slow adapting response to static force does not change after yellow light exposure in SAM mechanoreceptors from Sox10-ArchT, Sox10-Cre or Sox2-ArchTmice. Data shown as mean ± SEM.

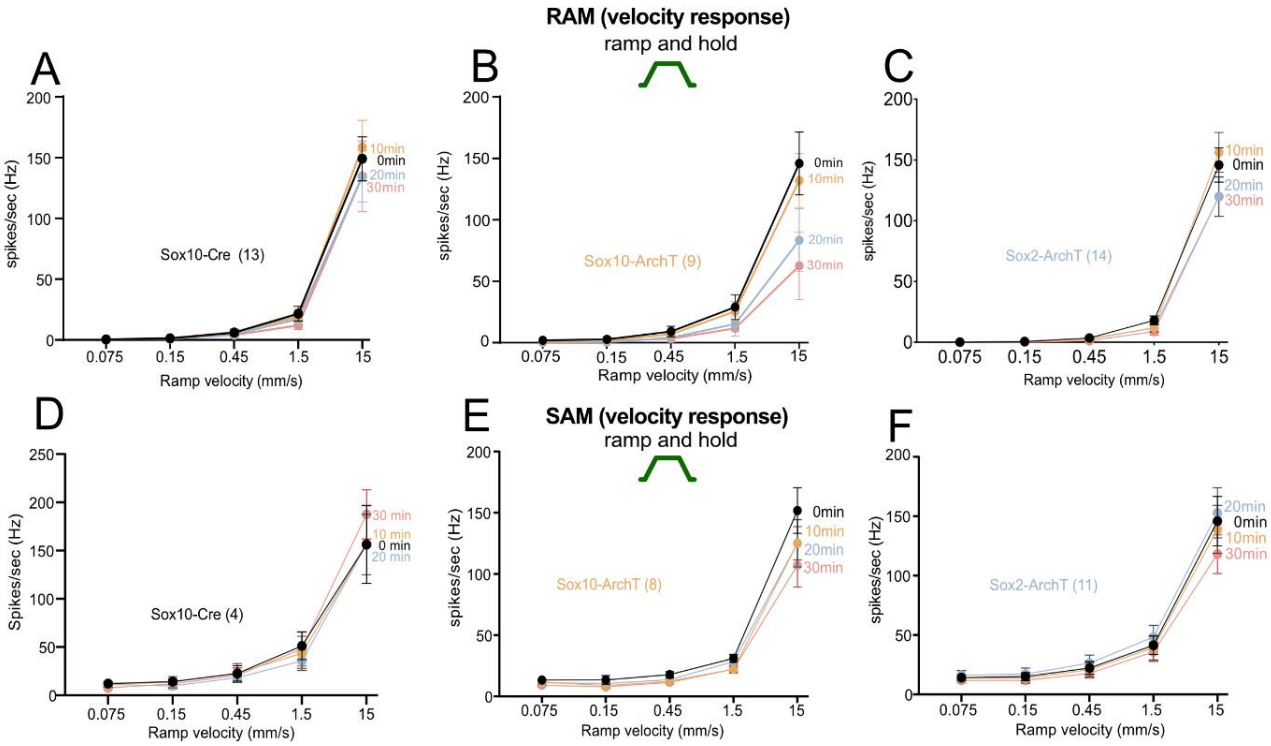

Figure 24. Fast velocity response of RAM mechanoreceptors decreases after sensory Schwann cells silencing. (A-C), ramp velocity response of RAM mechanoreceptors in control Sox10-Cre (left), Sox10-ArchT (middle) and Sox2-ArchT (right) decreases over the time after yellow light exposure. (D-F) ramp velocity response of SAM mechanoreceptors response does not change over time after yellow light silencing of Merkel, indicating these cells do not participate in fast movement detection. Left, Sox10-Cre; middle, Sox10-ArchT; right, Sox2-ArchT. Data shown as mean ± SEM.

Fast ramp stimulation protocols were used to test RAMs and SAMs sensitivity to ramp velocity stimuli. Only RAMs from Sox10-ArchT mice (Figure 24B) showed a significantly decreased sensitivity compared to controls of Sox10-Cre and Sox2-ArchT RAMs (Figure 20A, C). On the other hand, Merkel cells do not participate in the velocity response and sensitivity of SAMs (Maksimovic et al., 2014), no changes in ramp velocity sensitivity were observed in SAMS recorded from Sox10-ArchT or Sox10-Cre mice (Figure 24D, E). Additionally, SAMs responses to velocity does not change after yellow light silencing of $Sox2^{+}$ Merkel cells (Figure 24F), indicating these cells does not participate in AP initiation in Merkel cell-neurite complex.

9.1.3 Sensory Schwann cells mechanical indentation elicit mechanosensitive currents

Mechanosensitivity in nociceptive Schwann cells was suggested by Abdo et al. (2019) by whole-cell current-clamp recordings of voltages changes evoked by indentation in Schwann cells Sox10$^+$ culture. However, mechanically evoked depolarizations do not necessary implicate MS ion channel expression and activation in Schwann cells.

Here, in collaboration with Rakesh Kumar and Laura Enrique-Calvo, Schwann cells Sox10$^+$ cells were isolated from the skin and cultured for indentation in whole-cell recordings. Two main conditions were considered: first, whole-cell recordings were voltage-clamped to measure mechanically evoked currents and their kinetics; second, cell indentation was carried out in increasing steps where the probe was positioned close to the cell body and moving forward, and back to initial position, for each indentation step. Mechanically evoked currents were observed in Schwann cells Sox10$^+$ in a range of 2 to 12µm with relatively slow time constant for current activation (23±11ms) and inactivation (243±74ms) (Figure 25A, B). Normally, time constant of activation in sensory neurons is around 1ms, and only sensory neurons characterized with slowly adapting response (SA currents) reaches time constants of inactivation above 100ms (Hu & Lewin, 2006; Poole et al., 2014). Next, photostimulation of Schwann cells Sox10$^+$ was carried out isolating these cells from Sox10-ChR2 mice. The photostimulation protocol used was the same as in skin-nerve experiments, four blue light stimuli from 0.5 to 4.3mW/mm^2 of power (Figure 25C). Time constant of activation (24±5.9ms) and inactivation (765±97ms) by photostimulation and mechanical stimulation were comparable, although current inactivation was significantly higher after photostimulation (Figure 25E). Comparable current amplitudes were observed by photostimulation and indentation, the latest was slightly higher but not significant (Figure 25F).

Further experiments should be done to show if all Sox10$^+$ show similar mechanosensitive current kinetics. Considering that mechanoreceptors and nociceptors associated with sensory Schwann cells display very different mechanosensitive properties and response to different kind of mechanical stimulion.

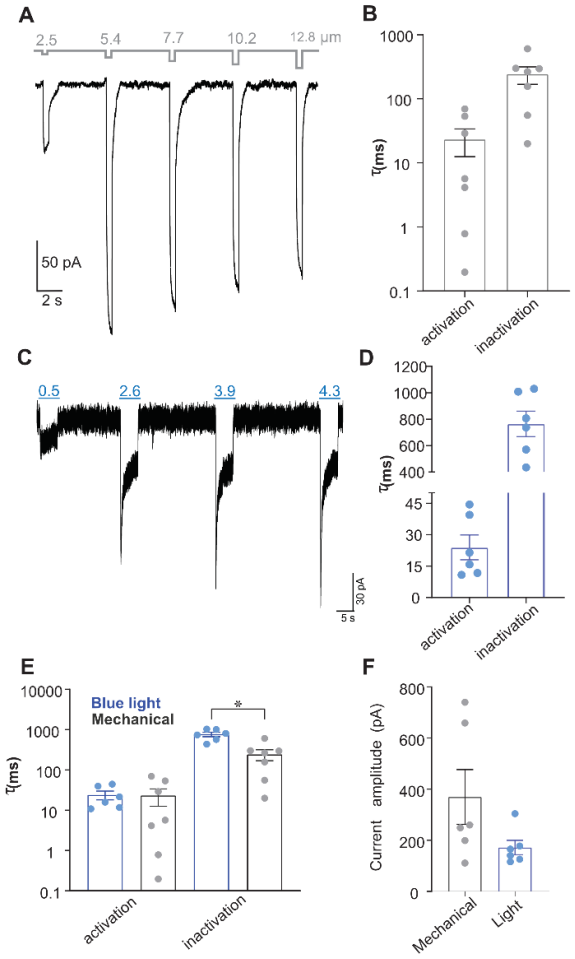

Figure 25. Schwann cells generate transient currents by mechanical or optogenetic stimulation. (A) Current traces evoked by increasing indentation stimuli in Schwann cells. Step displacement is pictured on top of the traces. (B) Current kinetics of activation (τ_1) and inactivation (τ_2) to mechanical stimulation. Data are displayed as individual values (n=7), activation= 23±11ms, inactivation= 243±74ms, Mean ± SEM. (C) Example traces of optogenetically activated currents (top, light intensity in mW/mm^2) in cultured terminal Schwann cells expressing channelrhodopsin-2 (2 DIV). (D) Activation and inactivation constants (τ) after blue light stimulation at saturating power (4.3mW/mm^2) in Sox10-ChR2$^+$, Data are displayed as individual values (n=6), activation 24±5.9ms, decay 765±97ms, Mean ± SEM. (E) Comparison of activation and inactivation constants to blue light (in blue) and mechanical stimulation (in gray). Unpaired t test, $P<0.05$, two-tailed. (F) Current amplitude values. Schwann cells tended to show larger currents in response to mechanical compared to blue light stimulation, but it is not statistically different. Patch clamp recordings and figure done by Rakesh Kumar and Laura Calvo-Enrique.

9.2 Role of TMEM150C/Tentonin3 protein in sensory mechanotransduction

Recently it was proposed that TMEM150C/Tentonin3 may be a mechanosensitive ion channel expressed in DRG neurons (Zhao et al., 2016). Whole-cell patch clamp recordings from DRG transfected with Ttn3 siRNA showed a reduction in slowly adapting mechanosensitive currents. Additionally, genetic ablation of the Ttn3 gene was shown to lead to a reduction in motor coordination indicating that TMEM150C/Tentonin3 may have a role in proprioception.

The results of Zhao et al (2016) became controversial when several researchers questioned the whole-cell recordings from HEK293T cells transfected with Ttn3 constructs as it was possible that mechanosensitive currents may have been due to low levels of Piezo1 channels in this cell line (Dubin et al., 2017). Using HEK293T cells in which the Piezo1 gene had been ablated (HEK293P1KO), these groups showed that overexpression of TMEM150C/Tentonin3 did not lead to the appearance of mechanosensitive currents evoked by cell indentation. Moreover, Anderson and colleagues (2018) repeated whole-cell recordings with TMEM150C/Tentonin3 co-expressed with mechanosensitive ion channels in HEK293P1KO and their results suggested that TMEM150C is an auxiliary subunit that enhanced the inactivation kinetics of mechano-gated ion channels like TREK-1 and Piezo channels (Anderson et al., 2018).

Regardless of whether TMEM150C/Tentonin3 is a mechano-gated ion channel or a mechanosensitive auxiliary subunit, its role in proprioceptor function and wide expression in the DRG suggested it might be involved in sensory neurons mechanotransduction. Here two TMEM150C knockout mutant mice were compared to test the role of TMEM150C gene in sensory neurons mechanotransduction.

9.2.1 N2a-P1KO cells overexpressing TMEM150C do not elicit mechanosensitive currents or enhancement of Piezo currents

N2a cells were used with a Piezo1 gene deletion generated by Moroni and collaborators (2018), now called N2a-P1KO, were used for whole-cell recordings and indentation (Figure 26A). N2aP1KO were transfected with mock DNA, TMEM150C or co-transfect with Piezo2 constructs, and whole-cell patch clamp recordings were made in these cells to measure mechanosensitive currents evoked by indentation. Recordings from N2aP1KO naïve compared to N2aP1KO transfected with TMEM150C show no apparent mechanosensitive current (Figure 26B, C), indicating that TMEM150C has no detectable intrinsic mechanosensitivity, as it has been shown before by Dubin and collaborators (2017) in HEK293 cells.

It has been proposed that TMEM150C enhances Piezo2 mechano-gated currents (Anderson et al., 2018). N2aP1KO transfected with Piezo2 and TMEM150C construct were compared to test mechanosensitive currents properties. The peak amplitude of mechanosensitive currents measured with increasing indentation of N2aP1KO cells transfected with Piezo2 channel and co-transfected with TMEM150C displayed a slightly higher amplitude, 953.2±242pA and 1109±232.7pA respectively, but this was not statistically different (Figure 26C, D). Additionally, the minimum indentation needed to elicit a mechanosensitive current considered as threshold was also not different between N2aP1KO transfected with Piezo2 channel and co-transfected with TMEM150C, 5±0.46 and 4.7±0.42µm, respectively (Figure 26E). Latency is considered as time needed to evoke the current after the indentation, similar values were observed in both cell recordings from Piezo2 channel and con-transfected with TMEM150C, 3.6±0.36 and 3.33±0.44ms, respectively. Finally, quantification of activation time constant (Ƭact) and inactivation time constant (Ƭact) from the mechanosensitive currents recorded showed no apparent differences between Piezo2 and double transfected N2aP1KO cells. Time constant of activation mean were 3.5±0.58ms and 3.6±0.5, in Piezo2 and co-transfected with TMEM150C, while time constant of inactivation were, 3.5±0.74 and 3.4±0.65, respectively.

In summary, no whole-cell recordings from cells transfected with Piezo2 or TMEM150C constructs indicated changes in the mechanosensitive properties and our data does not support a function for TMEM150C as a MS ion channel or modulator of Piezo2 channels.

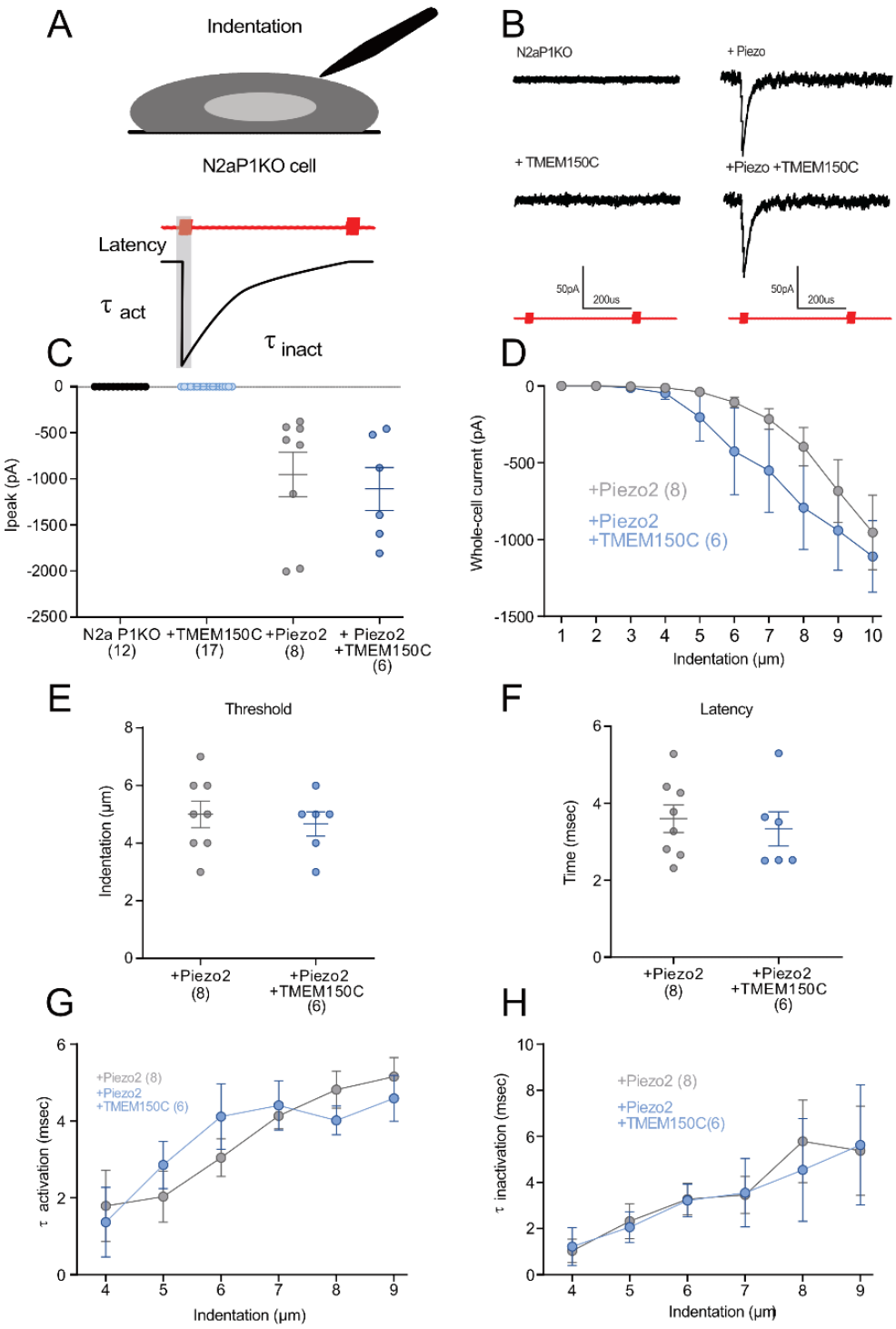

Figure 26. Overexpression of TMEM150C in N2aP1 KO cells does not evoke mechanosensitive currents or enhance mechano-gated currents of Piezo2 channels. (A) Schematic representation of cell indentation (on top) and mechanosensitive current evoked after mechanical stimulation (on bottom). Latency is measured as the time it takes

to evoke a current after the mechanical stimulation; Ƭact and Ƭinact rate, respectively. (B) Representative traces of mechanosensitive currents evoked after indentation. Left, N2aP1KO transfected with a vector or TMEM150C do not show mechanosensitive currents to stimulation. Right, Mechanosensitive currents to 5µm indentation in N2AP1KO overexpressing Piezo channel and a co-expressing TMEM150C. (C) Scatter plot showing the maximal whole-cell current observed in each cell recorded, only N2aP1KO overexpressing Piezo2 channel or in combination withTMEM150C showed mechanosensitive currents which comparable amplitudes. (D) Mechanosensitive current amplitude to increasing indentation with no significant differences. (E-F) Mechanosensitive current threshold (E) elicits by mechanical stimulation with not statistically differences and latency (F) as the time necessary to evoke a current, also with similar responses. (G-H) Activation and inactivation time constant, Ƭact and Ƭinact, are similar in cells transfected with Piezo2 or co-transfected with TMEM150C constructs. Data expressed as mean ± SEM.

9.2.2 Skin-nerve preparation in TMEM150C$^{LacZ/LacZ}$ by KOMP project

The same mouse line of TMEM150C knockout provided by KOMP project to Zhao and collaborators (2016) to describe the role of TMEM150C/Tentonin3 in proprioceptors, was used in this work to characterize cutaneous sensory receptor function. Sensory afferents from the saphenous nerve that innervates the hairy skin of the hindpaw were classified as mechanoreceptors low threshold rapidly and slowly adapting RAMs, SAMs and D-hairs; meanwhile nociceptors were considered as A-fiber nociceptors or C-fiber mechanonociceptors, displaying a high threshold and slow-adapting responses to mechanical stimulation.

The mechanical thresholds of RAMs (5.68±1.0mN), SAMs (5.61±1.08mN) and D-hairs (0.25±0.06mN) from wild-type mice and RAMs (4.6±1.1mN), SAMs (5.06±0.97 mN) and D-hair (0.37±0.12mN) from TMEM150C$^{LacZ/LacZ}$ mice to a 20Hz sine wave mechanical stimulation were similar (Figure 27A-C). Moreover, a series of increasing velocity ramp mechanical stimuli were applied to the same mechanoreceptors also revealed no differences between wild-type and TMEM150C$^{LacZ/LacZ}$ mice (Figure 27D-E). Additionally, SAMs and A-fiber and C-fiber nociceptors were analysed using increasing mechanical steps from 50 to 275mN to test their static force responses, where it was found again no differences between wild-type and TMEM150C$^{LacZ/LacZ}$ mice (Figure 27G-I). Finally, conduction velocities comparison as shown in Table 1 were unchanged between sensory afferents recorded from wild-type and TMEM150C$^{LacZ/LacZ}$ mice.

In summary, this deletion of TMEM150C using the KOMP strategy appeared to have no effect on cutaneous sensory neurons.

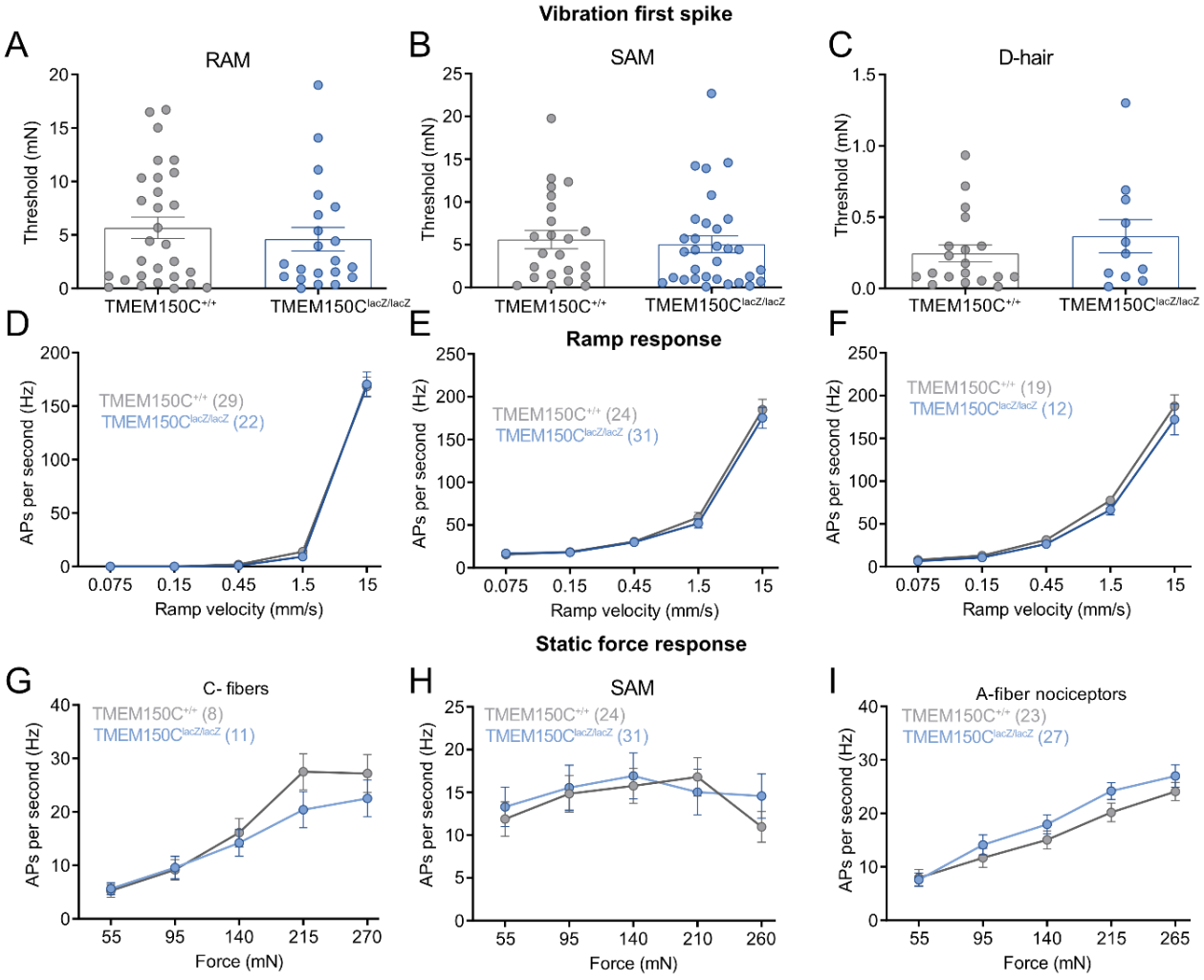

Figure 27. Mechanoreceptors responsive properties of TMEM150C KO to mechanical stimulation. (A-C) Mechanoreceptors threshold plot of TMEM150C$^{LacZ/LacZ}$ RAMs (A); SAMs (B); and D-hairs (C), showing similar sensitivity as WT recordings. (D-F) Ramp response to increasing velocities of ramp and hold stimulation show similar responses from mechanoreceptors recorded RAMs (D), SAMs (E) and D-hair (F) of wild-type and TMEM150C$^{LacZ/LacZ}$. (G-I) Mechanical static force stimulation of wild-type and TMEM150C$^{LacZ/LacZ}$ from C-fiber (G), SAM mechanoreceptors (H) and A-fiber nociceptors (I) showing similar response properties. Data expressed as mean ± SEM.

Table 1. Conduction velocities of sensory afferents recorded from Tmem150c$^{LacZ/LacZ}$ from hairy skin-nerve preparation.

	TMEM150C WT		Tmem150c$^{LacZ/LacZ}$
Aβ –fibers RAM CV (m/s)	13.44±0.65 (29)		14.43±0.86 (22)
t test		P>0.05	
SAM CV (m/s)	16.64±0.95 (24)		15.12±0.7 (31)
t test		P>0.05	
Aδ-fibers DH CV (m/s)	4.61±0.3 (19)		6.16±0.55 (12)
t test		P>0.05	
AM CV (m/s)	4.8±0.55 (23)		4.64±0.5 (27)
t test		P>0.05	
C-fibers C-M CV (m/s)	0.78±0.14 (8)		0.7±0.08 (11)
t test		P>0.05	
Total number	103		103

Mean values ± SEM are shown. Data set of wild-type were compared using a t test mutant TMEM150C KO.

9.2.3 Motor coordination in TMEM150C$^{Lacz/LacZ}$ seems to be similar to wild-type

Loss of motor coordination due to proprioceptors dysfunction in TMEM150C$^{LacZ/LacZ}$ was one of the major findings reported by Zhao and colleagues (2016).

Here, using the Mousewalk behavior test developed by Mendes and collaborators (2015), five mice from wild-type and TMEM150C$^{LacZ/LacZ}$ genotype were tested for motor performance. First, mice from both genotypes were placed on the walkway for habituation for half an hour, three days before testing. On the third day, 5 video recordings from each mouse were taken walking the length of the walkway (Figure 28A). Next, a 50cm length of the walk from each of the 5 videos per mouse was taken for analysis. The average speed of each walk (Figure 28B) considered as an overall motor performance was not different between wild-type and TMEM150C$^{LacZ/LacZ}$ mice. Swing speed and step distance represent the movement of the paw from the standing place to the next position and the distance covered respectively, separating anterior paws from posterior due to the differences in movement spread, none of these features were different between wild-type and TMEM150C$^{LacZ/LacZ}$ mice (Figure 28C-D). Swing regularity and leg distance dispersion show the standard deviation of each mice swing and footprint distance what it would indicate lack of step or limb coordination respectively, however no differences were observed between wild-

type and TMEM150C$^{LacZ/LacZ}$ mice (Figure 28E, F). Finally, legs and body linearity measure the ability of the mice to walk in a straight line considering the position of the legs and the body of stance respectively, also shown no differences between wild-type and TMEM150C$^{LacZ/LacZ}$ mice. In summary, there were no indications of loss of motor coordination in TMEM150C$^{LacZ/LacZ}$ in mousewalk recordings; speed, movement regularity and linearity were comparable to wild-type mice.

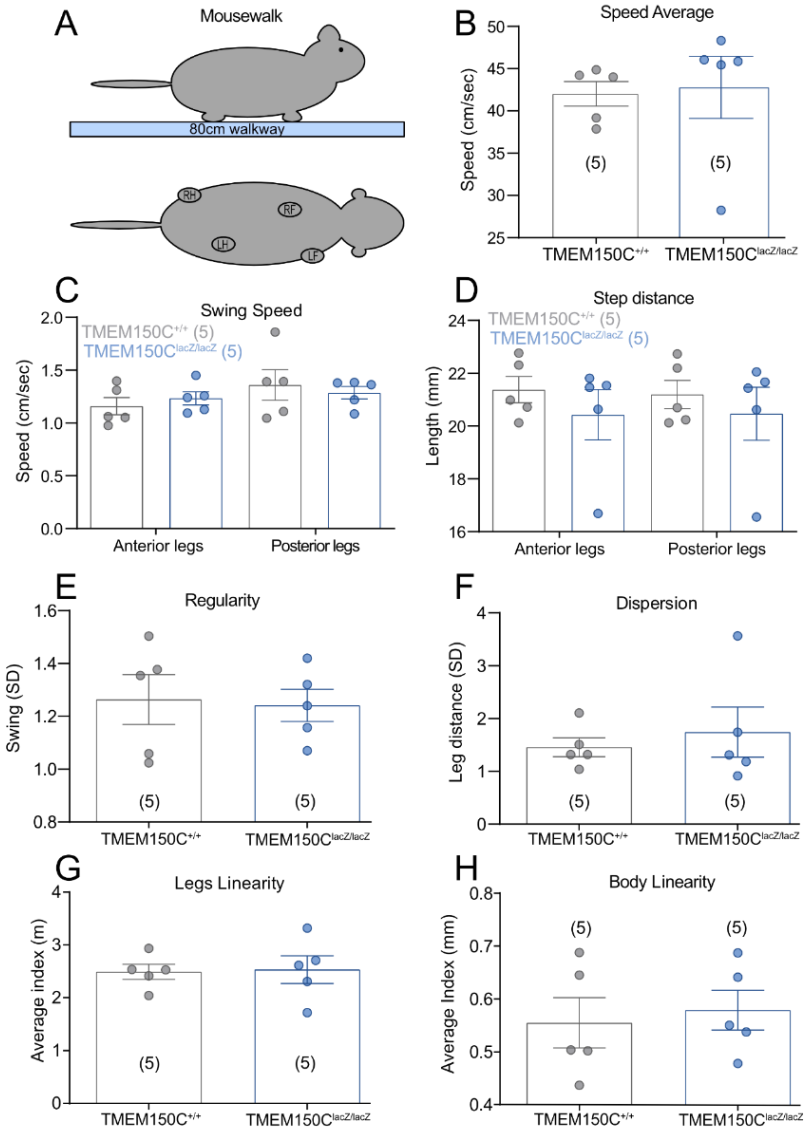

Figure 28. Mousewalk behavior test shows comparable motor coordination in TMEM150C KO to WT mice. (A) Scheme representing the Mousewalk configuration to test motor coordination. On top, a mouse is walking through a walkway of 80cm made of glass or acrylic allowing light illumination of the paws, body, tail and head of the mouse. On the bottom, there is a representative view of the mouse walking and how footprints are used to analyze each walk. (B) Average speed of each mouse from one extreme to the other in the walkway, showing no differences between WT

(42.02±1.45) and KO (42.79±3.67) mice. (C) Swing speed show the average for individual step from the anterior (WT 1.16±0.08; KO 1.23±0.06) and posterior legs (WT 1.36±0.14; KO 1.29±0.06) which have different features, however respectively comparable between the WT and mutant mice. (D) Step distance in between each swing, anterior legs (WT 21.38±0.5; KO 20.43±0.96) and posterior legs (WT 21.2±0.53; KO 20.47±1.0) are similar between WT and KO mice. (E) Regularity of swing plotting individual standard deviation per mice (WT 1.26±0.09; KO 1.24±0.06). (F) Dispersion of leg per step plotted as leg distance standard deviation (WT 1.46±0.18; KO 1.74±0.47) in general similar between wild-type and mutant. (G) Legs linearity measured as stance linearity index showing no difference between WT and KO (2.49±0.14; 2.53±0.26). (H) Body linearity shows the average index of stance, comparable linearity is found in WT and KO mice (WT 0.55±0.05; KO 0.57±0.04). Data expressed as mean ± SEM.

9.2.4 A new TMEM150C knockout mouse generated via CRISPR technology

The TMEM150C$^{LacZ/LacZ}$ mouse generated by the KOMP project inserted LacZ and neomycin cassettes between exons 5 and 6 of the gene locus from TMEM150C with a stop codon, resulting in a frame shift (Figure 29A). However, the start codon is conserved, and a truncated version of the protein could be generated by alternative splicing including the TM1, TM2, the pore-region like and part of TM3. A similar isoform is naturally generated from the gene that contains the three first transmembrane domains as well as the putative pore-like region (Lu et al., 2020). DRG showed no positive staining for β-galactosidase, yet it is present in epididymis staining (Figure 29B), alternative splicing could also elude the two cassettes inserted in the gene allele in DRG sensory neurons and express the wild-type protein. Moreover, an RT-PCR was carried out on cDNA from DRG tissue showing the bands of exon 4-6 and exon 6-8, prior and posterior to the targeted area of the allele, showing an inefficient ablation of the TMEM150C gene. Yet, in epididymis and live, used as positive and negative controls, the absence of the bands indicates an expected disruption of the gene (Figure 28C). Altogether, there is not enough evidence to indicate that TMEM150C$^{LacZ/LacZ}$ mouse has a global deletion of the gene. In DRGs, the TMEM150C could undergo a differential gene splicing that can generate a different isoform, or even, the wild-type protein.

A new knockout for TMEM150C gene was generated using CRISPR/Cas9 by the ingenious targeting laboratory, with this strategy a complete ablation of the gene was guaranteed, avoiding unspecific target mutations. Ablation of the gene Tmem150C using CRISPR/Cas9 technology was achieved by the deletion of nucleotide sequence between end of intron 1-2 and beginning of intron 5-6 (Figure 29D), from now on called TMEM150C$^{-/-}$, gRNA sequences were designed by Valérie Begay. The start codon and the three first transmembrane domains are removed, including the pore-like region, with a frame shift that avoids the translation of truncated versions of the TMEM150C/Ttn3 protein. A PCR performed on genomic DNA from ear biopsies from WT

and heterozygous and TMEM150C have shown the wild-type amplicon (179bp fragment) is not present in TMEM150C$^{-/-}$ tissue samples, while the null allele amplicon (886bp fragment) is founded (Figure 29D). It is worth noting that the full wild-type allele (3039bp fragment) was not possible to generate with the chosen PCR conditions, genotyping PCR was stablished by Valérie Begay.

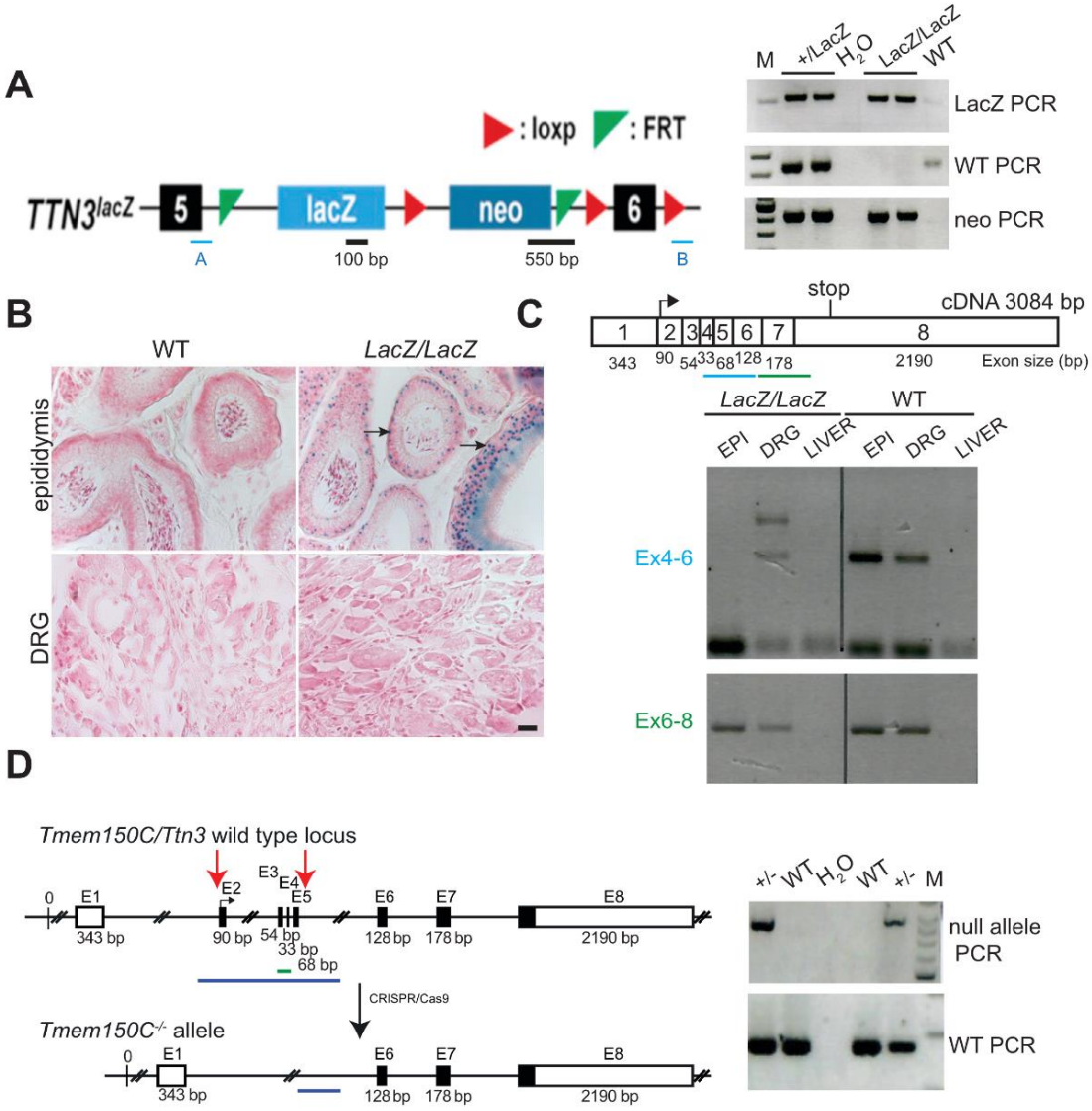

Figure 29. TMEM150C gene ablation with two gene editing techniques. (A) The Tmem150c/Ttn3 mouse (TMEM150C$^{LacZ/LacZ}$) was generated by the trans-National Institutes of Health Mouse initiative knockout Mouse project (KOMP). Briefly, a LacZ cassette and a neomycin cassette were inserted between exons 5 and 6 of the TMEM150C locus with a stop codon, which resulted in a frame shift. Gels of PCR results for neomycin cassette, LacZ cassette and wild type (WT) bands are shown. Genomic DNA from WT, heterozygous and homozygous mice were analyzed. (B) β-galactosidase staining (arrow) of epididymis (positive control) and DRG in WT and TMEM150C$^{LacZ/LacZ}$ mice, scale bar

= 20 µm. (C) Top panel shows a schematic representation of Tmem150c/Ttn3 cDNA containing 8 exons (1-8) with the start codon located in exon 2 (2) and the stop codon located in exon 8 (8). In the bottom panel, RT-PCR performed on cDNA prepared from tissues of WT mice and Tmem150c$^{LacZ/LacZ}$ mice with the blue line indicating amplicon covering exon 4 to 6 (the targeted area of Tmem150c$^{LacZ/LacZ}$ allele) and the green line indicating amplicon covering end of exon 6 to beginning of exon 8. EPI: epididymis (positive control), DRG: dorsal root ganglia, and liver (negative control). (D). Generation of Tmem150c knock-out (TMEM150C$^{-/-}$) using CRISPR/Cas9 technology leading to the deletion of nucleotide sequence between end of intron 1-2 and beginning of intron 5-6. In the left panel a schematic representation of the WT allele and null allele (KO): Exon1 (E1) encodes the 5'UTR and E8 the 3'UTR (white box). Black box: coding sequence. Red arrows indicate the location of gRNA sequences used for CRISPR/Cas9. In the Right panel a PCR performed on genomic DNA from WT and heterozygous mice are shown. The WT amplicon is represented by the green line in the scheme covering E3 and E4 (179 bp). The null allele amplicon is represented by the blue line producing an 886 bp fragment when the nucleotide sequence between intron 1-2 and intron 5-6 (3039 bp in WT) is deleted such in the null allele (+/-). M: DNA marker. Experiments and gRNA design of gRNA for CRISPR/cas9 ablation of TMEM150C gene was made by Valérie Begay.

9.2.5 Skin nerve preparation of TMEM150C$^{-/-}$ mouse

A comparison between wild-type mice and the new generated CRISPR knockout for TMEM150C gene, TMEM150C$^{-/-}$ mice, was carried out using the *ex vivo* skin-nerve preparation from the glabrous skin of the hindpaw of 5 wild-type mice and 4 mutant mice of both sexes, recording from sensory afferents of the tibial nerve.

Mechanoreceptors RAM, SAM and D-hair sensory afferents were recorded, and their conduction velocities measured, as it is shown in Table 2 no differences are found between wild-type and TMEM150C$^{-/-}$ mice. Two mechanical stimulation protocols were used to characterize mechanosensitivity of mechanoreceptors using a sinusoidal wave of 20Hz and a ramp and hold at increasing velocities. Threshold was quantified by measuring the force required to evoke the first spike and velocity sensitivity was measured by counting spikes evoked by different ramp and hold stimuli. There are no differences in the mechanical threshold of RAM (6.98±1.95mN), SAM (11.26±1.96mN) and D-hair (2.47±0.99) mechanoreceptors of wild-type and RAM (7.82±2.89mN), SAM (7.09±2.13mN) and D-hair (2.18±0.61) mechanoreceptors of TMEM150C$^{-/-}$ mice (Figure 30A-D). Moreover, SAMs first spike threshold to ramp and hold mechanical stimulation was also similar between wild-type and TMEM150C$^{-/-}$ mice (Figure 230A-E). Interestingly, SAMs responsive properties displayed a slightly increased firing rate to ramp velocity stimulation in TMEM150$^{-/-}$ mice (Figure 30D). Additionally, SAMs responsive properties to an increasing static force protocol also showed an increased firing rate from TMEM150$^{-/-}$ mice compared to WT, although this result was not statistically significant (Figure 30H). Further recordings are necessary

to determinate whether SAMs mechanoreceptors slowly adapting become more responsive after TMEM150C gene ablation.

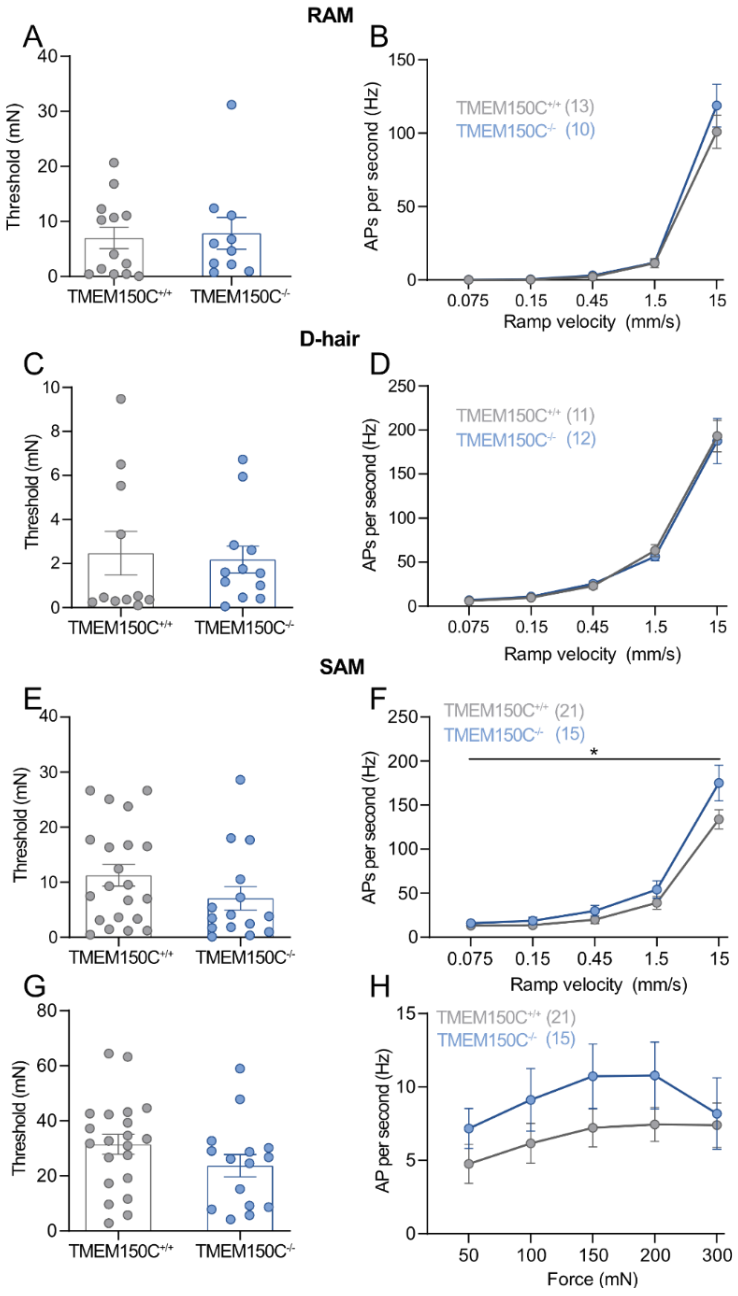

Figure 30. Mechanoreceptors response properties in TMEM150C$^{-/-}$ mice. (A) RAMs threshold plot from TMEM150C$^{+/+}$ and TMEM150C$^{-/-}$ mice showing no significant difference. (B) Ramp velocity response comparing wild-type and TMEM150C$^{-/-}$ mice, with no significant differences. (C) D-hairs threshold plot from TMEM150C$^{+/+}$ and TMEM150C$^{-/-}$ mice showing no significant difference. (D) Ramp velocity response comparing wild-type and TMEM150C$^{-/-}$ mice, with no significant differences. (E) SAMs threshold plot from TMEM150C$^{+/+}$ and TMEM150C$^{-/-}$ mice

showing no significant difference. (F) SAMs mechanoreceptors showing higher firing rate to velocity ramp and hold stimulation in TMEM150C$^{-/-}$ than WT (two-way ANOVA, P< 0.05, Bonferroni's multiple comparison test). (G) First spike threshold plot from TMEM150C$^{+/+}$ and TMEM150C$^{-/-}$ mice respectively, showing no significant difference to first spike. (H) SAMs mechanoreceptors AP activity to static force stimuli showing no significant difference between TMEM150C$^{+/+}$ and TMEM150C$^{-/-}$ mice. Data expressed as mean ± SEM.

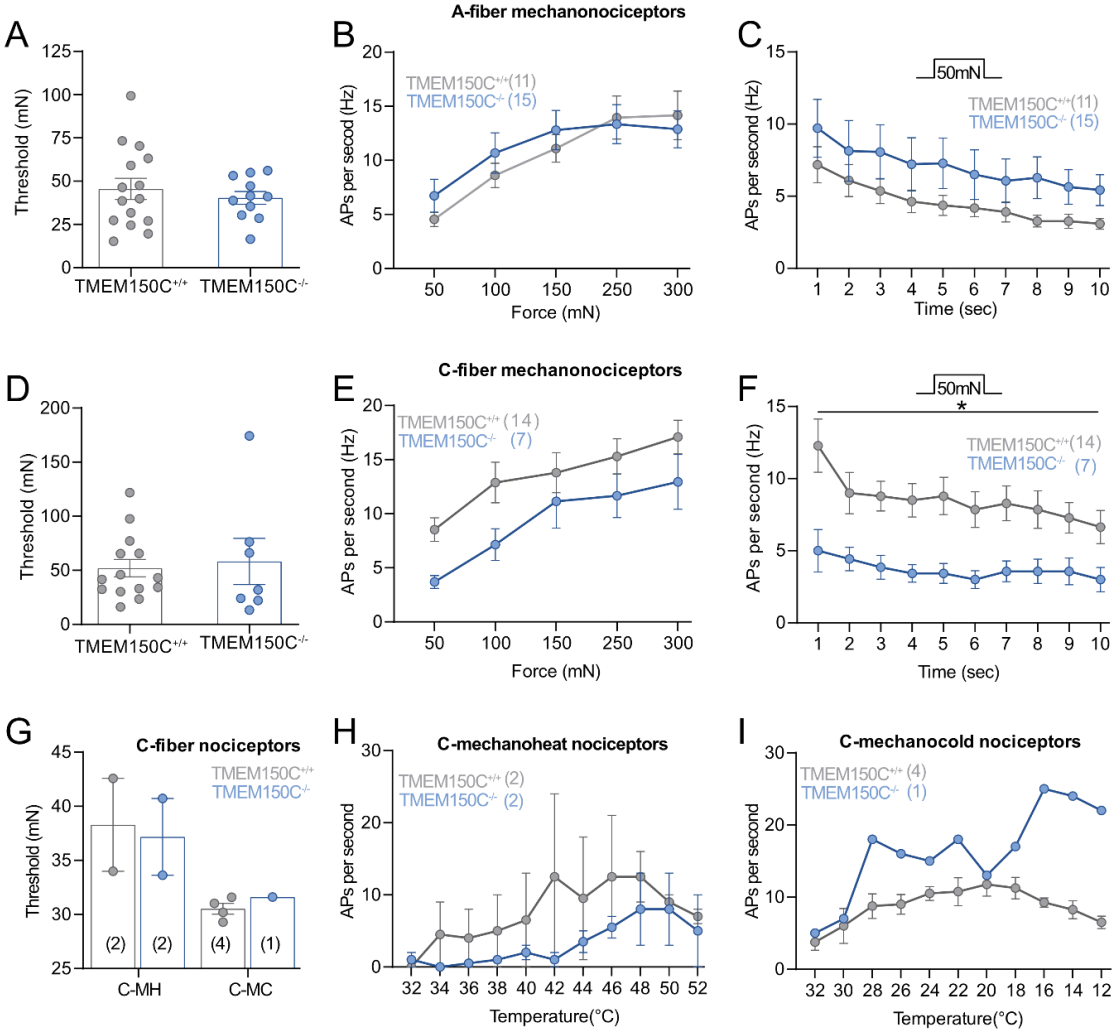

Figure 31. Response properties of nociceptors to static force stimulation in TMEMT150C$^{-/-}$ mice. (A) A-fiber mechanonociceptors first spike threshold from TMEM150C$^{+/+}$ and TMEM150C$^{-/-}$ mice which are not significantly different. (B) A-fiber mechanonociceptors firing rate to increasing static force stimulation are similar between wild-type and TMEM150C$^{-/-}$ mice. (C) APs activity to 50mN static force simulation showing TMEM150C$^{-/-}$ slightly higher firing rate than wild-type mice but not significant. (D) C-fiber mechanonociceptors first spike threshold stimulation from TMEM150C$^{+/+}$ and TMEM150C$^{-/-}$ mice are similar. (E) C-fiber mechanonociceptors firing rate to static force stimulation is slightly lower in TMEM150C$^{-/-}$ than wild-type mice, although not statistically significant. (F) C-fiber mechanonociceptors APs activity to 50mN static force showing TMEM150C$^{-/-}$ sensory afferents significantly lower firing

rate than wild-type mice (two-way ANOVA, P<0.05 Bonferroni's multiple comparison test). (G-H) C-fiber nociceptors response to thermal stimulation as threshold (G) of the first spike for C-MH and C-MC to heating and cooling ramp, respectively. (H) C-MH APs activity to heating ramp from 32°C to 52°C, apparently TMEM150C$^{-/-}$ thermosensitive afferents show less firing response. (I) C-MC APs activity to cooling ramp from 32°C to 12°C, TMEM150C$^{-/-}$ thermosensitive afferents show two spike burst firing response. Data expressed as mean ± SEM.

Table 2. Conduction velocities of TMEM150C$^{-/-}$ compared to WT mice.

	TMEM150C$^{+/+}$		TMEM150C$^{-/-}$
Aβ –fibers RAM CV (m/s)	14.55±1.04 (13)		12.24±0.66 (10)
t test		P>0.05	
SAM CV (m/s)	12.29±0.47 (21)		11.41±0.30 (15)
t test		P>0.05	
Aδ-fibers DH CV (m/s)	6.88±0.45 (11)		6.81±0.45 (12)
t test		P>0.05	
AM CV (m/s)	4.65±0.67 (11)		3.67±0.50 (15)
t test		P>0.05	
C-fibers CV (m/s)	0.56±0.07 (14)		0.68±0.11 (7)
t test		P>0.05	
Total number	70		59

Mean values ± SEM are shown. Data set of wild-type were compared using a t test mutant TMEM150C KO.

Nociceptive sensory afferents were also recording using the same skin-tibial nerve preparation. A-fiber and C-fiber nociceptors were evoked with increasing static force to measure their stimulus-response properties. Threshold was considered as the first spike elicited by the ramp before reaching the static force stimulation, no significant difference was observed between A-fiber mechanoreceptors, 40.35±3.7mN and 45.55±6.07 mN of wild-type and TMEM150$^{-/-}$ mice (Figure 31A, D, G). A-fiber nociceptors showed a slightly higher firing rates during the static force stimulation in TMEM150C$^{-/-}$ compared to WT mice (Figure 30B), the firing rate difference was

more prominent at lower forces such as 50mN force stimulation (Figure 31C). Although the differences between wild-type and TMEM150C$^{-/-}$ were not statistically significant, similar response was observed in SAMs mechanoreceptors (Figure 30H).

C-fiber nociceptor mechanical threshold of wild-type mice (51.99±8.05mN) and TMEM150C$^{-/-}$ (58.26±21.3MmN) were comparable. The responsive properties to static force stimuli showed overall reduced activity in TMEM150C$^{-/-}$ mice compared to WT mice (Figure 31E). Particularly at lower force magnitudes, comparison of the firing rate to a 50mN static force stimulation was 50% less in TMEM150C$^{-/-}$ compared to wild-type (Figure 31F), although the number of fibers recorded should be increased to assure that this result robust.

Finally, C-fiber thermosensitivity was also recorded using a heat ramp from 32° to 52°, or a cold ramp from 32° to 12° (Figure 31G-I). Although, it seemed that C-mechanoheat afferents from TMEM150C$^{-/-}$ were less responsive to heat ramp stimulation, it is necessary to increase the number of recordings to determinate if there is a statistically robust difference in TMEM150C$^{-/-}$ mice compared to WT. Conduction velocities from all sensory afferents recorded, mechanoreceptors and nociceptors, showed in Table 2 were comparable between wild-type and TMEM150C$^{-/-}$ mice.

10 . DISCUSSION

10.1 Sensory Schwann cells in sensory neurons mechanotransduction

Specialized cutaneous Schwann cells are coupled to terminal endings of sensory neurons as specialized lamellar cells in Meissner corpuscle, and nociceptive Schwann cells forming a glial-neural end organ in the skin. Here, the role of these sensory Schwann cells $Sox10^{+}$ as mechanosensitive cells and component of specialized receptors in the skin necessary to transduce mechanical stimulation was evaluated.

10.1.1 Role of specialized Schwann cells in nociception

Nociceptors have been considered as having free endings in the skin since they were initially described. In 2019, Abdo and collaborators proposed a specialized organization of nociceptors associated with epidermal Schwann cells called glio-neural end-organs, describing a functional connection between mechanosensitive nociceptors and Schwann cells. However, in that work it was impossible to determinate which kind of nociceptors were associated with this specialized structure. Central questions to address were thus, which specific kind of nociceptive sensory afferents are associated to nociceptive Schwann cells? What kind of connection is sustained between the two types of cells especially during noxious stimuli transduction? And finally, What is the contribution of Schwann cells to the sensory afferent functional response?

Here, I have shown that nociceptive Schwann cells are associated with all type of nociceptors that innervate the glabrous skin of the hindpaw of the mouse: A-fiber nociceptors, C-mechanonociceptors, C-fibers polymodal and C-thermoreceptors. However, the Schwann cell contribution to nociceptor function was distinctive for each of these receptor types.

A-Ms nociceptors are associated to pinprick pain responses, which evoke a coordinated and rapid paw-withdrawal reflex (Arcourt et al., 2017; Nagi et al., 2019). Blue light activation of nociceptive Schwann cells evoked a low-level activity in A-Ms nociceptors but with a relatively fast activation (Figure 16A-D). It is possible that nociceptive Schwann cells are necessary for AP initiation in A-Ms rather than a sustained firing activity. Slow frequency trains of 0.2Hz of photostimulation pulses to nociceptive Schwann cells, evoked one AP at the beginning of the stimulation in A-fiber nociceptors (data not shown). However, this protocol was tested only in two sensory fibers and further experiments are necessary with different frequency protocols to test this hypothesis.

C-fibers are a very diverse group of sensory receptors that has been classified by their responsive properties to modalities such as noxious mechanical or thermal stimuli in three major groups C-Mechanoreceptors (C-M), C-Mechanoheat (C-MH) and C-mechanocold (C-MC) (Moshourab & Lewin, 2004). Photostimulation of nociceptive Schwann cells elicited a sustained firing activity in C-M and C-fiber polymodal as long as the 10 seconds of blue light exposure. C-Ms showed a lower firing rate to nociceptive Schwann cells photostimulation than mechanical stimulation, between 6-2Hz and 15-5Hz, respectively. More interestingly, C-fiber polymodal (C-MH and C-MC) firing rates to nociceptive Schwann cell photostimulation evoked similar firing activity as static force mechanical stimulation, firing rate varies between 19-7Hz and 20-9Hz respectively. Thereafter, the firing rate decayed faster to blue light exposure than to mechanical stimulation, but this difference was not statistically significant (Figure 16F, D). C-fibers responding to thermal stimulation were qualitatively classified by applying hot or cold extracellular solution, C-fiber polymodal or thermoreceptors, showed a sustained firing activity to nociceptive Schwann cell photostimulation, but it was not possible to do a comparable quantification of both responses. Keratinocytes have been also proposed as modulators of nociceptors terminal endings for thermal and mechanical transduction, they form part of the epidermis and may directly contact with Aδ- and C-fiber terminal endings. Keratinocytes have been shown to express thermosensitive ion channels such as TRPV1 and the mechanosensitive ion channel Piezo 1, as well as produce neurotransmitters such as ATP, acetylcholine and glutamate that could influence sensory afferents function (Baumbauer et al., 2015; Moehring et al., 2018 (in bioRxiv); Sadler et al. 2020). Moreover, it has been shown the presence of synaptic vesicles in keratinocytes that could indicate a synaptic-like contact between sensory afferents and keratinocytes as it has been observed between Merkel cells and Aβ-fibers terminals (Tagalas et al., 2020).

There is one report of AP activity in nociceptors sensory afferents elicited by optogenetic keratinocytes stimulation. Baumbauer and collaborators (2015) used a similar strategy used in this work, where two opsins channelrhodopsin and halorhodopsin were expressed in keratinocytes under the promoter of keratin-14 (KRT14-Cre). After blue light stimulation the sensory afferents recorded in a skin-nerve preparation showed AP firing. However, no measurements of activation latency were reported, which could be considered as evidence of functional coupling between the two types of cells. Based on these results, it is possible that the artificial influx of cations in keratinocytes by ChR2 photostimulation indirectly affects nociceptors sensory endings activity in the epidermis without necessarily forming a direct coupling connection. In this present study, all types of Aδ- and C-fibers that were activated by blue light seemed to be tightly associated with nociceptive Schwann cells. In addition, during photostimulation of

nociceptive Schwann cells C-M, C-polymodal and C-thermoreceptors evoked a stimulus dependent sustained firing activity (Figure 16). Moreover, the first spike recorded during nociceptive Schwann cells activation had a shorter latency response than AP activity generated by mechanical stimulation, suggesting a direct coupling mechanism between nociceptive Schwann cells and C-fibers mechanosensitive to relay mechanical stimulation.

The fact that not all nociceptive sensory afferents responded to blue light stimulation of Schwann cells $Sox10^{+}$ (Figure 16C) could be due to efficiency of recombination after Tamoxifen injection leading to patchy expression of Channelrhodopsin in nociceptive Schwann cells. On the other hand, there were no differences between the mechanosensitivity of responsive and non-light responsive nociceptors (Figure17).

In order to determinate how much nociceptive Schwann cells contribute to the response properties of nociceptors, these cells were silenced by the expression of the Archeorhodopsin-3 (ArchT) that has been characterized as an outward proton pump with high selectivity and post-light recovery (Chow et al., 2010; El-Gaby et al., 2016). Then, an exposure to yellow light should cause an efflux of H^{+} and consequently membrane hyperpolarization of the Schwann cells.

Comparing the responses of mechanosensitive nociceptors such as A-Ms and C-fiber nociceptors (C-Ms and C-polymodal mechanical responses were pooled together for simplification) before and after yellow light stimulation (Figure 18), I have observed a significant decrease in firing of mechanosensitive nociceptors. A-M nociceptors showed increased mechanical threshold, but this was not statistically significant. Moreover, an unexpected long-lasting decrease in nociceptors mechanosensitivity was observed 20 minutes after nociceptive Schwann cell photoinhibition (Figure 18B). C-fiber nociceptors showed a lower firing rate to static force of 250mN after yellow-light exposure that also continued to decrease to 50% of the initial firing rate (Figure 18C), while the mechanical threshold increased after yellow light exposure, but this was not statistically significant and changed in a similar way than C-fiber nociceptors control recordings from no ArchT expressing Schwan cells of Sox10-Cre mice. Finally, C-fiber thermoreceptors showed no effect in thermosensitivity after yellow light exposure and their response properties such as thermal threshold and firing rate were similarly consistent after 20 minutes of recording, as was observed in C-fiber thermoreceptors recordings from Sox10-Cre mice.

In summary, we have shown that nociceptive $Sox10^{+}$ Schwan cells are not only associated to nociceptors, but specifically they have a functional contribution to mechanonociceptors sensitivity and firing properties (Figure 32). However, each type of nociceptor most probably form a specific type of coupling with nociceptive $Sox10^{+}$ Schwan cells because of the different functional roles in what they are involve.

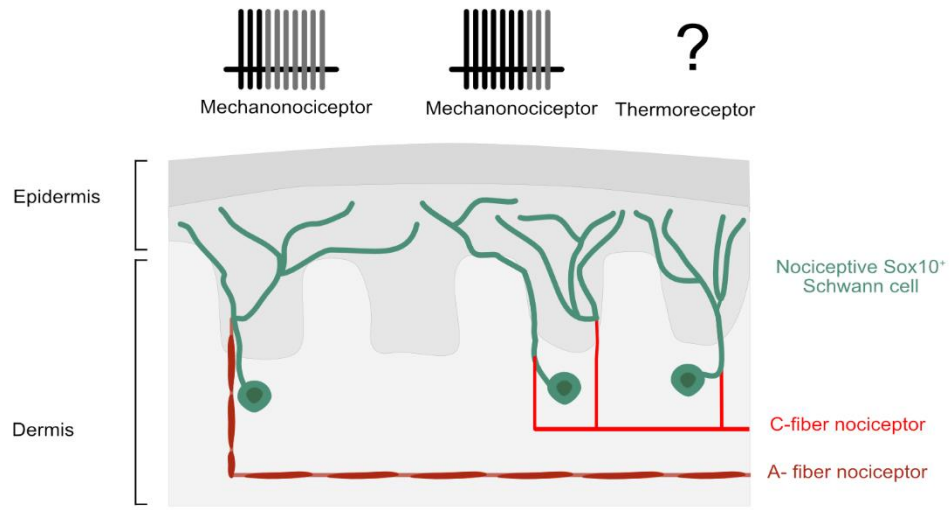

Figure 32. Nociceptive Schwann cells contribute to mechanosensitivity of mechanonociceptors. Schematic representation of nociceptive Sox10^{+} Schwann cells associated with A-fiber nociceptors, C-fiber nociceptors and C-thermoreceptors, where they contribute to the mechanotransduction properties of mechanonociceptors. In A-fiber nociceptors, Sox10^{+} Schwann cells participate in mechanical threshold and slightly to adaption properties. In C-fiber nociceptors, Sox10^{+} Schwann cells contribute to mechanotransduction speed and their slowly adapting firing rate. There is no evidence to demonstrate if Sox10^{+} Schwann cells are thermosensitive or participate in C-thermoreceptors response properties.

Long-lasting effects of ArchT photostimulation have not been reported as observed in the present study. However, it has been suggested that sustained activation of ArchT can increase presynaptic activity by enhancing spontaneous vesicle as an off-target effect in neurons from CNS (Mahn et al., 2016; Lafferty & Britt, 2020). Additionally, neurons express high level of ion channels and pumps to compensate rapidly for ion flux by opsin activation and little is known of ArchT function characterization in nonneuronal cells. Therefore, one possible explanation for the nociceptive Schwann cells photoinhibition long-lasting effect in nociceptor terminal endings is an indirect hyperpolarization of nociceptors causing a shut down in the cells, or an extracellular acidification due to the outward proton flux could block voltage-gated sodium channels and impair AP firing activity (Smith et al., 2011; Peters et al., 2018). Finally, another possibility is that the terminal endings from nociceptors get crushed after repetitive mechanical stimulation. Glabrous skin-tibial nerve recordings a performed in outside-out configuration, where it is impossible to discern skin innervation and avoid direct contact between the nerves and the mechanostimulator causing irreversible damage to the nerves and potentially degenerate. However, nociceptors mechanosensitivity recorded from Sox10-Cre mice, which do not express ArchT, showed no difference in their responsive properties before and 20 minutes after yellow-light stimulation

(Figure 18B, C). Thus, A-fiber and C-fiber nociceptors increased mechanical threshold and lower firing rate to static force recorded from Sox10-ArchT mice were most likely due to nociceptive Schwann cell photoinhibition.

10.1.2 Sensory Schwann cells and mechanoreceptor function

RAMs and SAMs form specialized receptors with distinct morphology and characteristic responses to mechanical stimulation. Here, I have shown that Schwann cells and Merkel cells $Sox10^+$ or $Sox2^+$ photostimulation generated firing activity in the terminal endings of Aβ-fibers that innervate Meissner corpuscle and Merkel cell-neurite complex. These results demonstrate a direct coupling between nonneuronal cells and the sensory afferents terminals, which could have a role in receptors function. Not all mechanoreceptors recorded, RAMs or SAMs, were excited by nonneuronal cell blue light stimulation, one possible explanation is a low efficiency of recombination after Tamoxifen injection in postnatal mice as observed in some nociceptors, or poor coupling between both type of cells.

Aβ-fiber firing activity evoked by photostimulation of Schwann cells $Sox10^+$ was achieved with all blue light intensities applied from 0.5 to 4.3mW/mm^2 but adapted after the first stimulation with the lower intensity. It is possible that calcium influx generated by ChR2 activation in the Schwann cell reached the terminal ending of the Aβ sensory afferent and after prolonged exposure to blue light, increasing the levels of intracellular calcium led to cytotoxicity in the sensory afferent. However, adaptation is also observed after repeated mechanical stimulation and it is a key property in mechanoreceptors to transduce different qualities of mechanical stimuli such as vibration, static indentation and stretch. Then, mechanoreceptors adaption after repetitive optogenetic stimulation of Schwann cells could reflect mechanoreceptors response to long-lasting repetitive mechanical stimulation. In contrast, Aβ-fiber firing activity evoked by photostimulation of Schwann cells $Sox2^+$ showed slow adapting firing rate in mechanically rapidly adapting mechanoreceptors. Such elevated mechanosensitivity and altered frequency response of RAMs has been previously described in mutations inactivating the potassium channel KCNQ4 (Kv7.4) shown by Heidendreich and collaborators (2012) and it might indicate Schwann cells $Sox2^+$ are closer to the AP generation region and adaptation is not a mechanical property that solely depend on terminal ending of A Aβ-fiber in Meissner corpuscles.

10.1.3 Sensory Schwann cells and Meissner corpuscle mechanoreceptors

Meissner corpuscles are innervated by Aβ-fibers, the terminal endings of which intercalate with specialized Schwann cells, and have a rapidly adapting response to mechanical stimulation. Here,

two subpopulation of sensory Schwann cells, or lamellar cells, were identified by their expression of the transcription factors Sox10 and Sox10/Sox2. Blue light activation of each kind of Schwann cells generated radically different firing patterns in Meissner corpuscles, indicating functional compartmentalization of Schwann cells and coupling to Aβ-fibers endings.

Photostimulation of $Sox10^{+}$ Schwann cells evoked a comparable rapidly adapting firing activity to mechanical stimulation in RAMs. A few spikes were generated immediately after blue light activation of sensory Schwann cells where had significantly faster latencies than mechanically evoked APs. On the other hand, photostimulation of $Sox2^{+}$ Schwann cells produced a very different response in the sensory afferents. For the first time, a tonic firing activity was recorded in Aβ-fibers terminals from Meissner corpuscles during the 10 seconds of blue light exposure, although with very long latencies mean of 368.3±173.1ms compared to mean latencies of 2.8±0.69ms measured for RAMs activated by photostimulation for sensory $Sox10^{+}$ Schwann cells (Figure 21C). These results suggests that $Sox2^{+}$ Schwann cells are placed in the Meissner corpuscles where their depolarization produce a high cation influx in the sensory terminals able to generate sustained AP activity during stimulation. More interestingly, it establishes that adaptation does not depend solely on the sensory afferent properties, non-excitable $Sox2^{+}$ Schwann cells can drive AP activity in the terminal ending of Aβ-fiber to which they are coupled as long as they have a constant cation inward current such as ChR2 photoactivation. In this study, a compartmentalization of two subpopulation of sensory Schwann cells in Meissner corpuscles is suggested, and their activation was able to switch mechanoreceptors response properties from rapidly to slowly adapting receptors.

In order to determinate the contribution of sensory $Sox10^{+}$ Schwann cells to mechanosensitivity of native Meissner corpuscles, photoinactivation of sensory $Sox10^{+}$ Schwann cells in Meissner corpuscles was achieved using Sox10-ArchT mice described previously. Similarly, I had observed three times increased mechanical threshold, from 22.9±7.6mN before yellow light exposure to 65.6±6.4mN after 20 minutes of recovery. In addition, vibration sensitivity of RAMs was tested with a sinusoidal wave of 20Hz with increasing indentation amplitude, I observed a following frequency response of RAMs reduction from 0.64±0.3Hz to 0.01±0.01Hz after 20 minutes of recovery from 10 minutes exposure to yellow light in Sox10-ArchT mice. In summary, these data suggest that Meissner corpuscle have a complex functional organization, where Schwann cells $Sox10^{+}$ are tight coupled to Aβ-fibers and the characteristic fast response of mechanoreceptors to light touch and vibration relay in the interaction of both cells. While, at the bottom of the Meissner corpuscle, Schwann cells $Sox2^{+}$ are able to excite voltage-gated ion channels of Aβ-

fiber terminal afferent and generate tonic firing activity probably in an independent way to mechanical stimuli transduction, but the physiological relevance of this is still unclear.

Recently, Neubarth and collaborators (2020) proposed that two types of Aβ-fibers innervate Meissner corpuscles. First characterized for their molecular identity, one expresses TrkB receptor while the other type of Aβ-fiber expresses c-Ret. Their responses to mechanical stimulation were found to be distinct, Aβ-fibers $TrkB^+$ have higher velocity sensitivity and respond to onset and offset indentation, while Aβ-fibers $c\text{-}Ret^+$ are less sensitive to velocity ramps and responded mostly to onset indentation in the Meissner corpuscles (Neubarth et al., 2020). In this work, all Aβ-fibers innervating Meissner corpuscles showed similar threshold, velocity sensitivity and onset/offset response properties to mechanical stimulation with no indicators of two functional types of Aβ-fibers as shown in Figure 22A-D, independently of wether Aβ-fiber were excited by sensory Schwann cells photostimulation. Meissner corpuscles are present in all mammals glabrous skin, and it has never been previously reported a tonic response by the Aβ-fibers that innervate them (Idé, 1977; Paré et al., 2001; Fleming and Luo, 2013). However recordings made from paw sensory afferents have two main limitations. First, in the mouse it has been shown that Meissner corpuscle are concentrated in the walking pads (Walcher et al., 2018) which are curved protrusions in the skin that narrow the stimulation area, and unintended contact with mechanical stimulator causes firing activity. Secondly, medium to high frequency protocols (above 20Hz) could cause unexpected vibration in the mechanical stimulator also causing artefactual firing activity. Therefore, there is little evidence in this study to support two functionally distinct Aβ-fibers innervating the Meissner corpuscles.

Photoactivation of $Sox2^+$ Schwann cells elicited tonic firing activity from mechanically activated rapidly adapting Aβ-fibers innervating the hair follicle in hairy skin-saphenous nerve preparation as observed for RAMs in the Meissner corpuscles of the glabrous skin from the same mouse Sox2-ChR2. However, there are no Meissner corpuscle in the hairy skin, Aβ-fibers terminal are organized as lanceolate -endings parallel to the hair shaft that they innervate. Thus, RAMs have a conserved functional organization of Schwann cells $Sox2^+$ and Aβ-fibers regardless of the specialized receptor that they form part such as Meissner corpuscle or lanceolate ending-terminal in the hair follicle.

Interestingly, RAMs excited by photostimulation of $Sox2^+$ Schwann cells showed distinct responsive properties to mechanical stimulation compared to the RAMs non-responsive to blue light activation (Figure 22G), with a lower firing rate to ramp velocity stimulation. It is important to highlight that RAMs responsive to blue light activation of $Sox2^+$ Schwann cells resembles Tap RAMs, that are described as rapidly adapting mechanoreceptors sensitive to very fast mechanical

stimulation such as velocity ramps of 15mm/s firing just one or two AP, while other wild-type RAMs can fire between three to four APs to the same stimuli (Wetzel et al., 2007), but further experiments should be performed to investigate if Tap RAMs afferents have a unique coupling with sensory Schwann cells and its physiological relevance.

The Aβ-fibers that innervate the hair follicles have been described as having an organizational distribution where two or more neurons innervate the same follicle and, simultaneously, one neuron can innervate more than one type of hair follicles (Kuehn et al. 2019). Therefore, a comparable Aβ-fibers somatotopic alignment could be consisted with sensory Schwann cells coupling and response properties in lanceolate-terminal endings. Future experiments in sensory $Sox10^+$ Schwann cells will be necessary to compare responsive properties of Aβ-fibers generated by $Sox10^+$ or $Sox10^+/Sox2^+$ photostimulation, as it has been observed in Meissner corpuscles.

In summary, with our results we have described sensory Schwann cells in touch receptors end-organs. In Meissner corpuscle, the $Sox10^+$ Schwann cell positive are involved in mechanotransduction and AP initiation (Figure 33A). $Sox2^+$ Schwann cells are related to sensory afferent excitability and adaptation properties in the Meissner corpuscle and hair follicle (Figure 33A, B). Our data suggests that sensory Schwann cells and terminal-endings from sensory afferents association have a functional role on mechanoreceptors function and is conserved along through diverse specialized receptors in the skin.

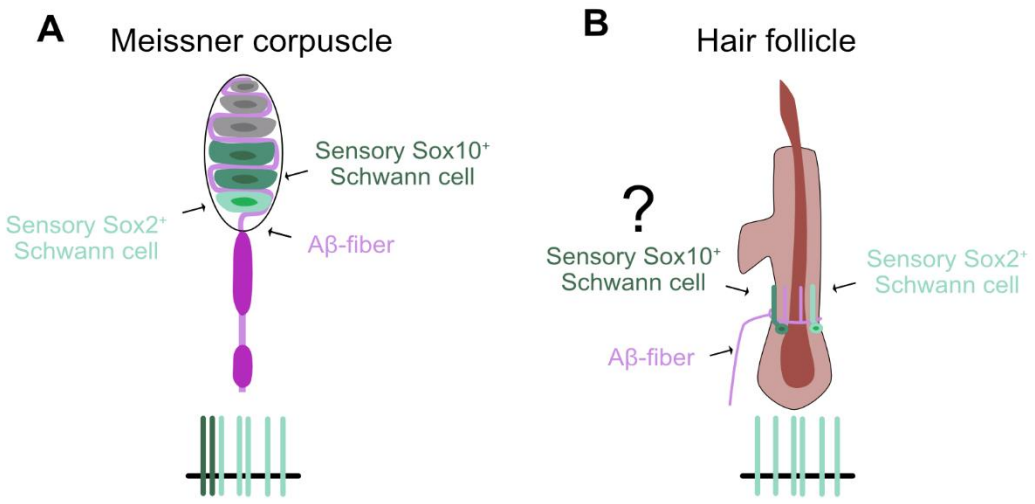

Figure 33. Rapidly adapting mechanoreceptors Aβ-fibers associated to sensory Schwann cells. (A) Schematic representation of a Meissner corpuscle in the glabrous skin, showing Aβ-fibers associated to Sensory $Sox10^+$ Schwann cells and Sensory $Sox2^+$. On the bottom, it is represented the possible contribution of sensory Schwann cells to RAMs firing activity. $Sox10^+$ Schwann cells seem to be involved in mechanotransduction and AP initiation (dark green) of Aβ-

fibers firing activity, while Sox2$^+$ could participate in the sensory afferent excitability and adaptation properties (light green). (B) Schematic representation of a hair follicle innervated by an Aβ-fibers (simplified). Sensory Sox2$^+$ Schwann are associated to Aβ-fibers and participate their excitability and adaptation properties (light green), as observed in sensory Sox2$^+$ Schwann cells - Aβ-fibers complex in the Meissner corpuscle. Further experiments are necessary to characterize the contribution of sensory Sox10$^+$ Schwann cells to rapidly adapting Aβ-fibers in the hair follicle.

10.1.4 Merkel cell photoactivation and SAM function

SAMs are single Aβ-fiber sensory afferent coupled to Merkel cells in a synapse-like configuration. Other than nonmyelinating glial cells, Merkel cells are the second type of epidermal cells expressing the transcription factor Sox2 (Kioke et al., 2014). Using Sox2-ChR2 mice, Merkel cells were photostimulated with blue light and SAMs firing activity recorded from glabrous skin-tibial nerve and hairy skin-saphenous nerve preparations. In both experiments, firing activity generated was a slowly adapting Aβ-fibers response comparable to mechanically evoked firing activity by static force. Previously, Maksimovic and collaborators (2014) have shown that Merkel cells photostimulation generates slowly adapting firing activity in Aβ-fibers. They used two photostimulation protocols, a 10 second blue light stimulation of increasing intensities and a long-lasting exposure over 3 minutes, in both cases a strong firing rate was observed from SAMs. Moreover, Maksimovic and collaborators (2014) pointed out two observations to achieve light-evoked activity in SAMs. First, firing activity of sensory afferents by Merkel cells photoactivation strongly depended on the site of stimulation, blue light stimulator must be positioned over the Merkel cells clusters, or no light-evoked activity was observed. Second, light-evoked activity of sensory afferents by ChR2 activation depended on the driver gene used. ChR2-tdTomato expression driven by the Cholecystokinin (Cck) gene locus was more efficient than ChR2-tdTomato expression driven by K14^{Cre} (Keratine-14). These two problems could be an explanation why only 30% of SAMs recorded showed light-evoked activity in the present study. Moreover, SAMs firing rate to blue light stimulation of Merkel cells from Sox2-ChR2 mice varies between 1-3Hz, while instantaneous firing frequency (IFF) of SAMs after Merkel cells photostimulation in Cck-ChR2 mice observed by Maksimovic et al. (2014) varies between 1-4Hz, which is comparable considering that IFF is always higher than firing rate (Lánský et al., 2004). Finally, it is important to note that light-responsive SAMs showed higher firing rates to velocity and static force mechanical stimulation than non-light-responsive SAMs (Figure 22E, F). Merkel cell form heterogeneous clusters of 4-40 Merkel cells in glabrous skin (Fleming & Luo, 2013). Thus, it is possible that photoactivation of large numbers of Merkel are required for efficient activation of SAMs.

SAMs response properties were tested after silencing Merkel cells in the skin nerve preparation of Sox2-ArchT mice. Ramp and hold mechanical stimulation protocols were applied to SAMs afferents before and after 10 minutes yellow light exposure, first spike threshold and static force firing rate did not change as observed in Sox10-Cre and Sox10-ArchT control recordings (Figure 23C, D), as well as velocity sensitivity responses (Figure 24D-F). In contrast, Maksimovic and collaborators (2014) showed firing frequency reduction during mechanical static force indentation to intermittent pulses of yellow light. It is important to consider that Merkel cells have a neuron-like phenotype and form a synapsis-like coupling with Aβ-fibers terminals, during mechanical indentation in the skin Piezo2 channels in Merkel cells activate and elicit norepinephrine vesicle release to excite the terminal afferent or Ca^{2+}-dependent AP (Ikeda et al., 2014; Hoffman et al., 2018). Given the morpho-functional structure of Merkel cell-neurite complex, it is possible that the present protocol of Merkel cells silencing used in this work, of yellow-light exposure intercalated with before and after mechanical stimulation, allows Merkel cells to recover and no inhibition is observed. Further experiments would be necessary where yellow light exposure is applied simultaneously with mechanical stimulation using the skin-nerve preparation.

10.1.5 What makes sensory Schwann cells mechanosensitive?

Mechanosensitive currents in whole-cell patch clamp sensory Schwann cells were recorded by indentation (Figure 25A, B). Yet, it was not possible to determine which kind of mechanosensitive ion channels are expressed in sensory Schwann cells, the mechanosensitive currents kinetics observed in nociceptive Schwan cells has a very slow kinetic with time constant of activation and inactivation of 23±11ms and 243±74ms, respectively. Sensory neurons and nonneuronal cells such as Merkel cells and chondrocytes also display mechanosensitive currents with different kinetics, but one common characteristic between them is a fast time constant of activation, below 5ms (Hu & Lewin, 2006; Maksimovic et al., 2014; Servin-Vences et al., 2018). However, the holding membrane potential of these cells was hyperpolarized between -60 to -80mV, while sensory Schwann cells resting membrane potential was at -40mV in this study. Depolarized membrane potentials can slow down current kinetics activation and inactivation such as Piezo channels and channelrhodopsin to depolarization (Coste et al., 2010; Chater et al., 2010). For example, Piezo1 channel inactivation time constant is 15ms at -80mV holding membrane potential but is above 30ms at -40mV holding membrane potential (Coste et al., 2010). Although it has not been reported changes in the inactivation time constant of hundreds of milliseconds. Given, the particular kinetics mechanosensitive currents in sensory Schwann cells, it is possible that multiple

mechanosensitive ion channels or auxiliary subunits are expressed by sensory neurons and Schwann cells to sense mechanical stimuli in the skin.

Piezo channels are promising candidates to be expressed by sensory Schwann cells. The Piezo1 channel has already been proposed to be expressed by epidermal cells (Herget Regina, unpublished data). Although, it has been also proposed that the Piezo1 channel is expressed by keratinocytes (in bioRxiv: Moehring et al., 2018), cells that also form part of the skin. Alternatively, Piezo2 channels are broadly express in the sensory neurons and it has already been demonstrated to be expressed by another nonneuronal cells able to generate mechanosensitive currents in the skin, Merkel cells (Woo et al., 2014). Recently, it has been characterized Piezo2 expression in different types of peripheral nonneuronal cells including perneuronal glial such as satellite glial cells, non-myelinating Schwann cells, sciatic nerve and cutaneous Schwann cells, skin epidermal melanocytes and Merkel cells (Shin et al., 2021, bioRxiv). Although, it is not shown a co-localization of Piezo2 channels and the transcription factors $Sox10^{+}$ or $Sox2^{+}$ with in Schwann cells, it is shown the expression of Piezo2 channels in Meissner corpuscles and epidermal Schwann cells associated with nociceptors terminal endings which strongly suggest that Piezo2 channels confers mechanosensitivity to sensory and nociceptive Schwann cells. Schwann cells $Sox10^{+}$ are involve in fast responses of RAMs associated with Meissner corpuscles and nociceptive Schwann cells seem to be involved in sustaining firing properties of nociceptors. The Piezo channels are able to conduct fast and large inward currents to the cell, an activation of Piezo channel in Schwann cells could push the receptor potential to generate action potentials, but it probably involves other mechanisms to generate the specific responses of RAMs and nociceptors. For example, tethers for tension-induced gating of associated to Piezo channels in Meissner corpuscle could explain fast activation, high sensitivity and rapid adaptation; while in nociceptors with high threshold, slow activation and adaption would require other mechanisms to allow mechanosensitive ion channels remain available like in the synapse-like structure between Merkel cells-neurite complex.

OSCA/TMEM63 is a recently described family of mechanically activated ion channels present in plants and animals (Murthy et al., 2018). The three members of theTMEM63 family are expressed in DRG neurons (Linnarsson.org/drg; Herget, Regina unpublished data) which could be also present in nociceptive Schwann cells. Interestingly, overexpression of TMEM63A and TMEM63B in HEK293 cells generates cell stretch-elicit currents with slow activation and inactivation kinetics, between 4-18ms and up to more than 200ms, respectively (Murthy et al., 2018). As it has been observed in nociceptive Schwann cells.

The TRPV4 channel is part of the superfamily of transient receptor potential (TRP) non-selective cations channels. Many of these channels have been involve in mechanosensory processes but have not been proven to be intrinsically mechanosensitive (Nikolaev et al., 2019). Originally considered as a potential osmotransducer, TRPV4 is a polymodal channel sensitive to temperature and chemical stimuli, and recently has been shown underlie mechanically gated currents in chondrocytes (Zhao et al., 2016; Servin-Vences et al., 2017). In the cartilage, chondrocytes are the most abundant cells embedded in the extracellular matrix, able to sense changes in the mechanical loading as tensile, compressive and shear forces. TRPV4 channels are also expressed in sensory neurons and vasculature cells (Servin-Vences et al., 2018). Recently, it has been proposed that TRPV4 is expressed in nonmyelinating Schwann cells in culture and in the sciatic nerve at the periphery (Feng et al., 2020), and it has an important role in losing myelinating phenotypes where gain of functionTRPV4 in the membrane of myelinating Schwann cells resembles nonmyelinating, or even, immature Schwann cells phenotype. TRPV4 channels have been also found astrocytes and microglia in the CNS, where enhances neuronal excitability and synchronize neuronal activity by releasing neurotransmitter such as ATP and glutamate through heat and lipid activation (Shibasaki, 2016). However, nociceptive behavior test of 2% saline injection in TRPV4$^{-/-}$ knockout mice shown a small decreased flinching reactions and no changes to high 10% saline solution (Alessandri-Haber 2005). Thus, it is possible that nociceptive Schwann in the epidermis Sox10^{+} express TRPV4 channels and contribute to their mechanosensitivity along with other mechanosensitive ion channels.

Auxiliary subunits associated to mechanosensitive ion channels function could be also express in Schwann cells Sox10^{+} such as STOML3, TACAN and TMEM150C/Ttn3. The particular kinetics of mechanosensitive currents recorded from Schwann cells Sox10^{+} could be also explain by the expression of auxiliary proteins that scaffold to the MS ion channels microdomain and alter their sensitivity or membrane composition. STOML3 has been shown to increase mechanosensitivity and slow down the inactivation time constant of Piezo channels (Poole et al., 2014). TACAN was originally described as a high threshold MS ion channel (Beaulieu-Laroche et al., 2020), however recent characterization of its structure is associated to a coenzyme-A molecule that can change the membrane constitution by lipid metabolism-related signaling (Batrakou et al., 2015; Niu et al., 2021; Rong et al., 2021 in bioRxiv). The TMEM150C/Ttn3 protein has also been described as a MS ion channel (Hong et al., 2016; Lu et al., 2020), a modulator of Piezo channels and TREK channels (Anderson et al., 2018) and a potential modulator of the lipids composition in the plasma membrane as other members of the TMEM150C family (Chung et al., 2015). There is not enough evidence to probe the role of TMEM150C/Ttn3 in sensory neurons function but still can be part of

the complex Schwann cell and sensory terminal-ending, a more detailed discussion about TMEM150C/Ttn3 function in mechanotransduction is approached in the next section.

Finally, nociceptive Schwann cells coupled to nociceptors and sensory Schwann cells coupled to Meissner corpuscles express the transcript factor Sox10 that is used as a glial marker. However, given the different kind of mechanical stimulation that they transduce, and the firing response elicited by the sensory afferents that are coupled, it is possible that cutaneous Schwann express different kind of mechanosensitive ion channels. Particularly, sensory Schwann cells or lamellar cells in the Meissner corpuscle can evoke APs in the Aβ-fiber in less than 5ms after photostimulation (Figure 21C). Nikolaev and collaborators (2020) have proposed that lamellar cells of Meissner corpuscles in the duck bill skin are intrinsically mechanosensitive and generate Ca^{2+} - dependent action potentials. In addition, Ikeda and colleagues (2014) have also shown that Merkel cells fire Ca^{+2}-APs in a long-lasting and slowly adapting manner which can trigger neurotransmitters release to the terminal-ending of Aβ-fiber, in the Whisker hairs from mouse. Then, Piezo2 and Ca^{+2}-APs and synaptic-like transmission participate in Whisker hairs tactile responses. Although it is plausible that the mammalian counterpart of Meissner corpuscles uses a similar mechanotransduction strategy as in the duck, or even express other kinds of voltage-gated ion channels, the lamellar cells form less interdigitation with the neurons which it could imply a different coupling.

10.1.6 How are sensory neurons and sensory Schwann cells coupled?

In the epidermis, nociceptive Schwann cells have been described as forming a mesh-like network where individual nociceptive Schwann cells ensheath several unmyelinated nerve endings in a tight coupled conformation called glio-neural complex (Abdo et al., 2019). In the hair follicle, a comparable structure has been described between terminal Schwann cells processes, axon terminals and hair follicle outer root sheath cells (Li & Ginty, 2014). Different end organs in the skin with similar organization between axon terminals and glial cells suggest a morpho-functional role in mechanotransduction. In this work, it has been shown than photostimulation of $Sox10^{+}$ Schwann cells can evoke firing activity in terminal sensory afferents faster than mechanical stimulation on the same afferent, suggesting a tight and direct electrical coupling between both cells. One of the fastest and synchronized ways of cell-cell communication are gap junctions, which are clusters of intercellular channels between adjacent cell membranes allowing low-resistance cell to cell ion transfer (Simon & Paul, 1998). Connexins are the proteins that form the connexon from each cell and fuse to form the channel between them, these proteins are very dynamic in the membrane and have a short half-life, which make them perfect candidates to

communicate receptor potential arriving after mechanical stimuli (Goodenough & Paul, 2009). Particularly, connexin 32 (Cx32) and connexin 43 (Cx43) are found in myelinating and nonmyelinating Schwann cells and sensory neurons, respectively. Cx32 and Cx43 have been reported to be involve in voltage-gating, cross-excitation and pain sensitization (Goodenough & Paul, 2009; Huang et al., 2019; Spray & Hanani, 2019), which makes these connexins good candidates to participate in nociceptive Schwann cells and terminal axons coupling in the epidermis.

In Meissner corpuscles, terminal endings and sensory afferents may have an additional coupling mechanism to ensure fast mechanical stimuli transduction. A tether protein model was proposed by Hu and colleagues (2010) in the somatosensory system, a protein link of 100nm length may gate mechanosensitive ion channels in the membrane of sensory neurons to a laminin matrix, in the absence of this protein RA- currents were abolished indicating that tether proteins could have a role in mechanotransduction by directly gating the ion channel or the lipid environment in the membrane that finally tune the mechanosensitivity of LTMRs for touch and vibration. Recently, the extracellular protein Usher2a has been described as a tether protein expressed by Schwann cells that could tune fast mechanotransduction to ensure the transmission of the fast message in mechanoreceptors, corroborating the tether protein model tuning Meissner corpuscles for vibration and other mechanical stimuli (Lewin & Moshourab, 2004; Schwaller et al., 2020). Mechanosensitive ion channels, especially in mammals cells, are rarely alone in the membrane and scaffold proteins form a complex with the channels that integrate the cytoskeleton and extracellular matrix (Cox et al., 2016). Meissner corpuscles could be deformed by extracellular forces that simultaneously pulls Schwann cells tethers connected to the mechanosensitive (MS) ion channels in the sensory to generate action potentials, removing the mechanical force could release MS ion channels from inactivation and generate the second round of APs in the sensory afferent (Hu et al., 2010; Piccini et al. 2021).

10.2 Does TMEM150C/Ttn3 play a role in sensory neuron mechanosensitivity?

TMEM150C/Ttn3 was proposed as a component of a mechanosensitive ion channels after heterologous expression in naïve cells as HEK293T and was associated with the appearance of mechanosensitive currents to indentation. In sensory neurons, immunofluorescence analysis of TMEM150C/Ttn3 showed high expression in myelinated neurons such as mechanoreceptors and proprioceptors (approximately 60%) while in peptidergic and nonpeptidergic nociceptors TMEM150C/Ttn3 is expressed at low levels (less than 25%). After genetic ablation of the gene, whole-cell patch clamp recordings from DRG showed a reduction of slow-adapting currents, as in sensory neurons transfected with Ttn3 siRNA. Additionally, a reduction in motor coordination in mouse walk and grid griping behaviour test suggested TMEM150/Tentonin3 has a role in proprioception (Hong et al., 2016). In this work, I have investigated the role of TMEM150C/Ttn3 in mechanosensitivity of cutaneous sensory neurons and function.

10.2.1 TMEM150C/Ttn3 is not associated with mechanosensitive currents

Mechanosensitive properties of TMEM150C/Ttn3 became questionable after several researchers in the field performed whole cell recordings using HEK293T cells and F11 cells. The scientist suggested that such cells express endogenous mechanosensitive currents that could mask the intrinsic mechanosensitivity of TMEM150C/Tenotonin3 (Dubin et al., 2017). Instead, using HEK293T cells where Piezo1 channel gene (HEK-293P1KO) had been ablated making them mechanically insensitive, these groups showed overexpression of TMEM150C/Tentonin3 was not associated with the appearance of mechanosensitive currents when the cells are stimulated by indentation (Dubin et al., 2017; Anderson et al., 2018).

In this study, TMEM150C/Ttn3 was expressed in N2a cells where the Piezo1 channel gene was ablated denominated Na2P1KO cells developed by Moroni and collaborators (2018), which are also mechanically insensitive cells. After TMEM150C/Ttn3 heterologous expression in N2aP1KO cells, no mechanosensitive current was recorded using indentation stimuli (Figure 26B, C) or pressure clamp in outside-out membrane patches (data not shown). With these results, TMEM150C/Tn3 has been assessed as a mechanosensitive protein in two types of cell lines (HEK-293P1KO and N2aP1KO), and with two different techniques for mechanical stimulation (indentation and pressure-clamp) by five different research groups showing no mechanically activated currents (Dubin et al., 2017; Anderson et al., 2018). Recently, it has been suggested that TMEM150C/Ttn3 mechanosensitivity depend on cytoskeletal integrity, which might be low in

Piezo1- deficient cells such as HEK293P1KO and N2aP1KO (Lu et al. 2020). In the same study, overexpression of TMEM150C/Ttn3 in HEK-P1KO cells treated with Jasplakinolide (Jas), an actin-stabilizing agent, evoked slowly adapting mechanosensitive currents to indentation stimuli. In addition, Anderson and colleagues (2018) suggested TMEM150/Tentonin3 is an auxiliary subunit that modulates inactivation kinetics of mechano-gated ion channels like TREK-1 and Piezo channels. Interestingly, in their experiments a large amount of plasmid DNA for transfection was used, 1µg of DNA for each gene Piezo or TMEM150C/Ttn3. Therefore, I tested different concentrations of plasmid DNA to co-express Piezo2 and TMEM150C (data not shown), and I found that Piezo2 mechanosensitive currents had large amplitudes and slower inactivation only when 1µg of Piezo2 and 0.5 µg of TMEM150C plasmid DNA was used for transfection.

For example, Niu and collaborators (2021, in bioRxiv) using a different transmembrane protein also postulated as a mechanosensitive ion channel TMEM120A/TACAN, they have observed transient currents when the protein was expressed at high concentration and produced a non-selective, heterogeneous conduction amplitude that are not related to mechanosensitive currents kinetics previously reported (Niu et al., 2021, in bioRxiv).

Finally, Anderson and collaborators (2018) have also shown that TMEM150C co-immunoprecipitated with TREK-1 and Piezo2 and both proteins could form a complex in the membrane. Although, it is worth mentioning that overexpression of Piezo2 and TMEM150C in cell lines might not represent the physiological interaction of these two proteins in wild-type sensory neurons, and therefore TMEM150C/Ttn3 role in mechanotransduction might be only relevant in conditions where both proteins are upregulated.

10.2.2 The TMEM150C$^{LacZ/LacZ}$ mouse generation and phenotype

Hong and collaborators (2016) used a mutant mouse generated by KOMP and denominated TMEM150C$^{LacZ/LacZ}$ to show that TMEM150C/Ttn3 ablation in sensory neurons whole-cell recordings showed reduced slowly adapting currents evoked by indentation, and loss of motor coordination in mouse walk and grid gripping analysis from mice. In the present study, sensory neuron mechanotransduction properties were tested using the *ex vivo* hairy skin-saphenous nerve preparation and motor coordination using a similar mousewalk behavior test analysis in the same TMEM150C$^{LacZ/LacZ}$ mice established in our lab. Given the phenotype described by Hong et al. (2016), slowly adapting responsive properties of sensory afferents such as SAMs, A-Ms and C-fibers were of particular interest in skin-nerve preparation from TMEM150C$^{LacZ/LacZ}$ mice. However, all sensory afferents recorded displayed almost identical response properties as observed in wild-type mice. For example threshold, velocity sensitivity and adaptation were all

unchanged (Figure 27). In addition, motor ability measured as speed, limb coordination and regularity have similar values between wild-type and TMEM150C$^{LacZ/LacZ}$ mice indicating that the sensory neurons that innervate the muscles, or proprioceptors, were largely unaffected (Figure 28).

There are 6 transcripts variants produced from the mouse gene TMEM150C, two of them can be translated into a protein. One corresponds to the full-length protein isoform denominated Ttn3, a protein with 6 transmembrane (TM) domains with a putative pore-like region between the TM1 and TM2, localized in the cell membrane and associated to mechanosensitivity in sensory neurons (Hong et al., 2016; Lu et al., 2020). The second isoform of the protein is a truncated version of TMEM150C/Ttn3 that contains the three first transmembrane domains as well as the putative pore-like region. Interestingly, the TMEM150C knockout generated by the KOMP project used a LacZ and neomycin cassette inserted between exons 5 and 6 of the locus with a stop codon, resulting and a shift of the reading frame (Figure 29A). However, the exons 1 to 4 of the gene are still intact and a truncated version of TMEM150C/Ttn3 could be translated. This truncated version TMEM150C/Ttn3 protein is very similar to the second isoform of the protein and might have a role in sensory neurons mechanosensitivity in TMEM150C$^{LacZ/LacZ}$, because it containsTM1, TM2, part of TM3 and the pore-like region.

The TMEM150C$^{LacZ/LacZ}$ mouse established in our lab did not show a TMEM150C/Ttn3 knockout genotype in DRG neurons. First, the enzyme-based histochemical staining in DRG neurons from TMEM150C$^{LacZ/LacZ}$ showed no expression of beta-galactosidase as in wild-type mice. Secondly, a qPCR assay of TMEM150C exons 4-6 and exons 6-8 sequences was expressed in DRGs from TMEM150C$^{LacZ/LacZ}$ (Figure 23B, C), where the insertion of LacZ and neomycin cassette should had disrupted that region of the gene. Thus, in my experiments the TMEM150C gene was probably not efficiently ablated in DRG neurons from TMEM150C$^{LacZ/LacZ}$ mice and displayed a wild-type phenotype as showed in mechanosensitive response properties of sensory neurons from skin-nerve preparation (Figure 27) and motor coordination of mousewalk (Figure 28).

10.2.3 A new TMEM150C$^{-/-}$ mouse generation and phenotype

Until now, there is not enough evidence that TMEM150C plays a role in sensory neurons function. Yet, TMEM150C has been found by two different screens (Hong et al., 2016; Herget, Regina unpublished data) in large-size soma mechanoreceptors. Also, TMEM150C gene encodes for a protein with 6 transmembrane domains able to modulate Piezo channels kinetics under certain conditions (Anderson et al., 2018).

In our lab, we generated a new TMEM150C knockout, this mouse was designed using CRIPSR/Cas9 technology. The gRNA was designed to delete the region between exon 2 and 5 of the cDNA sequence of TMEM150C, that includes the start codon and leads to a frame shift where is not possible to produce truncated proteins because the N-terminal, including TM1, the pore-like region and part of TM2 are deleted to generate a mutant mouse with an efficient ablation of the gene, called TMEM150C$^{-/-}$.

The responsive properties of sensory afferents were evaluated with skin-nerve preparation from TMEM150C$^{-/-}$ mice. Surprisingly, SAMs recording showed a significant increased sensitivity to ramp velocity stimulation in TMEM150C$^{-/-}$ mice compared to wild-type (Figure 30F). In addition to reduced mechanical threshold and increased firing rate to static force, although not statistically significant (Figure 30E-H). A similar tendency was observed in A-fiber mechanonociceptors (Figure 31A-C). In contrast, C-fiber mechanonociceptors showed a statistically significant lower firing rate to low-intensity static force stimulation (Figure 31D-F).

Further experiments are necessary to characterize TMEM150C$^{-/-}$. However, these preliminary results showed slightly increased sensitivity of slow-adapting mechanoreceptors; and second, loss of sensitivity in nociceptors, suggesting that TMEM150C gene ablation changes mechanosensitivity in cutaneous sensory neurons. At first, these results might seem to be contradictory, yet mechanoreceptors and nociceptors form distinct specialized receptors, express a different set of proteins involve in mechanotransduction and membrane constitution. For example, TMEM150 family has been associated to lipid membrane composition and could have a different role in mechanoreceptors and nociceptors (Romanet, 2017).

10.2.4 The TMEM150 family contains three members

The Tmem150 family is evolutionary recent family of genes are only found in vertebrates, comprising three members: TMEM150A, TMEM150B and TMEM150C, encoding proteins with six transmembrane domains with both the amino- and carboxil-termini in the intracellular region. These proteins are involved in autophagy induction and are known as part of the Damage-Regulated Autophagy Modulators (DRAM) family (Romanet, 2017).

The TMEM150A gene encodes a protein is known as DRAM-5 and can play a role in TLR4 (Toll-like receptor 4) signaling transduction by modulating cytokines (Romanet, 2017). Also, it has been found to be a functional homologue of Sfk1, a yeast protein that interacts with plasma membrane protein PI 4-kinase type IIIα (PI4KIIIα) and EFR3 (peripheral membrane protein) to generate PI4P (Phosphatidylinositol 4-phosphate) that regulates metabolic pathways including the presence of other lipids in the membrane (Chung et al., 2015).

The DRAM-related protein, DRAM3, is encoded by the gene TMEM150B. It has been reported as a transmembrane protein that regulates autophagy and cell death after glucose deprivation (Mrschtic & Ryan, 2016). In mouse, TMEM150B is highly expressed in ovary, and it has been associated with premature and natural menopause but is not essential for follicle maturation or oocyte development when the gene is deleted (Liu et al., 2020). The genes TMEM150A and TMEM150C are also expressed in the ovary, then it is possible that these genes have a functional redundancy.

The TMEM150C gene encodes also a transmembrane protein known as Tentonin3 and also DRAM4, however it has not yet implicated in autophagy modulation (Romanet, 2017). Surprisingly, TMEM150C/Ttn3 is the only member of the TMEM150C family associated to mechanotransduction. The TMEM150C is less related to the other two members, sharing 26.5% and 28.1% of the sequence identity with TMEM150A and TMEM150B, respectively (Hong et al., 2016). TMEM150C/Ttn3 has been proposed as a mechanosensitive ion channel expressed in sensory neurons from DRGs and nodose ganglia in close association with Piezo channels. In cells where Piezo channels has been ablated, TMEM150C/Ttn3 is not able to activate mechanosensitive currents because it depends on specific level of membrane tension and Piezo channels contribute to cytoskeletal integrity or traction force in cells. (Lu et al., 2020).

There is strong correlation between the mechanosensitivity of the channel and the lipid bilayer composition of the membrane. The TMEM150 family encodes for transmembrane proteins associated to membrane lipid composition, autophagy and mechanotransduction.

It is not possible yet to discard TMEM150C/Ttn3 as mechanosensitive ion channels. The other two members of TMEM150 family are not found in DRG neurons (Linnarssonlab.org/drg), then after ablation of TMEM150C/Ttn3 seem to have a role in mechanotransduction of sensory neurons and could form part of the complex of proteins necessary to keep the membrane composition adequate to transduce mechanical stimuli.

11. CONCLUSION

In this thesis, I have presented evidence that $Sox10^+$ Schwann cells form part of a diverse glio-neural end-organs in the skin necessary for light touch and noxious mechanical stimuli transduction. Lamellar cells have been described as specialized Schwann cells in the Meissner corpuscles since they were characterized more than 150 years ago by George Meissner and Rudolf Wagner (Johnson, 2001; Paré, 2001).

Now, we start to understand that Schwann cells are not only specialized to form the Meissner corpuscle and support the terminal endings of sensory afferents to transduce mechanical stimuli. Schwann cells are specialized to sense mechanical stimuli and contribute actively to mechanotransduction. More interestingly, sensory Schwann functions are compartamelized in Meissner corpuscles, $Sox2^+$ Schwann cells are able to trigger slowly adapting AP activity. Such phenomenon has been never described for rapidly adapting mechanoreceptors and represents a step forward over the paradigm that adaptation is an exclusive property of sensory neurons terminal endings. Similarly, $Sox2^+$ Schwann cells associated with rapidly adapting Aβ-fibers to mechanical stimulation in the hair follicle, can change their excitability and show slowly adapting activity, although the physiological implications and function still unclear.

Nociceptors in the skin have been described as ‘free endings’ (2019) that are directly activated by noxious stimuli in the skin. Recently, Abdo and collaborators have proposed a specialized cutaneous Schwann cells forming a mesh-like network in the subepidermal border and associating to nociceptors to convey noxious stimuli. Here, we have shown that nociceptive Schwann cells are associated with all types of nociceptors in the skin, but their connection is distinctive with each of them. As for mechanoreceptors, $Sox10^+$ Schwann cells are involved in sensitivity and transduction of mechanical stimulation. The tight connection between Schwann cells and nociceptors terminal endings allows that photostimulation of $Sox10^+$ trigger AP activity faster than mechanical stimulation on the same receptor field of mechanonociceptors.

In conclusion, we have shown that the sensory Schwann cells and terminal endings have a conserved morphologically and functionally connection through diverse specialized receptors in the skin, and mechanosensation depends on the intrinsic properties of both cell types.

Mechanotransduction relay on the mechanosensitive ion channels able to sense force changes in the membrane cell and transduce the stimuli into electrical and chemical intracellular signals. The search for mechanosensitive ion channels in the animal kingdom has been specially challenging because of the difficulties to prove intrinsic mechanosensitivity and the complex of

proteins that are involve in mechanotransduction from the cytoskeleton and the extracellular matrix. Here, we have taken the TMEM150C/Ttn3 protein associated with mechanosensitive currents in sensory neurons and recently proposed as a mechanosensitive ion channel (Hong et al., 2016; Lu et al., 2020). In our hands, indentation of cells that express TMEM150C/Ttn3 failed to evoke mechanosensitive currents or modulate the mechanically gated Piezo2 channel. Moreover, we have tested two mouse lines were TMEM150C/Ttn3 gene was ablated using *ex vivo* skin nerve preparation showing that this transmembrane protein does not play a direct role in mechanotransduction of cutaneous sensory neurons, but it could be involved in slowly adapting properties of mechanoreceptors and nociceptors. Although further experiments are necessary to characterize the function of TMEM150C/Ttn3 in this set of sensory neurons function. For example, given that the TMEM150 family is involve in lipid metabolism, it is possible that TMEM150C/Ttn3 participates indirectly in the mechanosensitive properties of sensory neurons by modifying the constitution of the membrane and protein complex where MS ion channels are immersed.

Mechanotransduction in the somatosensory system is a basic and complex phenomenon that it is present in all kinds of organisms. Here, we have shown that it depends on the functional organization of sensory neurons and nonneuronal cells in the specialized receptors that they form in the skin. As well as diverse mechanosensitive proteins that are expressed in the membrane and can directly, or indirectly, set the conditions to transmit mechanical information.

12. REFERENCES

Abdo, H., Calvo-Enrique, L., Lopez, J. M., Song, J., Zhang, M. D., Usoskin, D., ... & Ernfors, P. (2019). Specialized cutaneous Schwann cells initiate pain sensation. *Science*, *365*(6454), 695-699.

Abraira, V. E., & Ginty, D. D. (2013). The sensory neurons of touch. *Neuron*, *79*(4), 618-639.

Alessandri-Haber, N., Joseph, E., Dina, O. A., Liedtke, W., & Levine, J. D. (2005). TRPV4 mediates pain-related behavior induced by mild hypertonic stimuli in the presence of inflammatory mediator. *Pain*, *118*(1-2), 70-79.

Anderson, E. O., Schneider, E. R., Matson, J. D., Gracheva, E. O., & Bagriantsev, S. N. (2018). TMEM150C/Tentonin3 is a regulator of mechano-gated ion channels. *Cell reports*, *23*(3), 701-708.

Árnadóttir, J., & Chalfie, M. (2010). Eukaryotic mechanosensitive channels. *Annual review of biophysics*, *39*, 111-137.

Arcourt, A., Gorham, L., Dhandapani, R., Prato, V., Taberner, F. J., Wende, H., ... & Lechner, S. G. (2017). Touch receptor-derived sensory information alleviates acute pain signaling and fine-tunes nociceptive reflex coordination. *Neuron*, *93*(1), 179-193.

Assaraf, E., Blecher, R., Heinemann-Yerushalmi, L., Krief, S., Vinestock, R. C., Biton, I. E., ... & Zelzer, E. (2020). Piezo2 expressed in proprioceptive neurons is essential for skeletal integrity. *Nature communications*, *11*(1), 1-15.

Bagriantsev, S. N., Gracheva, E. O., & Gallagher, P. G. (2014). Piezo proteins: regulators of mechanosensation and other cellular processes. *Journal of biological Chemistry*, *289*(46), 31673-31681.

Batrakou, D. G., de Las Heras, J. I., Czapiewski, R., Mouras, R., & Schirmer, E. C. (2015). TMEM120A and B: nuclear envelope transmembrane proteins important for adipocyte differentiation. *PLoS One*, *10*(5), e0127712.

Baumbauer, K. M., DeBerry, J. J., Adelman, P. C., Miller, R. H., Hachisuka, J., Lee, K. H., ... & Albers, K. M. (2015). Keratinocytes can modulate and directly initiate nociceptive responses. *Elife*, *4*, e09674.

Beaudry, H., Daou, I., Ase, A. R., Ribeiro-da-Silva, A., & Séguéla, P. (2017). Distinct behavioral responses evoked by selective optogenetic stimulation of the major TRPV1+ and MrgD+ subsets of C-fibers. *Pain*, *158*(12), 2329-2339.

Beaulieu-Laroche, L., Christin, M., Donoghue, A., Agosti, F., Yousefpour, N., Petitjean, H., ... & Sharif-Naeini, R. (2020). TACAN is an ion channel involved in sensing mechanical pain. *Cell*, *180*(5), 956-967.

Bernal Sierra, Y. A., Haseleu, J., Kozlenkov, A., Bégay, V., & Lewin, G. R. (2017). Genetic tracing of Cav3. 2 T-type calcium channel expression in the peripheral nervous system. *Frontiers in molecular neuroscience*, *10*, 70.

Biernaskie, J., Paris, M., Morozova, O., Fagan, B. M., Marra, M., Pevny, L., & Miller, F. D. (2009). SKPs derive from hair follicle precursors and exhibit properties of adult dermal stem cells. *Cell stem cell*, *5*(6), 610-623.

Boudjadi, S., Chatterjee, B., Sun, W., Vemu, P., & Barr, F. G. (2018). The expression and function of PAX3 in development and disease. *Gene*, *666*, 145-157.

Bunge, R. P. (1993). Expanding roles for the Schwann cell: ensheathment, myelination, trophism and regeneration. *Current opinion in neurobiology*, *3*(5), 805-809.

Caspary, T., & Anderson, K. V. (2003). Patterning cell types in the dorsal spinal cord: what the mouse mutants say. *Nature Reviews Neuroscience*, *4*(4), 289-297.

Chater, T. E., Henley, J. M., Brown, J. T., & Randall, A. D. (2010). Voltage-and temperature-dependent gating of heterologously expressed channelrhodopsin-2. *Journal of neuroscience methods*, *193*(1), 7-13.

Chen, C. C., & Wong, C. W. (2013). Neurosensory mechanotransduction through acid-sensing ion channels. *Journal of cellular and molecular medicine*, *17*(3), 337-349.

Cho, H., Shin, J., Shin, C. Y., Lee, S. Y., & Oh, U. (2002). Mechanosensitive ion channels in cultured sensory neurons of neonatal rats. *Journal of Neuroscience*, *22*(4), 1238-1247.

Chow, B. Y., Han, X., Dobry, A. S., Qian, X., Chuong, A. S., Li, M., ... & Boyden, E. S. (2010). High-performance genetically targetable optical neural silencing by light-driven proton pumps. *Nature*, *463*(7277), 98-102.

Chung, J., Nakatsu, F., Baskin, J. M., & De Camilli, P. Plasticity of PI4KIII interactions at the plasma membrane.

Coste, B., Mathur, J., Schmidt, M., Earley, T. J., Ranade, S., Petrus, M. J., ... & Patapoutian, A. (2010). Piezo1 and Piezo2 are essential components of distinct mechanically activated cation channels. *Science*, *330*(6000), 55-60.

Cox, C. D., Bavi, N., & Martinac, B. (2017). Origin of the force: the force-from-lipids principle applied to piezo channels. *Current topics in membranes*, *79*, 59-96.

Denk, F., Bennett, D. L., & McMahon, S. B. (2017). Nerve growth factor and pain mechanisms. *Annual review of neuroscience*, *40*, 307-325.

Delmas, P., & Coste, B. (2013). Mechano-gated ion channels in sensory systems. *Cell*, *155*(2), 278-284.

Delmas, P., Hao, J., & Rodat-Despoix, L. (2011). Molecular mechanisms of mechanotransduction in mammalian sensory neurons. *Nature Reviews Neuroscience*, *12*(3), 139-153.

Douarin, N. L., Dulac, C., Dupin, E., & Cameron-Curry, P. (1991). Glial cell lineages in the neural crest. *Glia*, *4*(2), 175-184.

Dubin, A. E., & Patapoutian, A. (2010). Nociceptors: the sensors of the pain pathway. *The Journal of clinical investigation*, *120*(11), 3760-3772.

Dubin, A. E., Murthy, S., Lewis, A. H., Brosse, L., Cahalan, S. M., Grandl, J., ... & Patapoutian, A. (2017). Endogenous Piezo1 can confound mechanically activated channel identification and characterization. *Neuron*, *94*(2), 266-270.

Eastwood, A. L., Sanzeni, A., Petzold, B. C., Park, S. J., Vergassola, M., Pruitt, B. L., & Goodman, M. B. (2015). Tissue mechanics govern the rapidly adapting and symmetrical response to touch. *Proceedings of the National Academy of Sciences*, *112*(50), E6955-E6963.

El-Gaby, M., Zhang, Y., Wolf, K., Schwiening, C. J., Paulsen, O., & Shipton, O. A. (2016). Archaerhodopsin selectively and reversibly silences synaptic transmission through altered pH. *Cell reports*, *16*(8), 2259-2268.

Feng, R., & Wen, J. (2015). Overview of the roles of Sox2 in stem cell and development. *Biological chemistry*, *396*(8), 883-891.

Feng, X., Takayama, Y., Ohno, N., Kanda, H., Dai, Y., Sokabe, T., & Tominaga, M. (2020). Increased TRPV4 expression in non-myelinating Schwann cells is associated with demyelination after sciatic nerve injury. *Communications biology*, *3*(1), 1-14.

Fleming, M. S., & Luo, W. (2013). The anatomy, function, and development of mammalian Aβ low-threshold mechanoreceptors. *Frontiers in biology*, *8*(4), 408-420.

Fontenas, L., & Kucenas, S. (2017). Livin'on the edge: glia shape nervous system transition zones. *Current opinion in neurobiology*, *47*, 44-51.

Goodenough, D. A., & Paul, D. L. (2009). Gap junctions. *Cold Spring Harbor perspectives in biology*, *1*(1), a002576.

Hao, J., & Delmas, P. (2010). Multiple desensitization mechanisms of mechanotransducer channels shape firing of mechanosensory neurons. *Journal of Neuroscience*, *30*(40), 13384-13395.

Hao, J., Bonnet, C., Amsalem, M., Ruel, J., & Delmas, P. (2015). Transduction and encoding sensory information by skin mechanoreceptors. *Pflügers Archiv-European Journal of Physiology*, *467*(1), 109-119.

Heidenreich, M., Lechner, S. G., Vardanyan, V., Wetzel, C., Cremers, C. W., De Leenheer, E. M., ... & Lewin, G. R. (2012). KCNQ4 K+ channels tune mechanoreceptors for normal touch sensation in mouse and man. *Nature neuroscience*, *15*(1), 138-145.

Hoffman, B. U., Baba, Y., Griffith, T. N., Mosharov, E. V., Woo, S. H., Roybal, D. D., ... & Lumpkin, E. A. (2018). Merkel cells activate sensory neural pathways through adrenergic synapses. *Neuron*, *100*(6), 1401-1413.

Hong, G. S., Lee, B., Wee, J., Chun, H., Kim, H., Jung, J., ... & Oh, U. (2016). Tentonin 3/TMEM150c confers distinct mechanosensitive currents in dorsal-root ganglion neurons with proprioceptive function. *Neuron*, *91*(1), 107-118.

Hong, G. S., Lee, B., & Oh, U. (2017). Evidence for mechanosensitive channel activity of tentonin 3/TMEM150C. *Neuron*, *94*(2), 271-273.

Hu, J., & Lewin, G. R. (2006). Mechanosensitive currents in the neurites of cultured mouse sensory neurones. *The Journal of physiology*, *577*(3), 815-828.

Hu, J., Chiang, L. Y., Koch, M., & Lewin, G. R. (2010). Evidence for a protein tether involved in somatic touch. *The EMBO journal*, *29*(4), 855-867.

Huang, T. Y., Belzer, V., & Hanani, M. (2010). Gap junctions in dorsal root ganglia: possible contribution to visceral pain. *European journal of pain*, *14*(1), 49-e1.

Idé, C. (1976). The fine structure of the digital corpuscle of the mouse toe pad, with special reference to nerve fibers. *American Journal of Anatomy*, *147*(3), 329-355.

Idé, C. (1977). Development of Meissner corpuscle of mouse toe pad. *The Anatomical Record*, *188*(1), 49-67.

Ikeda, R., Cha, M., Ling, J., Jia, Z., Coyle, D., & Gu, J. G. (2014). Merkel cells transduce and encode tactile stimuli to drive Aβ-afferent impulses. *Cell*, *157*(3), 664-675.

Hudspeth, A. J., Jessell, T. M., Kandel, E. R., Schwartz, J. H., & Siegelbaum, S. A. (Eds.). (2013). *Principles of neural science*. McGraw-Hill, Health Professions Division.

Jenkins, B. A., & Lumpkin, E. A. (2017). Developing a sense of touch. *Development*, *144*(22), 4078-4090.

Jessen, K. R., & Mirsky, R. (2005). The origin and development of glial cells in peripheral nerves. *Nature Reviews Neuroscience*, *6*(9), 671-682.

Jessen, K. R., & Mirsky, R. (2016). The repair Schwann cell and its function in regenerating nerves. *The Journal of physiology*, *594*(13), 3521-3531.

Jessen, K. R., Mirsky, R., & Lloyd, A. C. (2015). Schwann cells: development and role in nerve repair. *Cold Spring Harbor perspectives in biology*, *7*(7), a020487.

Jessen, K. R., & Mirsky, R. (2019). Schwann cell precursors; multipotent glial cells in embryonic nerves. *Frontiers in molecular neuroscience*, *12*, 69.

Johnson, K. O. (2001). The roles and functions of cutaneous mechanoreceptors. *Current opinion in neurobiology*, *11*(4), 455-461.

Kastriti, M. E., & Adameyko, I. (2017). Specification, plasticity and evolutionary origin of peripheral glial cells. *Current opinion in neurobiology*, *47*, 196-202.

Kioke, T., Wakabayashi, T., Mori, T., Takamori, Y., Hirahara, Y., & Yamada, H. (2014). Sox2 in the adult rat sensory nervous system. *Histochemistry and cell biology*, *141*(3), 301-309.

Kress, M., Koltzenburg, M., Reeh, P. W., & Handwerker, H. O. (1992). Responsiveness and functional attributes of electrically localized terminals of cutaneous C-fibers in vivo and in vitro. *Journal of neurophysiology*, *68*(2), 581-595.

Lafferty, C. K., & Britt, J. P. (2020). Off-Target Influences of Arch-Mediated Axon Terminal Inhibition on Network Activity and Behavior. *Frontiers in neural circuits*, *14*, 10.

Lallemend, F., & Ernfors, P. (2012). Molecular interactions underlying the specification of sensory neurons. *Trends in neurosciences*, *35*(6), 373-381.

Lamkin, E. R., & Heiman, M. G. (2017). Coordinated morphogenesis of neurons and glia. *Current opinion in neurobiology*, *47*, 58-64.

Lánský, P., Rodriguez, R., & Sacerdote, L. (2004). Mean instantaneous firing frequency is always higher than the firing rate. *Neural computation*, *16*(3), 477-489.

Laranjeira, C., Sandgren, K., Kessaris, N., Richardson, W., Potocnik, A., Berghe, P. V., & Pachnis, V. (2011). Glial cells in the mouse enteric nervous system can undergo neurogenesis in response to injury. *The Journal of clinical investigation*, *121*(9).

Lechner, S. G., Frenzel, H., Wang, R., & Lewin, G. R. (2009). Developmental waves of mechanosensitivity acquisition in sensory neuron subtypes during embryonic development. *The EMBO Journal*, *28*(10), 1479-1491.

Lechner, S. G., & Lewin, G. R. (2013). Hairy sensation. *Physiology*, *28*(3), 142-150.

Lewin, G. R., & Moshourab, R. (2004). Mechanosensation and pain. *Journal of neurobiology*, *61*(1), 30-44.

Lewis, A. H., Cui, A. F., McDonald, M. F., & Grandl, J. (2017). Transduction of repetitive mechanical stimuli by Piezo1 and Piezo2 ion channels. *Cell reports*, *19*(12), 2572-2585.

Li, L., & Ginty, D. D. (2014). The structure and organization of lanceolate mechanosensory complexes at mouse hair follicles. *Elife*, *3*, e01901.

Li, L., Rutlin, M., Abraira, V. E., Cassidy, C., Kus, L., Gong, S., ... & Ginty, D. D. (2011). The functional organization of cutaneous low-threshold mechanosensory neurons. *Cell*, *147*(7), 1615-1627.

Light, A. R., & Perl, E. R. (1979). Reexamination of the dorsal root projection to the spinal dorsal horn including observations on the differential termination of coarse and fine fibers. *Journal of Comparative Neurology*, *186*(2), 117-131.

Liu, R., Ke, H., Shao, T., Qin, Y., & Zhao, S. (2020). TMEM150B is dispensable for oocyte maturation and female fertility in mouse. *Scientific Reports*, *10*(1), 1-7.

Lingueglia, E. (2007). Acid-sensing ion channels in sensory perception. *Journal of Biological Chemistry*, *282*(24), 17325-17329.

Lu, H. J., Nguyen, T. L., Hong, G. S., Pak, S., Kim, H., Kim, H., ... & Oh, U. (2020). Tentonin 3/TMEM150C senses blood pressure changes in the aortic arch. *The Journal of clinical investigation*, *130*(7).

Mahn, M., Prigge, M., Ron, S., Levy, R., & Yizhar, O. (2016). Biophysical constraints of optogenetic inhibition at presynaptic terminals. *Nature neuroscience*, *19*(4), 554-556.

Maricich, S. M., Wellnitz, S. A., Nelson, A. M., Lesniak, D. R., Gerling, G. J., Lumpkin, E. A., & Zoghbi, H. Y. (2009). Merkel cells are essential for light-touch responses. *Science*, *324*(5934), 1580-1582.

Marmigère, F., & Ernfors, P. (2007). Specification and connectivity of neuronal subtypes in the sensory lineage. *Nature Reviews Neuroscience*, *8*(2), 114-127.

Marshall, K. L., Clary, R. C., Baba, Y., Orlowsky, R. L., Gerling, G. J., & Lumpkin, E. A. (2016). Touch receptors undergo rapid remodeling in healthy skin. *Cell Reports*, *17*(7), 1719-1727.

Marshall, K. L., Saade, D., Ghitani, N., Coombs, A. M., Szczot, M., Keller, J., ... & Patapoutian, A. (2020). PIEZO2 in sensory neurons and urothelial cells coordinates urination. *Nature*, 1-6.

Martinez-Salgado, C., Benckendorff, A. G., Chiang, L. Y., Wang, R., Milenkovic, N., Wetzel, C., ... & Lewin, G. R. (2007). Stomatin and sensory neuron mechanotransduction. *Journal of neurophysiology*, *98*(6), 3802-3808.

Maksimovic, S., Nakatani, M., Baba, Y., Nelson, A. M., Marshall, K. L., Wellnitz, S. A., ... & Lumpkin, E. A. (2014). Epidermal Merkel cells are mechanosensory cells that tune mammalian touch receptors. *Nature*, *509*(7502), 617-621.

McCarter, G. C., Reichling, D. B., & Levine, J. D. (1999). Mechanical transduction by rat dorsal root ganglion neurons in vitro. *Neuroscience letters*, *273*(3), 179-182.

McGlone, F., & Reilly, D. (2010). The cutaneous sensory system. *Neuroscience & Biobehavioral Reviews*, *34*(2), 148-159.

Mendes, C. S., Bartos, I., Márka, Z., Akay, T., Márka, S., & Mann, R. S. (2015). Quantification of gait parameters in freely walking rodents. *BMC biology*, *13*(1), 1-11.

Melzack, R., & Wall, P. D. (1965). Pain mechanisms: a new theory. *Science*, *150*(3699), 971-979.

Milenkovic, N., Wetzel, C., Moshourab, R., & Lewin, G. R. (2008). Speed and temperature dependences of mechanotransduction in afferent fibers recorded from the mouse saphenous nerve. *Journal of neurophysiology*, *100*(5), 2771-2783.

Moehring, F., Halder, P., Seal, R. P., & Stucky, C. L. (2018). Uncovering the cells and circuits of touch in normal and pathological settings. *Neuron*, *100*(2), 349-360.

Moehring, F., Mikesell, A. R., Sadler, K. E., Menzel, A. D., & Stucky, C. L. (2020). Piezo1 Mediates Keratinocyte Mechanotransduction. *bioRxiv*.

Moroni, M., Servin-Vences, M. R., Fleischer, R., Sánchez-Carranza, O., & Lewin, G. R. (2018). Voltage gating of mechanosensitive PIEZO channels. *Nature communications*, *9*(1), 1-15.

Morrison, K. M., Miesegaes, G. R., Lumpkin, E. A., & Maricich, S. M. (2009). Mammalian Merkel cells are descended from the epidermal lineage. *Developmental biology*, *336*(1), 76-83.

Moshourab, R. A., Wetzel, C., Martinez-Salgado, C., & Lewin, G. R. (2013). Stomatin-domain protein interactions with acid-sensing ion channels modulate nociceptor mechanosensitivity. *The Journal of physiology*, *591*(22), 5555-5574.

Mrschtik, M., & Ryan, K. M. (2016). Another DRAM involved in autophagy and cell death. *Autophagy*, *12*(3), 603-605.

Murthy, S. E., Dubin, A. E., & Patapoutian, A. (2017). Piezos thrive under pressure: mechanically activated ion channels in health and disease. *Nature Reviews Molecular Cell Biology*, *18*(12), 771-783.

Murthy, S. E., Dubin, A. E., Whitwam, T., Jojoa-Cruz, S., Cahalan, S. M., Mousavi, S. A. R., ... & Patapoutian, A. (2018). OSCA/TMEM63 are an evolutionarily conserved family of mechanically activated ion channels. *Elife*, *7*, e41844.

Murthy, S. E., Loud, M. C., Daou, I., Marshall, K. L., Schwaller, F., Kühnemund, J., ... & Patapoutian, A. (2018). The mechanosensitive ion channel Piezo2 mediates sensitivity to mechanical pain in mice. *Science translational medicine*, *10*(462).

Nagi, S. S., Marshall, A. G., Makdani, A., Jarocka, E., Liljencrantz, J., Ridderström, M., ... & Olausson, H. (2019). An ultrafast system for signaling mechanical pain in human skin. *Science advances*, *5*(7), eaaw1297.

Neubarth, N. L., Emanuel, A. J., Liu, Y., Springel, M. W., Handler, A., Zhang, Q., ... & Ginty, D. D. (2020). Meissner corpuscles and their spatially intermingled afferents underlie gentle touch perception. *Science*, *368*(6497).

Nikolaev, Y. A., Feketa, V. V., Anderson, E. O., Schneider, E. R., Gracheva, E. O., & Bagriantsev, S. N. (2020). Lamellar cells in Pacinian and Meissner corpuscles are touch sensors. *Science Advances*, *6*(51), eabe6393.

Nikolaev, Y. A., Cox, C. D., Ridone, P., Rohde, P. R., Cordero-Morales, J. F., Vásquez, V., ... & Martinac, B. (2019). Mammalian TRP ion channels are insensitive to membrane stretch. *Journal of cell science*, *132*(23).

Niu, Y., Tao, X., Vaisey, G., Olinares, P. D. B., Alwaseem, H., Chait, B. T., & MacKinnon, R. (2021). Analysis of the Mechanosensor Channel Functionality of TACAN. *bioRxiv*.

Nourse, J. L., & Pathak, M. M. (2017, November). How cells channel their stress: Interplay between Piezo1 and the cytoskeleton. In *Seminars in cell & developmental biology* (Vol. 71, pp. 3-12). Academic Press.

Omerbašić, D., Schuhmacher, L. N., Sierra, Y. A. B., Smith, E. S. J., & Lewin, G. R. (2015). ASICs and mammalian mechanoreceptor function. *Neuropharmacology*, *94*, 80-86.

Owens, D. M., & Lumpkin, E. A. (2014). Diversification and specialization of touch receptors in skin. *Cold Spring Harbor perspectives in medicine*, *4*(6), a013656.

Pare, M., Elde, R., Mazurkiewicz, J. E., Smith, A. M., & Rice, F. L. (2001). The Meissner corpuscle revised: a multiafferented mechanoreceptor with nociceptor immunochemical properties. *Journal of Neuroscience*, *21*(18), 7236-7246.

Paricio-Montesinos, Ricardo, Frederick Schwaller, Annapoorani Udhayachandran, Florian Rau, Jan Walcher, Roberta Evangelista, Joris Vriens, Thomas Voets, James FA Poulet, and Gary R. Lewin. "The sensory coding of warm perception." *Neuron* (2020).

Patkunarajah, A., Stear, J. H., Moroni, M., Schroeter, L., Blaszkiewicz, J., Tearle, J. L., ... & Poole, K. (2020). TMEM87a/Elkin1, a component of a novel mechanoelectrical transduction pathway, modulates melanoma adhesion and migration. *Elife*, *9*, e53308.

Piccini Meghan A., Miao Julia H., Janice Schwartz. (Updated: 2021). Histology, Meissner Corpuscle. In StatPearls Publishing. Treasure Island. From: https://www.ncbi.nlm.nih.gov/books/NBK518980/

Poole, K., Herget, R., Lapatsina, L., Ngo, H. D., & Lewin, G. R. (2014). Tuning Piezo ion channels to detect molecular-scale movements relevant for fine touch. *Nature communications*, *5*(1), 1-14.

Poole, K., Moroni, M., & Lewin, G. R. (2015). Sensory mechanotransduction at membrane-matrix interfaces. *Pflügers Archiv-European Journal of Physiology*, *467*(1), 121-132.

Ranade, S. S., Syeda, R., & Patapoutian, A. (2015). Mechanically activated ion channels. *Neuron*, *87*(6), 1162-1179.

Ranade, S. S., Woo, S. H., Dubin, A. E., Moshourab, R. A., Wetzel, C., Petrus, M., ... & Patapoutian, A. (2014). Piezo2 is the major transducer of mechanical forces for touch sensation in mice. *Nature*, *516*(7529), 121-125.

Riethmacher, D., Sonnenberg-Riethmacher, E., Brinkmann, V., Yamaai, T., Lewin, G. R., & Birchmeier, C. (1997). Severe neuropathies in mice with targeted mutations in the ErbB3 receptor. *Nature*, *389*(6652), 725-730.

Romanet, J. L. (2017). A Role for TMEM150A in Cytokine Regulation.

Rong, Y., Jiang, J., Gao, Y., Guo, J., Song, D., Liu, W., ... & Liu, Z. (2021). TMEM120A contains a specific coenzyme A-binding site and might not mediate poking-or stretch-induced channel activities in cells. *bioRxiv*.

Roudaut, Y., Lonigro, A., Coste, B., Hao, J., Delmas, P., & Crest, M. (2012). Touch sense: functional organization and molecular determinants of mechanosensitive receptors. *Channels*, *6*(4), 234-245.

Sadler, K. E., Moehring, F., & Stucky, C. L. (2020). Keratinocytes contribute to normal cold and heat sensation. *Elife*, *9*, e58625.

Syeda, R., Florendo, M. N., Cox, C. D., Kefauver, J. M., Santos, J. S., Martinac, B., & Patapoutian, A. (2016). Piezo1 channels are inherently mechanosensitive. *Cell reports*, *17*(7), 1739-1746.

Schwaller, F., Bégay, V., García-García, G., Taberner, F. J., Moshourab, R., McDonald, B., ... & Lechner, S. G. (2020). USH2A is a Meissner's corpuscle protein necessary for normal vibration sensing in mice and humans. *Nature Neuroscience*, 1-8.

Servin-Vences, M. R., Moroni, M., Lewin, G. R., & Poole, K. (2017). Direct measurement of TRPV4 and PIEZO1 activity reveals multiple mechanotransduction pathways in chondrocytes. *Elife*, *6*, e21074.

Servin-Vences, M. R., Richardson, J., Lewin, G. R., & Poole, K. (2018). Mechanoelectrical transduction in chondrocytes. *Clinical and Experimental Pharmacology and Physiology*, *45*(5), 481-488.

Shibasaki, K. (2016). TRPV4 ion channel as important cell sensors. *Journal of anesthesia*, *30*(6), 1014-1019.

Shin, S. M., Moehring, F., Itson-Zoske, B., Fan, F., Stucky, C. L., Hogan, Q. H., & Yu, H. (2021). Piezo2 mechanosensitive ion channel is located to sensory neurons and non-neuronal cells in rat peripheral sensory pathway: implications in pain. *bioRxiv*.

Simon, A. M., & Goodenough, D. A. (1998). Diverse functions of vertebrate gap junctions. *Trends in cell biology*, *8*(12), 477-483.

Smith, E. S. J., & Lewin, G. R. (2009). Nociceptors: a phylogenetic view. *Journal of Comparative Physiology A*, *195*(12), 1089-1106.

Spray, D. C., & Hanani, M. (2019). Gap junctions, pannexins and pain. *Neuroscience letters*, *695*, 46-52.

Szczot, M., Pogorzala, L. A., Solinski, H. J., Young, L., Yee, P., Le Pichon, C. E., ... & Hoon, M. A. (2017). Cell-type-specific splicing of Piezo2 regulates mechanotransduction. *Cell reports*, *21*(10), 2760-2771.

Usoskin, D., Furlan, A., Islam, S., Abdo, H., Lönnerberg, P., Lou, D., ... & Ernfors, P. (2015). Unbiased classification of sensory neuron types by large-scale single-cell RNA sequencing. *Nature neuroscience*, *18*(1), 145-153.

Walcher, J., Ojeda-Alonso, J., Haseleu, J., Oosthuizen, M. K., Rowe, A. H., Bennett, N. C., & Lewin, G. R. (2018). Specialized mechanoreceptor systems in rodent glabrous skin. *The Journal of physiology*, *596*(20), 4995-5016.

Walsh, C. M., Bautista, D. M., & Lumpkin, E. A. (2015). Mammalian touch catches up. *Current opinion in neurobiology*, *34*, 133-139.

Wetzel, C., Hu, J., Riethmacher, D., Benckendorff, A., Harder, L., Eilers, A., ... & Lewin, G. R. (2007). A stomatin-domain protein essential for touch sensation in the mouse. *Nature*, *445*(7124), 206-209.

Woo, S. H., Ranade, S., Weyer, A. D., Dubin, A. E., Baba, Y., Qiu, Z., ... & Patapoutian, A. (2014). Piezo2 is required for Merkel-cell mechanotransduction. *Nature*, *509*(7502), 622-626.

Woo, S. H., Lukacs, V., De Nooij, J. C., Zaytseva, D., Criddle, C. R., Francisco, A., ... & Patapoutian, A. (2015). Piezo2 is the principal mechanotransduction channel for proprioception. *Nature neuroscience*, *18*(12), 1756-1762.

Woodhoo, A., & Sommer, L. (2008). Development of the Schwann cell lineage: from the neural crest to the myelinated nerve. *Glia*, *56*(14), 1481-1490.

Woolf, C. J., & Ma, Q. (2007). Nociceptors—noxious stimulus detectors. *Neuron*, *55*(3), 353-364.

Wu, J., Lewis, A. H., & Grandl, J. (2017). Touch, tension, and transduction–the function and regulation of Piezo ion channels. *Trends in biochemical sciences*, *42*(1), 57-71.

Yue, F., Cheng, Y., Breschi, A., Vierstra, J., Wu, W., Ryba, T., ... & Ren, B. (2014). A comparative encyclopedia of DNA elements in the mouse genome. *Nature*, *515*(7527), 355-364.

Zelená, J. (1978). The development of Pacinian corpuscles. *Journal of neurocytology*, *7*(1), 71-91.

Zhao, Q., Wu, K., Geng, J., Chi, S., Wang, Y., Zhi, P., ... & Xiao, B. (2016). Ion permeation and mechanotransduction mechanisms of mechanosensitive piezo channels. *Neuron*, *89*(6), 1248-1263.

Zhao, Q., Wu, K., Chi, S., Geng, J., & Xiao, B. (2017). Heterologous expression of the Piezo1-ASIC1 chimera induces mechanosensitive currents with properties distinct from Piezo1. *Neuron*, *94*(2), 274-277.

Zhao, X., Yan, X., Liu, Y., Zhang, P., & Ni, X. (2016). Co-expression of mouse TMEM63A, TMEM63B and TMEM63C confers hyperosmolarity activated ion currents in HEK293 cells. *Cell biochemistry and function*, *34*(4), 238-241.

Zheng, Y., Liu, P., Bai, L., Trimmer, J. S., Bean, B. P., & Ginty, D. D. (2019). Deep sequencing of somatosensory neurons reveals molecular determinants of intrinsic physiological properties. *Neuron*, *103*(4), 598-616.

13. ACKNOWLEDGMENTS

First, I will thank my supervisor Prof. Dr. Gary R. Lewin. I have learned more than I could imagine from him and his lab. It was a great journey, and I am taking with me a lot of inspiration for the rest of my academic carrier.

I would like to take the chance to thank Dr. Ursula Koch for accepting to be my supervisor. As well as Dr. James Poulet and Dr. Niccolo Zampieri for being part of my committee meeting and helped me with their comments and suggestions to improve my project.

I want to specially thank to Dr. Valérie Begay for helping me and supporting me during all these years with experiments, advice and dedication.

I also wish to thank all the members of Lewin lab. To the technicians for their dedication and help that recued me more than once. To all my colleagues for sharing knowledge, time, laughs and trying to make the best of our time in the lab. Special thanks to Dr. Jan Walcher for introduced me to what would become a long carrier in skin-nerve.

My mom Julia, my dad Toño and my brother Toño, for their love and remaining me where home is. My friends Cledi, Carol, Irene, Marina and Ana for their unconditional support at all moments.

Finally, I would like to thank Aljoscha Overkamp, your motivation, support and love were essential for this process. Without you this path would have been impossible, or at least, less fun.